GLOBAL PROTEOME RESPONSE OF HUMAN CANCER CELL LINES TO LOW DOSE eIF4E/eIF4G INHIBITION

Rory Nicholas Besaans

Supervised by Dr Paul Teesdale-Spittle

A thesis submitted to the Victoria University of Wellington in fulfilment of the degree of Master of Science in Biotechnology

Victoria University of Wellington

2019

1.1 Abstract

Cachexia is a debilitating muscle wasting disease and co-morbidity strongly associated with chronic inflammatory conditions such as cancer, chronic heart failure, chronic obstructive pulmonary disease and sepsis. Cachexia has a strong negative impact on quality of life and research suggests that 20% of cancer patients will die of cachexia. Translation initiation is the most highly regulated step of protein synthesis and the eukaryotic initiation factor 4F (eIF4F) translation initiation complex is the gatekeeper of this process; the eIF4F complex is composed of eIFG, a scaffolding protein, eIF4E, an mRNA cap-recognition protein and eIF4A, an RNA helicase. Inhibition of eIF4A by pateamine A has been shown to rescue muscle wasting *in vitro* and *in vivo*, this result has been reproduced with other eIF4A inhibitors. Pateamine A is a sponge-derived natural product with nanomolar toxicity to cancer cells. Surprisingly, at doses well below its anti-neoplastic activity it exerts distinct effects on cachexia. The research in this thesis follows on from previous work in our laboratory with pateamine A in human cell lines. Work on the effects of pateamine A on the proteome suggests that not all the proteins changing in expression are explainable by stressing the translation initiation complex. A model by which motifs in the 5' UTRs of transcripts are a recognised and removed from the system in a selective manner could help explain these effects. We aimed to target eIF4E, another component of the eIF4F system, with two compounds to see if a comparable dose of eIF4E inhibitors could elicit a pateamine-like response. DMSO, a solvent used extensively in this thesis, had unexpected effects on translation. We conclude that 4E1RCat, a compound developed as a selective inhibitor of eIF4E, is not likely to be useable in further work, due to its window of activity coinciding with an unacceptable concentration of DMSO. Ribavirin, our second compound, showed a proteomic response consistent with its classification as an eIF4E translation initiation inhibitor. The proteome response seen with our eIF4E inhibitors is consistent with disruption of translation initiation. However, the data for 4E1RCat was deemed untrustworthy in the wake of revelations that DMSO, the vehicle in which it is dissolved, exerts an almost identical response. From the results obtained, it was not possible to confidently test whether protein downregulation occurred in response to a 5'UTR sequence motif, as seen for inhibitors of eIF4A. Coupled with the uncertainty associated with the 4E1Rcat results, there were relatively few downregulated proteins from the treatments, and many of these could be explained by the direct biological response to the function of the compound in the treatment. All in all, we have obtained new insights into the effects of DMSO on the proteome which will aid further experimentation. This thesis has laid the groundwork for further investigation of the effects of eIF4F inhibition in the context of better understanding the remediation of cachexia through the eIF4F system.

1.2 **Acknowledgements**

I cannot remember a time when I have felt so utterly burnt-out, while simulatenously feeling such a great sense of contentment. In the words of the late Christopher Hitchens “I burned the candle at both ends . . . and it gave a lovely light”. This has truly been an amazing and formative experience for me and there are simply too many people to thank. That being said there are some people whose contribution to both my development as an individual, and to this thesis warrants extra thanking.

Paul, I feel like you are too modest to want or expect credit for someone else’s achievement, but it would be wrong for me to not attribute part of my success to your guidance, mentorship and seemingly infinite patience. I cannot express how grateful I am for all the times you walked me through concepts I should know and explained them to me in words I could understand. I try my best to extend this same patience to those who require my help and guidance. Needless to say, I have a long way to go, but it has been awesome to have such a great role model to show how to be an excellent teacher and mentor. I think some of why the School of Biological Sciences is such a well-functioning department and such a friendly and collaborative place is attributable to your outlook and the outlook of others like you, such as Anne La Flamme, John Miller and Peter Pfeffer all of whom I remember fondly from my days as an undergraduate. I haven’t forgotten about you Melanie, Andrew and Darren, thank you for being great teachers and academics too.

Vimal, many of the things I have thanked Paul for are things you provided me with too, in a different sense perhaps. Thank you for all the help, thoughtful conversations and laughs. It’s been a pleasure sharing an office with you. Clint, I get the feeling that I was in some way a kindred proteomics-spirit, if you ever get a chance, look for the CLINT1 node I left in the STRING diagram in homage. It should be in the DMSO downregulated hits diagram! The one node in SBS with no friends! I hope you remember the joke for my sake! Richard, thank you for always helping me out with your process, you saved me innumerable headaches. Leti, thanks for being so damn efficient and organised and helping me out in tissue culture. Carl, thanks for encouraging me, perhaps unintentionally, not to pander or clamour for attention and for reinforcing my belief that being nice doesn’t make you a good person, you are not nice, and undeniably a good person. I miss your sense of humour greatly.

Ali, although I may not express it, I am incredibly sad that we are no longer on speaking terms. I am so glad that we got to know each other so well this year, you were definitely an overall net positive addition to my life. I cherish the memories we share. Alvey, thanks for being such good fun, and always being down to nerd-out about science and the like. Sonja, despite being so different in our approaches to life, I love your take on things, despite it being blunt at times. Don’t change too much, I care about you deeply and hope your new chapter in America works out well for you!

Reigh, Stephen, John, Holly, Sam, Alex and Madge, thank you for being such amazing friends, I am so glad that we are still friends this far out of our undergraduate degrees. I’ve never been a clique person, but I’d clique with you guys any day!

To my family, Mark, Ginelle, Kevin and Rob, thank you for putting up with me, I suspect I have not been the most fun to be around in the last year. I miss you all dearly and hope to be able to spend more time with you in the future. I am slowly realising how important my family is to me. Thank you for always being there for me.

Lots of love,
Rory

1.3 Abbreviations

BMI	Body mass index
CHCA	α-Cyano-4-hydroxycinnamic acid
CHX	Cycloheximide
CID	Collision-induced dissociation
DMSO	Dimethyl sulfoxide
dH_20	Distilled water
eIF4(A/E/F/G)	Eukaryotic initiation factor 4 (A/E/F/G)
FBS	Fetal bovine serum
FDR	False discovery rate/s
GO	Gene ontology
GOAT	Gradient optimisation and analysis tool
iBAQ	Intensity based absolute quantification
LBM	Lean body mass
LC	Liquid chromatography
LTQ	Linear trap quadrupole
MALDI-TOF	Matrix-assisted laser desorption/ionisation – time of flight
MS	Mass spectrometer/spectrometry
MS/MS	Tandem mass spectrometry
MTT	3-(4,5-dimethylthiazol-2-yl)-2,5-diphenyltetrazolium bromide
PatA	Pateamine A
PBS	Phosphate buffered saline
PEG	Polyethylene glycol
PSM	Peptide spectrum match
RBV	Ribavirin
RIPA buffer	Radioimmunoprecipitation assay buffer
SDC	Sodium deoxycholate
SDS	Sodium dodecyl sulfate
STAT3	Signal transducer and activator of transcription 3
TIC	Total ion current

1.4 Table of contents

Contents

1 Introduction

Cachexia is a wasting disorder that affects millions of people world-wide and is generally associated with chronic inflammatory conditions. Research suggests it could be responsible for as many as 1 in 5 deaths in cancer patients. Systemic inflammation is central to the development of cachexia, and pro-inflammatory cytokines are a feature of all forms of cachexia. Translation initiation is controlled by the eIF4F complex and is the most highly regulated step in protein expression and is the gateway to cellular production of protein. The three-part eIF4F complex consists of a scaffolding protein, eIF4G, a cap-recognition protein, eIF4E, and the helicase eIF4A, responsible for melting secondary structure and giving the ribosome access to mRNAs that might otherwise have their translation hindered. Inhibition of eIF4A, by the marine natural product pateamine A (PatA) has recently been demonstrated to reverse cachexia *in vitro*, in lab-grown muscle fibres and *in vivo* in mice. Pateamine A is an exceptionally potent anti-cancer compound isolated from marine sponges in New Zealand and has a unique method of disrupting translation. PatA has been shown to have applications outside the realm of cancer treatment, at doses well-below its anti-cancer effects. PatA is unfortunately in short supply, and despite being the first therapy to address the cachexia at the molecular level, the transition of PatA from pre-clinical to clinical trials has been delayed. Efforts are being made to find a commercially viable method of procuring PatA, however, in the meantime lessons can be learned from the molecular effects of PatA on the eIF4F system. The precise mechanism by which PatA rescues cachexia has not been elucidated and it is not known whether inhibiting eIF4A is solely responsible, or if the eIF4F complex is also involved. Our lab group has previously observed the effects of PatA on the proteome of a selection of human cell lines, the work in this thesis is done in parallel and mirrors the treatment conditions and cell lines used. This research aims, in part, to establish whether eIF4F has a role in the anti-cachectic effects of eIF4A inhibition. By partially disabling cap-recognition by inhibiting eIF4E in human cell lines and observing the effects on the proteome, we hope to see whether there are shared outcomes between the cells subjected to inhibition of eIF4E and eIF4A.

1.1 Cachexia

Cachexia is a metabolic wasting disorder that results in the involuntary progressive loss of weight through atrophy of muscle and fat tissues. It is co-morbid with many chronic diseases, and its etiology is grounded in inflammatory processes, anorexia, and muscle and fat tissue catabolism (Argilés, Busquets, Stemmler, & López-Soriano, 2014). In the United States alone approximately 27 million people suffer from cachexia with around 5.5 million requiring treatment (Morley, Thomas, & Wilson, 2006). There are two clinical consensus definitions of cachexia. Fearon (2011) focus on weight loss, BMI, and sarcopenia, whilst Evans (2008) definition is based on decreased muscle strength, fatigue, anorexia, low fat-free mass index and abnormal biochemistry (an in increase in inflammatory markers; anemia; and low serum albumin. The Evans definition has been shown to be especially effective (Vanhoutte et al., 2016). The Evans' cohort identified chronic heart failure, chronic obstructive pulmonary disease (COPD), chronic kidney disease, chronic infection, sepsis and cancer as a set of disease states associated strongly with cachectic wasting. Loss of muscle, loss of fat, and anemia are key identifiers of cachexia (Evans et al., 2008).

1.1.1 Effects on survival prospects and quality of life

The most significant contributor to cachectic disease is COPD with 16 million sufferers, followed by heart failure with 4.8 million and rheumatoid arthritis at 2.1 million (Morley et al., 2006). In contrast, cancer cachexia at 1.4 million, ranks below even nursing home sufferers of cachexia at 1.6 million. The literature tends to focus heavily on cancer cachexia despite only about 6% of cachexia sufferers

being in this group. Decreases in lean body mass (LBM) and functional impairment lead to a decreased quality of life. Along with this is increased risk of mortality, as shown in a study from 1932, documenting the cause of death in 500 cases of cancer with cachexia. In the study, fully one fifth of the cancer deaths were attributed to cachexia (Warren S, 1932).

1.1.2 The molecular basis of cachectic disease

Despite the complex and convoluted etiology of cachexia, research has implicated several molecular mechanisms and pathways of interest which are thought to account for the loss of lean muscle and fat tissues. Skeletal muscle accounts for 40% of an individuals' body mass and its loss is an obvious, visual sign of disease. However, focusing too heavily on skeletal muscle loss is misleading and does not address the nuances inherent in this disease state. A correct assessment of cachexia involves acknowledgement of the syndrome as multi-organ, multi-factorial and typified by abnormal biochemistry (Argilés et al., 2014). Cancers' meagre contribution to the overall number of cachexia sufferers' contrasts with the extensive insights the study of cancer cachexia has bestowed upon the field. 'Adipose browning' or conversion of white adipose tissue to brown adipose is driven by tumour secreted molecules including IL-6 from the inflammatory response, and parathyroid-hormone-related protein (PTHrP) generally secreted by tumour cells. Neutralising PTHrP caused a decrease in both white adipose tissue browning and the loss of muscle mass in mice (Serkan Kir et al., 2014). UCP1, an uncoupling protein commonly known as thermogenin, causes increased levels of thermogenesis and is responsible for fat-mass loss and contributes to the wasting process. The expression of thermogenin in brown adipose is caused by conversion of white adipose to brown adipose by IL-6 and PTHrP. Weight loss is a common symptom of cachexia, as a function of a negative tilt on an individual's energy balance and homeostasis of muscle tissue caused by increased thermogenesis and increased levels of inflammatory cytokines. Commonly associated with cachexia is a loss of appetite, also indicating effects on the brain and hypothalamus and providing more support for the theory of cachexia as a multi-organ syndrome (Argilés et al., 2014). Decreased food intake is common in cancer patients and speeds up the decline of body mass. In these patients, weight loss is also driven by the high protein, glucose, and fat demands of tumours. Activated immune cells and tumours are the main producers of inflammatory cytokines in cancer cachexia. One of these cytokines, TNF-α, is known to have direct catabolic effects on skeletal muscle and adipose tissue (Reid & Li, 2001).

1.1.3 Cachexia management and current therapeutic approaches

The systemic inflammatory response seems to be the connection between the major pathologies that cause cachexia, and as such anti-inflammatory drugs are a logical way to counteract cachexia by reducing systemic inflammation. The most common way to achieve this is by suppression of pro-inflammatory cytokine production. TNF-α is a pro-inflammatory and pro-catabolic cytokine, in 2005 a randomised placebo controlled trial showed that thalidomide was well-tolerated and effective at attenuating weight loss, and LBM loss in pancreatic cancer patients suffering from cachexia (Gordon et al., 2005). Another suggested therapeutic option for addressing weight loss in cancer cachexia on a molecular level is β-adrenergic blockade. In a recent trial in severe chronic heart failure patients, carvedilol attenuated the development of and partially reversed cachexia (Clark et al., 2017). However, most research into cachexia treatments is aimed at management through symptom-focused therapies. Appetite stimulant therapies are a direct way of addressing loss of appetite often seen in cancer patients, as well as the weight loss associated with reduced food intake. These stimulants are therapeutic interventions that do not directly address cachexia on the molecular level but address the loss of fat and muscle tissue indirectly by addressing the weight loss associated with cachectic wasting. Megestrol acetate, an orally accessible synthetic progesterone, and L-carnitine have, in combination and individually, shown promise at helping with the loss of weight and LBM

(Von Haehling & Anker, 2015). Megestrol acetate has also shown promise in dealing with cachectic weight loss in children suffering from cancer and the weight loss associated with chemotherapy; there was a mean increase in LBM of 19.7% in comparison to the placebo group with a loss of 1.2% over the course of the 90 day trial period (Frey & Davis, 2016). In terms of sarcopenia, nutritional support and exercise have marked effects on muscle loss; however, the effects of these measures are less clear in cachexia. A Cochrane meta-analysis of nutritional support and mortality in elderly people at risk of malnutrition indicates small benefits such as increased weight gain and a potential to lower the risk of complications in hospital conditions. The authors state that nutritional support may lower the risk of mortality in people who are malnourished (Milne, Potter, & Avenell, 2005). Since cachexia is in many ways a catabolic syndrome, the use of anabolic steroids may seem like a logical way to counteract the disease. Unfortunately, anabolic steroid therapies are limited to 2-week treatment periods due to concern about side effects (Von Haehling & Anker, 2015; Yu et al., 2014) . In response, clinical trials of enobosarm, a selective androgen receptor modulator, in 2013 were completed and suggested some benefits (Dobs, 2013). However, no new clinical data has recently been reported.

1.1.4 The lack of progress in the realm of cachexia treatment is a driver of our research

The lack of a cachexia therapeutics is not a symptom of the biomedical science field's failure to explore therapeutic options. The effective treatment of cachexia is littered with the bodies of clinical trials showing modest to marginal improvements in cachexia endpoints. These endpoints include hand grip strength, performance in the 6-minute walk test, LBM and quality of life. Anamorelin, an appetite stimulant and anabolic therapeutic, showed marginal improvements in LBM, with no improvement in hand-grip strength or quality of life (Katakami et al., 2018; Von Haehling & Anker, 2015). On 14 September 2017, the European Medicines Agency confirmed the refusal of marketing authorisation for amorelin in cachexia treatment. Frustratingly, reading between the lines is necessary with therapeutics in clinical trials, it takes a significant amount of time to work out if some of the promising clinical agents have progressed in the cachexia therapy space. This may be economically motivated as there is no incentive for a company to actively broadcast that a therapeutic in development has marginal effects on the disease it has been formulated to treat. Enobosarm seems to have stalled in clinical trials and may be awaiting regulatory approval to proceed. Taken together, the attempts at addressing cachexia have highlighted several therapeutic options for clinicians with modest improvements in symptomatic consequences of cachectic muscle wasting. Nonetheless, therapy addressing the underlying molecular cause of cachexia is still needed. Studies in murine models of cachexia and *in vitro* at the level of protein production using inhibitors of the translation initiation factor eIF4A are a promising avenue to explore. The next step is to better understand the mechanistic underpinning of these effects, which may ultimately lead to effective treatments for this disease.

1.2 eIF4F

The eukaryotic initiation factor 4F (eIF4F) has been described as a nexus for cancer therapy (Pelletier, Graff, Ruggero, & Sonenberg, 2015). The eIF4F complex is necessary for recruitment of mRNA to the ribosome in cap-dependent translation. It is composed of three components: eukaryotic initiation factors 4A, 4G, and 4E. eIF4A is an RNA helicase; eIF4E, an m7G cap recognition protein, and eIF4G a large scaffolding protein (Figure 1-1). Unlike other translation regulatory pathways, eIF4F, with the exception of translation mediated by internal ribosome entry sites (IRESes), is an unavoidable 'bottleneck' that cancers have a hard time circumventing. Enzymes which regulate eIF4F-mediated translation by phosphorylation, such as Mnk1 and 2, encounter redundancy issues whereby cancer cells can subvert the regulatory nature of these pathways by finding another way to favourably regulate key proteins that promote oncogenesis or maintenance of the cancer

cell. For example, the eIF4F complex is typically indispensable for translation and if Mnk1/2 inhibitors are being used to prevent activating the eIF4F complex by phosphorylation, the cancer cell will find another way to phosphorylate and activate eIF4F to meet its protein requirements.

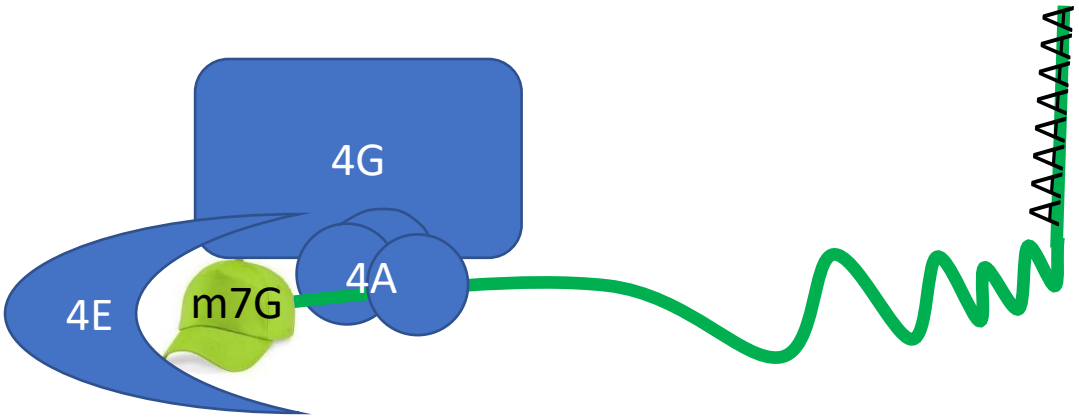

Figure 1-1 A simplistic diagrammatic representation of the eIF4F complex engaged in cap-binding. In green, a messenger RNA possessing both a methyl guanosine (m7G) cap and a poly-A tail is shown, eIF4A the dumb-bell shaped protein, has assisted in melting secondary structure allowing the 40S ribosomal subunit (not shown) to be recruited. Also shown is eIF4G the scaffolding protein and eIF4E the protein involved in cap-binding and recognition.

1.2.1 Eukaryotic initiation factor 4A

The eukaryotic initiation factor 4A (eIF4A), is a dumb-bell shaped protein with two major domains connected by a linker. It is an ATP-dependent DEAD-box RNA helicase of the eukaryotic initiation factor-4A family of proteins (Bordeleau et al., 2005). The two eIF4A domains move between an open and closed conformation; in the closed conformation, the two domains interact in a way that favours the binding of mRNA and ATP (Sun et al., 2014). eIF4A unwinds secondary structure in mRNA, and mRNAs with any secondary structure in the 5'UTR ultimately require this activity for translation. The helicase activity of eIF4A is increased as a by-product of stabilisation of the 'closed' conformation; the ATP binding pocket and mRNA binding region require both eIF4A domains to interact to be fully form in the closed conformer, this becomes clear when viewing the binding pocket and mRNA binding region *in silico* (Ho et al., 2009). The weak helicase activity of unbound eIF4A increases 20-fold when bound to the eIF4G scaffold (Oberer, Marintchev, & Wagner, 2005; Rozen et al., 1990). eIF4A is vital because it is a requirement for 40S ribosomal subunit binding to the mRNA for translation, and by extension, protein synthesis. Some mRNA molecules are ready to be translated into protein with little or no requirement for the action of eIF4A. Other mRNAs have stable secondary structures in their 5' untranslated regions (UTRs) like RNA duplexes, or even G-quadruplexes which require enzymatic activity to 'unwind'. The degree of requirement for the RNA helicase eIF4A for translation is dependent on both the length and complexity of the transcript. Longer transcripts and those with greater secondary structure are more dependent on eIF4A for translation (Svitkin, Pause, Haghighat, & Pyronnet, 2001).

There are three isoforms of eIF4A in humans: 4AI, 4AII and 4AIII. 4AI and 4AII share 90-95% homology and *in vitro* assay work suggests they are functionally interchangeable (Yoder-Hill, Pause, Sonenberg, & Merrick, 1993) but differentially expressed (Merrick, 1992). 4AI is expressed in all growing tissues while 4AII preferentially binds to eIF4G and is expressed in organs with low proliferative capacity (Nielsen & Trachsel, 1988; Williams-Hill, Duncan, Nielsen, & Tahara, 1997). 4AIII shares 65% homology with 4AI and 4AII and is a core component of the exon junction complex

involved in mRNA surveillance and nonsense mediated decay (Le Hir, Gatfield, Izaurralde, & Moore, 2001). Due to its different function, eIF4AIII is not found in the eIF4F complex.

1.2.2 Eukaryotic initiation factor 4E

The role of the eukaryotic initiation factor 4E (eIF4E) component of the eIF4F complex in eukaryotic translation initiation is to bind and recognise the 5' m7G cap, consisting of the sequence m7GpppN (where N is any nucleotide). There are three isoforms of eIF4E in humans: 4EI, 4EII and 4EIII (Joshi, Lee, Maeder, & Jagus, 2005). The isoforms differ in their ability to engage in cap-binding, with isoforms II and III being 40-fold weaker binders of the m7G cap (Frydryskova et al., 2016). eIF4EI is the main isoform involved in global cap-dependent translation, eIF4EII is involved in translational repression of a subset of mRNAs through AU-rich sequences in the 3' UTR and involving the protein Bicoid (Bcd) (Cho, Osler, & Hg, 2008; Tao, 2015). Overexpression of eIF4E is present in 30% of all cancers and is generally associated with a poor prognosis (Volpin et al., 2017). A hallmark of many cancers is over-expression of eIF4E because unregulated growth increases demand for protein. In a given non-cancerous eukaryotic cell, protein synthesis is indirectly controlled by the stoichiometry of the eIF4F components. Under normal conditions, the rate-limiting component of eIF4F is eIF4E, which is available at the lowest abundance in comparison to eIAF4A and eIF4G. The activity of eIF4F is regulated through eIF4E by 4E binding proteins (4EBPs), which in turn are regulated by hyperphosphorylation. The addition of multiple phosphate groups decreases the 4EBP binding affinity for eIF4E, freeing it to interact with eIF4G thus permitting cap-recognition to take place and allowing the eIF4F complex to assemble. 4EBPs and eIF4G share a binding motif involved in eIF4E binding, research shows that eIF4G and eIF4E interface at a single canonical alpha-helical motif (Zhao, Liu, Miller, & Goss, 2017). The eIF4E canonical binding motif has been characterised as Tyr-X-X-X-X-Leu-ϕ where X is any amino-acid and ϕ is a hydrophobic residue (Marcotrigiano, Gingras, Sonenberg, & Burley, 1999). Awareness of this motif is important when considering how drugs target eIF4E.

1.2.3 Eukaryotic initiation factor 4G

The eukaryotic initiation factor 4G (eIF4G) is the scaffolding protein and core of the eIF4F complex. At least 2 genes for eIF4G exist in humans, eIF4G1 and eIF4G2. The N-terminal third binds to eIF4E and poly-A binding proteins (PABPs), the middle third binds eIF4A and eIF3, and the C-terminal third represents the regulatory portion, containing a second eIF4A binding site and a docking sequence for the ser/thr kinase Mnk1 (Morino, Imataka, Svitkin, Pestova, & Sonenberg, 2000). Mnk1 has been identified as the main kinase that acts on eIF4E, and the phosphorylated form shows increased affinity for the m7G cap (Minich, Balastat, Gosst, & Rhoads, 1994). Thus, eIF4G has two eIF4A binding sites, one in the central domain and one in the carboxylic acid terminal domain (Korneeva, Lamphear, Hennigan, Merrick, & Rhoads, 2001). The association of eIF4E with eIF4G and is likely to cause conformational changes in the scaffold, modulating its capacity to interact with other eIFs.

1.2.4 eIF4F inhibitors

The eIF4F complex has been identified as an excellent target for cancer therapy, as such an extensive number of drugs have been identified or synthesised that target components of the complex. Although the impetus for identifying eIF4F inhibitors came from the fields interested in cancer therapy, inhibitors of the eIF4F complex are also a useful tool to study the functional consequences of disturbing the translation initiation machinery. Several compounds exist that interact with the eIF4F machinery in various mechanistically distinct ways. Known eIF4A inhibitors include hippuristanol, pateamine A, elatol, the rocaglate family drugs and include an eIF4A aptamer (Cencic & Pelletier, 2016; Iwasaki, Floor, & Ingolia, 2016; James H. Matthews, Maass, Northcote, Atkinson, & Teesdale-Spittle, 2013; Oguro, Ohtsu, Svitkin, Sonenberg, & Nakamura, 2003; Peters et al., 2018).

eIF4E inhibitors include 3 commercially available inhibitors, 4EGI-1, 4E1RCat, and ribavirin. Two of these inhibitors, 4E1Rcat and ribavirin, are the subject of this research, as their effects have not been extensively studied in the context of translation. These two compounds are described in more detail below. A short review of other eIF4F inhibitors and their mechanisms of inhibiting eIF4F components, and by extension translational output is also included.

1.2.4.1 4E1RCat

4E1RCat, is a small molecule inhibitor of eIF4E that functions by preventing 4EBP from binding eIF4E, as well as preventing eIF4E-eIF4G interaction. 4E1Rcat has provided evidence that targeting the eIF4F machinery can have positive outcomes for cancer treatment. Mice bearing $Pten^{+/-}$Eμ-Myc, and $Tsc2^{+/-}$Eμ-Myc lymphomas showed similar regression patterns when treated with a 4E1RCat-doxorubicin combination in comparison to rapamycin-doxorubicin combination therapy (Cencic et al., 2010). 4E1RCat had no effect on tumour regression as a standalone treatment, whereas rapamycin and doxorubicin were individually capable of causing moderate tumour regression. (Cencic et al., 2010). *In silico* modelling of the molecular interaction of 4E1RCat with eIF4E suggests that the eIF4G/4EBP binding pocket is occupied by 4E1RCat preventing it from associating with eIF4G (Cencic et al., 2010). Disruption of the eIF4E/eIF4G interaction occurs at the canonical eIF4E binding motif previously mentioned. This mechanism is unlike 4EGI-1 which increases the binding affinity of eIF4E for 4EBP (Moerke et al., 2007), the effect of 4E1RCat prevents 4EBP from binding eIF4E as well as preventing eIF4E-eIF4G interaction signifying two molecular interactions to be aware of.

1.2.4.2 Ribavirin

Ribavirin is an FDA approved drug of the nucleotide analogue variety, it is used primarily for the treatment of Hepatitis C viral infection. Ribavirin in combination with radiation therapy or temozolomide has shown increased efficacy in cancer treatment, in comparison to either treatment alone. This was demonstrated by an in increase in the median survival of rats and mice with orthotopically implanted gliosarcoma, and stem-like glioma cells respectively (Volpin et al., 2017). Unlike 4E1RCat, which can be considered pharmacologically 'clean', ribavirin has a host of molecular interactions and despite being approved by the FDA in 1986 some of ribavirin's interactions are still debated. Even the ability of ribvarin to inhibit eIF4E has been hotly contested, especially the notion that it is an m7G mimic (Kentsis et al., 2005; Kentsis, Topisirovic, Culjkovic, Shao, & Borden, 2004; Westman et al., 2005; Yan, Svitkin, Lee, Bisaillon, & Pelletier, 2005). In a letter to the editor Kentsis et al, defend ribavirin as an eIF4E-cap interactor mimicking the m7G cap, citing the pleiotropic, concentration dependent effects of ribavirin and usage errors made in the papers contesting their findings. They also direct the attention to the low-micromolar dose range in which ribavirin has been shown to interact with eIF4E, as well as questioning the validity of the use of lysates as a tool to study a process as complex and highly regulated as translation initiation (Kentsis et al., 2005)

1.2.4.3 A brief mechanistic appraisal of other eIF4F inhibitors

The eIF4F complex is well characterised, and many inhibitors of the individual components have been identified using high-throughput screens and affinity assays. As eIF4E is the main eIF4F component investigated in this thesis, this section aims to briefly introduce other inhibitors and their mechanisms of (inter)action to demonstrate the range of inhibitory compounds available to biologists studying eIF4F. This section also aims to indicate the role and context of this research in the field.

Pateamine A (PatA) is perhaps the most well-known eIF4A inhibitor, it has an IC_{50} in the low-nanomolar range and is suspected to function by increasing the binding affinity of eIF4A for mRNA, 'locking' it onto a transcript, and disrupting protein-protein interactions with eIF4G, thereby

preventing translation initiation (Low, Dang, Bhat, Romo, & Liu, 2007). Hippuristanol, is a polyhydroxysteroid with an IC_{50} in the high nanomolar range, it has a mechanistically distinct mode of action from PatA whereby the allosteric binding of the drug prevents association of mRNA with both free and eIF4F complex bound eIF4A (Waldron, Raza, & Le Quesne, 2018). Elatol is another natural product inhibitor of eIF4AI. Elatol's IC_{50} is in the low-micromolar range, it binds eIF4AI with 2:1 (elatol:eIF4A1) stoichiometry and has been identified as a specific inhibitor of ATP hydrolysis (Peters et al., 2018). The rocaglate family a class of cyclopenta[*b*]benzofuran drugs including rocaglamide A (RocA), silvestrol and episilvestrol originate from *Aglaia sp* these compounds tend to have IC_{50} values in the mid-to-low nanomolar range. The mechanism of RocA interaction involves a binding interface created by the mRNA:eIF4A complex (Iwasaki et al., 2019), with an initial increase in helicase activity, but ultimately leading to eIF4A inhibition (Sadlish et al., 2014). Silvestrol and episilvestrol interact with eIF4AI/II but do not interact with any other molecular targets, and all molecular effects are traceable to their interaction with eIF4AI/II (Chambers et al., 2013). The use of RNA aptamers involved development of an eIF4A aptamer that 'staples' the two domains of eIF4A into a closed conformation preventing the conformational changes necessary for ATP hydrolysis and helicase activity (Oguro et al., 2003). Antisense oligonucleotides have been developed against the eIF4E transcript preventing production of the eIF4E subunit, and are in Phase I/II clinical trials in combination with the chemotherapy drug, irinotecan (Duffy, Makarova-Rusher, & Ulahannan, 2016).

1.3 The Pateamine A Story

Pateamine A is an immunosuppressive, cytotoxic, and anti-fungal inhibitor of eukaryotic translation initiation (Kuznetsov et al., 2009; Low et al., 2005; Northcote, Blunt, & Munro, 1991). It is a thiazole-containing macrodiolide. This small molecule sits at the motivational core of this project as it has been identified as a potential treatment of cachexia, through inhibition of the function of the eIF4F complex (Di Marco et al., 2012). PatA was isolated from *Mycale* sp. sponges found off west coast of New Zealand. In 1991, an initial report published a description of its 2-D structure and its cytotoxicity in human cell lines (Northcote et al., 1991). A simplified synthetic analogue des-methyl, des-amino Pateamine A (DMDA-PatA) (see Figure 1-2A) has been synthesized and shows near equal potency (Romo et al., 2004) and has been used as a tool to study the behaviour of PatA by proxy. As a demonstration of DMDA-PatA toxicity researchers compared the cytotoxicity of PatA with an existing cancer therapy, vinblastine (see Figure 1-2B). A notable feature is the striking uniformity of the IC_{50} values in cell lines responding to PatA, almost all clustering at 10 nM, with few exceptions (Kuznetsov et al., 2009). DMDA-PatA, and by extension PatA has proven to be insensitive to P-glycoprotein mediated efflux. This resistance to efflux suggests that these molecules are likely to be more effective therapies against multi-drug resistant cancers (Kuznetsov et al., 2009), than therapeutics sensitive to removal by cancers employing a drug efflux strategy. Significantly, there are currently no therapeutics in the clinic that target translation initiation through the eIF4F complex, an exploitable target for cancer therapy (Pelletier, Graff, Ruggero, & Sonenberg, 2015). If PatA made it through clinical trials it would be the first compound to enter this new therapeutic territory.

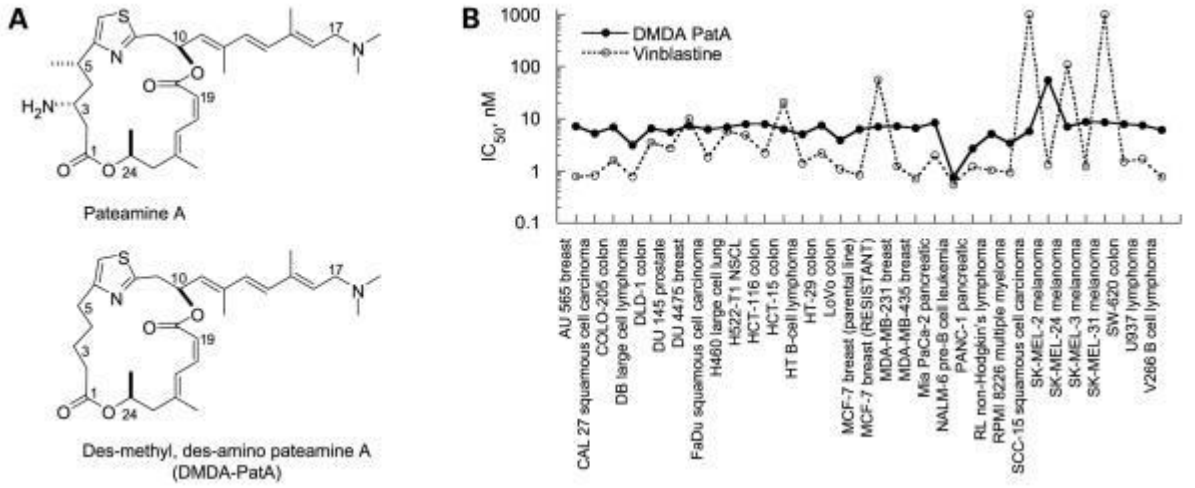

Figure 1-2 In growing cells DMDA-PatA (and by extension PatA) shows nearly uniform IC_{50} values across 32 cell lines demonstrating comparable cytotoxicity to vinblastine an existing anti-neoplastic agent (Kuznetsov et al., 2009)*. The simplified synthetic analogue DMDA-PatA had previously been deemed equipotent with its natural counterpart pateamine A in an* in vitro *reporter assay (Romo et al., 2004). Reprinted from Molecular Cancer Therapeutics, 2009, 8(5), 1250–60, Galina Kuznetsov, Potent in vitro and in vivo anticancer activities of des-methyl, des-amino pateamine A, a synthetic analogue of marine natural product pateamine A with permission from AACR.*

1.3.1 Therapeutic window of Pateamine

Cancer therapies are infamous for having a raft of unpleasant, severe, and debilitating side-effects. This drives the biomedical field to search for new therapeutics with not only the ability to kill a range of cancers, but also considers the side-effect profiles and tolerability of a therapeutic. Early on in PatA's discovery, researchers noted the contrast between toxic effects on cells under static growth conditions and those actively dividing (Northcote, Blunt, & Munro, 1991). P388, a murine cell line under active growth conditions exhibited an IC_{50} of 0.15 ng/mL whereas at 90% confluence, under static growth conditions the BSC kidney epithelial cell line had a high tolerance to the cytotoxic effects of PatA evidenced by an IC_{50} of 300 ng/mL. These outcomes were mirrored in more recent work with DMDA-PatA treated quiescent human fibroblasts, showing little to no toxic effects at the low nanomolar concentrations associated with its toxicity to cancer cells (Kuznetsov et al., 2009). These effects suggest that PatA would be tolerated by somatic cells while being incredibly cytotoxic to rapidly growing cells - on the order of 1,000-2,000 times by these early studies. On paper, this indicates an acceptable therapeutic window, which refers to the range of useable concentrations between a drugs' effectiveness as a therapy and unacceptable toxic side-effects. *In vivo* work in nude mice shows utility in the treatment of cancerous xenografts in MDA-MDB-435 melanoma regression was achieved in 9 of 10 mice in comparison to 7 of 10 in paclitaxel at day 44 of the study (Kuznetsov et al., 2009). At study closure at day 65, half of the study's cohort of mice were tumor free compared with a fifth of paclitaxel treated mice. It should be noted that the concentration of drug administered for success in these xenografts was extremely close to an empirically determined maximum tolerable dose. Despite this, not all xenograft models showed such promising results, some showed modest tumor regression. In LOX melanoma, less durable tumor regression was observed in comparison to paclitaxel. Modest regression was also reported in the remaining three tumor models, DLD-1 human colon cancer model, H522-T1 human non-small cell lung cancer model, and the NALM-6 leukemia model. Two other xenograft models, MiaPaca-2 pancreatic cancer and HT29 colon cancer, showed no significant response to therapy (Kuznetsov et al., 2009). This body of research indicates that pateamine A is in many ways a promising treatment for select cancers. The translation of this therapy to human trials is uncertain; the anti-cancer effects being close to a maximum tolerable dose is a concern for use as a therapy. Whether pateamine A finds a place in the

therapeutic space, either as a stand-alone therapy, in combination with existing therapies or in another therapeutic domain entirely (e.g. treatment of cachexia), it is undoubtedly a fascinating natural product with plenty of insights still to yield.

1.3.2 The problem: Pateamine availability

Total synthesis of Pateamine A was reported in a 1998 article by Daniel Romo (Romo et al., 1998), citing the compound's unique structure, potent immunosuppressive effects, and high levels of cytotoxicity as key drivers of synthesis efforts. A few years later a near equipotent simplified analogue, DMDA-PatA was synthesised with 10 fewer steps in the chemical synthesis (Romo et al., 2004). Despite this, Pateamine A is not commercially available. Efforts to cultivate *Mycale sp*. Sponges for semi-commercial production of peloruside A, another *Mycale sp*. derived anti-neoplastic agent, were largely unsuccessful. This method of procuring marine natural products was never intended to be commercially feasible and was done on a small scale for research in what was described as an 'interim supply' of compounds (M. J. Page, Handley, Northcote, Cairney, & Willan, 2011). Unfortunately, predation of these farmed Mycale sponges by the nudibranch *Hoplodoris nodulosa* meant that over the course of 6-7 years just over a 1.12 g peloruside A was obtained (M. J. Page et al., 2011). Had the endeavour to obtain peloruside A from sponges been successful, it would be reasonable to believe this means of production could have been mirrored for pateamine A. There are significant efforts being made at Victoria University of Wellington by the Harvey and Teesdale-Spittle group to produce peloruside A as well as pateamine A using synthetic chemistry approaches (Hemi Cumming et al., 2016). There are also retrosynthetic approaches using bacterial gene clusters expressed in a lab-culturable bacterial species (Owen et al., 2015) similar enough to the bacterial symbiont in *Mycale* to recombinantly express PatA by the Owen group.

1.3.3 What can Pateamine and eIF4A inhibition teach us about cachexia

The story of pateamine does not end at cancer and the applications do not stop at cancer therapy. Low dose (20 μg kg^{-1}) treatment with pateamine A has shown to rescue muscle wasting *in vivo* in mice with both C26 tumour induced muscle wasting, and the tumour-free TNF-α/IFN-γ model (Di Marco et al., 2012). More recent work has confirmed that eIF4A inhibition by several compounds with varied mechanisms proves that these effects are the result of eIF4A inhibition (Cramer et al., 2018). It was noticeable that low doses of PatA were still able to ameliorate the muscle wasting phenotype. These doses were well below concentrations where its anti-cancer effects tend to manifest, evidenced by no noticeable regression of the C26 tumours, suggesting it would also be well below the threshold for toxic effects. Although higher doses (50 μg kg^{-1}) both ameliorated cachexia and decreased the size of the tumours (Di Marco et al., 2012). The pleiotropic, dose-dependent effects alone hint at interesting biochemistry, with two effects mediated by treating the translation initiation complex at different dosage regimes. Perhaps more interesting from a clinical standpoint was the observation that at low doses there were no noticeable toxic manifestations of the compound on the treated animals. In the treatment of cachexia, a growing body of research has implicated factors including the cytokine IL-6 and the inducible nitric oxide synthase (iNOS) as well as the loss of myogenin and MyoD mRNA as the causative agents for muscle wasting (Di Marco et al., 2012). More recently, the signal transducer and activator of transcription 3 (STAT3) protein, a transcription factor and upstream effector of cytokines IL-6, TNF-α and IFN-γ, has been shown to be translationally repressed by eIF4A inhibition (Cramer et al., 2018). Cramer showed that that STAT3 protein levels are affected by eIF4A inhibitors without an effect on STAT3 mRNA levels suggesting that the effect is happening at the level of translation. *In vitro* INF-γ and TNF-α treatment of myotubes results in cytokine induced atrophy of the muscle fibres. The eIF4A inhibtors, pateamine A (PatA), hippuristanol, and silvestrol have all been shown to ameliorate these effects. New research has also added silvestrol and hippuristanol to the list of compounds affecting the iNOS/NO pathway

cementing eIF4A inhibition as a potential central therapeutic target in the rescue of cachexia (Cramer et al., 2018).

1.3.4 How does eIF4A inhibition ameliorate cachexia at the molecular level?

Although PatA is known to interact with all three isoforms of eIF4A (Bordeleau et al., 2005), PatA's anti-cancer and anti-cachectic effects are likely to be mediated primarily by its interaction with eIF4AI. There is a 4:1 abundance ratio in comparison to the eIF4AII isoform suggesting that at least based on abundance, eIF4AI is the main isoform (Yoder-Hill et al., 1993). Pateamine A encourages stabilisation of the favourable mRNA and ATP binding closed conformer, increasing helicase activity but preventing interaction with eIF4G (Iwasaki et al., 2019). Mechanistically, the anti-cancer properties of PatA at concentrations that lead to cell death are due to generalised protein synthesis inhibition. The sensitivity of tumor cells to its cytotoxic effects is likely a function of the protein demands of tumour cells going through unregulated division and the observation that many oncogenic transcripts are reliant on eIF4F for their efficient translation (Wolfe et al., 2015). Consequently, eIF4F components are often upregulated in cancers. The effects of eIF4A treatment can be direct, at the level of translation, whereby the mRNA level is unaltered, but the protein expression level is decreased. For example, as noted above STAT3 mRNA levels remain unaffected by eIF4A inhibition. However, eIF4A inhibition leads to a decrease in STAT3 and phospho-STAT3 protein in response to eIF4A. This was evidence that eIF4A inhibition was affecting STAT3 at the level of translation. The effects can also be indirect. STAT3 is a transcription factor, with many targets including IL-6. It is notable that IL-6 mRNA expression is lower after eIF4A inhibition. The decreased mRNA levels suggest that IL-6 protein levels have been indirectly affected, because inhibiting the production of protein should theoretically have no immediate effects on mRNA levels. STAT3 is the likely culprit for this disturbance.

A mechanism for the seemingly selective process by which inhibiting eIF4A lowers protein expression in a non-uniform manner has not been fully identified. Some relatively recent research proposes a model of stress granule-mediated translational repression as a mechanism by which eIF4A inhibitors could remove specific mRNAs. This repression of translation by removal to stress granules in this model ultimately leads to reversal of cachexia (Di Marco et al., 2012). It has been established that the degree of secondary structure present in the 5' UTR is in direct proportion to the requirement for eIF4A for translation (Svitkin et al., 2001). Eukaryotic initiation factors are capable of binding and scanning unstructured 5' UTRs however, even weak secondary structures enforce the requirement of the helicase activity of eIF4A for translation (Pestova & Kolupaeva, 2002). Di Marco implies that the therapeutic effects of eIF4A inhibition on models of cachexia are the result of the amount of 5' UTR secondary structure present in eIF4A sensitive transcripts (Di Marco et al., 2012). In other words, that the amount of secondary structure in the 5' UTR is the defining feature of an eIF4A-sensitive transcript. Our understanding of this system is evolving as new inhibitors of the system are developed and evaluated. Some of these are described in section 1.2.4, above. For example, recent research pertaining to the interactions of the rocaglates with eIF4A have shifted the understanding from translation dependent on 5' UTR length and complexity, to one of sequence-specific binding (Iwasaki et al., 2016). By implication, other eIF4A inhibitors that strengthen the ability of eIF4A to bind mRNA may also be manifesting their effects on the proteome in a similar manner. Rocaglates have been shown to increase the affinity of the binding interaction of eIF4A to select for polypurine sequences present in the 5' UTR (Iwasaki et al., 2016). X-ray crystallography also showed that the formation of the mRNA-eIF4A dimer is required for rocaglates to 'lock' the complex together (Iwasaki et al., 2019). PatA's interaction with mRNA and eIF4A has not been confirmed but is suspected to share this mechanism with rocaglates.

1.3.5 Is all mRNA born equal in the eyes of eIF4A?

It is clear that at high concentrations of eIF4A inhibitors, the reduction in availability of free eIF4A impacts on transcripts based on the 5' UTR requirement for functional eIF4A (Wolfe et al., 2015). However, at lower concentrations, such as used in cachexia control, (Di Marco et al., 2012),it is possible that the selective removal of STAT3 and iNOS protein expression are a consequence of complex enzyme kinetics. The formation of the enzyme-substrates complex between eIF4A, ATP and mRNA are a requirement for rocaglate binding. In this sense rocaglates can be considered uncompetitive inhibitors of eIF4A as they require the assembled mRNA-eIF4A interface. The substrate preference of eIF4A for different sequences of mRNA is only beginning to be explored (Iwasaki et al., 2016). It is likely that eIF4A inhibitors bind more effectively to some mRNA sequences than they do to others. For example, recent publications suggest that rocaglates may favour binding to eIF4A-mRNA complexes at polypurine motifs. The field has not crystallised the characteristics of eIF4A dependent transcripts or whether interfering with other components of the eIF4F complex has the same effect. This preference for particular sequence motifs may arise through the strength of binding interaction of the inhibitor with the eIF4A-mRNA complex, with some sequences offering optimal binding sites. Alternatively, processing time may be an important factor. The rate of translation could be highly variable across the range of mRNAs the eIF4F system is responsible for translating. There is strong evidence that eIF4A responds differently to structurally differing mRNAs, including exclusively Poly-U containing, mRNAs containing a mixture of duplex and single stranded RNA, and mRNAs that are extensively duplexed. It was noted that the mRNA variety used had highly variable effects on the conformational dynamics of eIF4A (Harms, Andreou, Gubaev, & Klostermeier, 2014). Therefore, the time it takes for mRNA to be processed may be variable, and this could be a factor determining the seemingly selective effects of eIF4A inhibition, as uncompetitive inhibition is impacted by the lifetime of the enzyme-substrate complex.

PatA binding has been shown to be either a very strong or irreversible inhibitor of the function of eIF4A (James Henry Matthews, 2010). If PatA shares the other trait of rocaglates, namely the selectivity for polypurine motifs, this could also potentially explain the selectivity seen with eIF4A inhibition. However, recent work shows that hippuristanol still rescues the muscle wasting seen with *in vitro* models of caxechia (Cramer et al., 2018). This is notable, as hippuristanol is an allosteric regulator of eIF4A, and linked to a decreased affinity for mRNA (Cencic & Pelletier, 2016; Lindqvist et al., 2008), in contrast to PatA and the rocaglates). This is seeming evidence against the model of selective effects of eIF4A inhibition being a product of sequestering into SGs of mRNAs with specific 5' UTR sequences or motifs such as polypurine motifs, hairpin loops or G-quadruplexes. Recent research suggests that the formation of classical secondary structures by $(GGC)_4$ motifs is favoured in comparison to G-quadruplexes and the role that G-quadruplexes play in 5' UTR motif mediated translation initiation repression may have been overestimated (Waldron et al., 2018). Unpublished experiments done by Richard Little (R Little 2018, personal communication, 11 October) at Victoria University of Wellington laboratories suggest that polypurine motifs may be an enriched sequence in PatA sensitive transcripts.

Pateamine A and other eIF4A inhibitors show potential for the treatment of cachexia. There is ample evidence that the inhibition of eIF4A is responsible for the anti-cachectic outcomes' researchers see *in vivo*. Current models implicate a loss of specific transcripts including iNOS and STAT3, while anabolic, muscle-generating transcripts such as myogenin and MyoD are rescued. The studies creating links between eIF4A inhibition and transcript loss or retention based on specific sequences and structural motifs are preliminary. Currently, nothing is known about the sequence selective effects of inhibiting other members of the eIF4F complex, and therefore whether any other eIF4F inhibitors should be considered for anti-cachectic drug development. The goal of this research is to

capture the effects both direct and indirect of translation inhibition by a selection of eIF4E inhibitory compounds. These effects on translation should manifest in the proteome as a change in protein expression when compared to a population of untreated control cells.

2 Aims and objectives

Cachexia is a debilitating and sometimes fatal condition without current therapeutics. Targeting eIF4A with inhibitory drugs like Pateamine A leads to a non-uniform drop in protein expression across the proteome. The goal of this study is to determine whether there is merit in targeting the components of eIF4F individually. We aim to perturb the eIF4F system in a targeted manner to study the global proteomic effects of treatment. We ask if we can achieve the same proteomic outcomes seen with Pateamine A using inhibitors for the other constituents of the eIF4F system: ribavirin and 4E1RCat.

The objectives of this research were:

1) To determine the effective inhibitor concentrations (e.g. IC_{50} , IC_{10} and IC_1) of two eIF4E inhibitors, and a relevant control inhibitor, by pharmacologically challenging a model cell system.

2) To quantify proteomic effects, pharmacologically challenge cells with inhibitors of eIF4E, and a control inhibitor, at concentrations determined in Objective 1, and extract, purify and analyse cellular protein abundance changes using LC-MS/MS.

3) To use gene ontologies and co-expression analysis to assess the cellular processes affected by eIF4E inhibition, with the ultimate goal of generating insight pathways effected by low dose eIF4E inhibitor treatment.

4) To identify any sequence motifs in the 5’ UTRs of proteins that change in response to eIF4E inhibition, but that are not explained by the direct biological response to the treatment. Finally, to evaluate whether 5’UTR sequence motifs are equivalent to those that respond to low-dose eIF4A treatment.

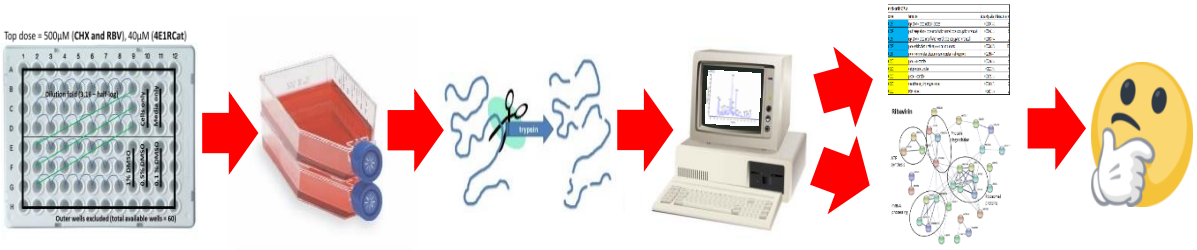

Figure 2-1 A simple diagrammatic representation of the work done in this thesis, from MTT assay through to treatment, tryptic digestion, LC-MS² analysis and to gene ontology (GO) and STRING analysis.

3 Materials and methods

3.1 Reagents

3.1.1 Cell Culture

96 well plates	Corning, USA
Dulbecco's Phosphate-Buffered Saline (DPBS)	Life Technologies, NZ
Foetal Bovine Serum (FBS)	Sigma-Aldrich, NZ
Roswell Park Memorial Institute-1640 media (RPMI-1640) HyClone™	GE Life Sciences, USA
Dulbecco's Modified Eagle's Media (DMEM) High modified +45000mg/L glucose +110mg/L sodium pyruvate	GE Life Sciences, USA
T25 flasks	Corning, USA
T75 flasks	Corning, USA
Trypan Blue, 0.4 %	Life Technologies, NZ
Trypsin-EDTA, 0.05 %	Life Technologies, NZ

3.1.2 Chemicals and Miscellaneous

α-Cyano-4-hydroxycinnamic acid (CHCA), 99 %	Sigma-Aldrich, NZ
Acetone, >99 %	Romil Ltd, UK
Acetic acid, glacial	Merck, NZ
Acetonitrile, >99.9 %	Carl Roth, NZ
Acetonitrile gradient grade for liquid chromatography	Merck, NZ
Bovine serum albumin (BSA)	ICP Biologicals, NZ
Chloroform	BDH, UK
Complete protease inhibitor cocktail	Sigma-Aldrich, NZ
Dithiothreitol (DTT)	BioRad, NZ
Dimethyl sulfoxide, ≥99.9 % (DMSO)	Sigma-Aldrich, NZ

Formic acid, 98-100 %	Merck, NZ
GlutaMAX™, 200 mM	ThermoFisher, NZ
Iodoacetamide, >99 %	GE Healthcare UK Limited
Kimwipes®	Kimberly-Clarke, USA
LoBind tubes®	Eppendorf, GER
Methanol, 99.9 %	ThermoFisher, NZ
N, N-dimethylformamide (DMF), ≥99 %	Sigma-Aldrich, NZ
Parafilm M®	Bemis, USA
Sinapinic acid	Sigma-Aldrich, NZ
Sodium deoxycholate (SDC), ≥97 %	Sigma-Aldrich, NZ
Sodium dodecyl sulphate (SDS)	Calbiochem, NZ
Thiourea, 99 %	Merck, NZ
Trifluoroacetic acid (TFA), 0.1 % in H_20	Sigma-Aldrich, NZ
Triton-X-100	ThermoFisher, NZ
Trypsin, Mass Spectrometry Grade	ThermoFisher, NZ
Urea	Sigma-Aldrich, NZ
dH_20 – water used was purified by reverse osmosis and distilled	High-Q Inc.™, USA
ZipTip® pipette tips	Agilent Technologies, USA

3.1.3 Kits

DC™ Protein Assay	Bio-Rad, USA

3.1.4 Buffers and Solutions

3-(4,5-dimethylthiazol-2-yl)-2,5-diphenyl tetrazolium bromide (MTT) solution: 5mg/mL of MTT, in PBS thoroughly vortexed and stored in a foil sheath.

MTT solubiliser: 10 % SDS: 50.0 g, 45 % *N, N*-dimethylformamide: 225.0 mL, dilute to 500 mL with dH2O, pH adjusted to 4.5 with glacial acetic acid

Radioimmunoprecipitation assay (RIPA) lysis buffer: 25mM Tris, pH 7–8, 150 mM NaCl, 0.1% sodium dodecyl sulfate (SDS), 0.5% sodium deoxycholate (SDC), 1% Triton X-100, protease inhibitor - RIPA buffer was made to 0.99x final volume, protease inhibitor tablets were dissolved to 0.01x in dH_20 to produce a 10x solution and combined to the produce the working solution.

Crude cell lysis buffer: 8M urea in dH_2O.

Urea SDC solution: 8M urea, 5% (w/v) SDC in dH_2O.

Urea-thiourea lysis solution: 6M urea, 2M thiourea in dH_2O.

Alkylation buffer: 100 mM iodoacetamide in dH_2O. Made fresh, tube covered in foil to minimise light exposure.

Reducing buffer: 10mM DTT in dH_2O

Buffer A: 0.1% formic acid in H_2O Optima® liquid chromatography/mass spectrometry.

Buffer B: 0.1% formic acid in acetonitrile.

CHCA matrix: 8 mg/mL α-Cyano-4-hydroxycinnamic acid (CHCA) in 50% acetonitrile, 0.1% TFA in H_2O.

Sinapinic acid matrix: 10 mg/mL sinapinic acid in 50% acetonitrile, 0.1% TFA in dH_2O.

Trypan blue solution: dH_20, 0.4% w/v trypan blue

Trypsin solutions: 20µg trypsin of trypsin was resolubilised in 20µL of dH_20 and split into 1µg aliquots

3.2 Drug stocks (CHX, RBV and 4E1RCAT) – preparation and storage

Ribavirin (RBV) and 4E1RCat were purchased from Sigma-Aldrich and stored at -20 °C. Cycloheximide (CHX) was stored at 4 °C. Drugs were dissolved in DMSO and stored at −20 °C at a concentration of 50 mM for RBV and CHX. 4E1RCAT was dissolved at 4 mM. Drugs diluted in aqueous solutions were used within 24 hours to avoid degradation. Drug stock tubes were wrapped in parafilm to avoid water adsorption, a well-known property of DMSO.

3.3 Software

Xcalibur™	ThermoFisher Scientific, USA
Scaffold™ 4	Proteome Software, USA

Proteome Discoverer™ 2.1	ThermoFisher, NZ
Prism	GraphPad Software, USA
Excel	Microsoft, USA

3.4 Cell culture

3.4.1 Cell culture - strains and maintenance conditions HL60 and HT29

All cultures originated from existing liquid N_2 freezer stocks at the Centre for Biodiscovery at Victoria University of Wellington. The HT29 cell line is derived from the colorectal adenocarcinoma of a 44-year-old caucasian female, originally isolated in 1964. The HT29 cell line has been used extensively in research, some examples of its use include its use as a measure of the effectiveness of anti-neoplastic compounds in drug discovery (Volpin et al., 2017) and to express genes due to its amenability to transfection (Morin, Vogelstein, & Kinzlertt, 1996). The HL60 cell line is an acute promyelocytic leukemia derived line originating from a 36-year-old caucasian female. The HL60 cell line are well-used to study myeloid differentiation (Birnie, 1988), it is commonly used as a first step assessing a compounds toxicity against human cells in MTT assays in drug discovery at the Victoria University of Wellington. Cell cultures were maintained at 37 °C in an incubator with a humidified atmosphere supplemented with 5% CO_2. HL60 Cells were seeded by default at a density of $1x10^5$ cells/mL, HT29 cells were seeded at $2x10^5$ cells/mL, cells were maintained in the exponential phase of growth and were kept from reaching confluency by regular passaging. Generally, 3 days passed between passages for both cell lines this was a good general rule.

3.4.2 Cell culture media

HT29 and HL60 cells were cultured in RPMI media containing 10% (v/v) FBS and 2.05 mM L-Glutamine. DMEM was required when thawing cells stored in DMEM or when growing cells from the stocks of another lab in which the cells were previously cultured in DMEM. In these cases the media was supplemented with 10% (v/v) FBS and L-Glutamine, 2.05 mM. Cells grown in DMEM were transferred to RPMI and given at least one passage before they were used in any experiments.

3.4.3 Cell counting

Culture cell counts were performed using light microscopy and a 0.4% trypan blue solution to facilitate cell counting using a hemocytometer. The outer 4 and the middle squares in the grid were most commonly used. If cell counts were extremely consistent across 3 squares diagonally across the grid and were at enough numbers i.e. over 100 cells, then no more squares were counted. If cell numbers in a grid were below 50, depending on the consistency of the first 5 squares counted, it was sometimes deemed necessary to count all 9 squares in the grid, or re-count a new set of cells.

3.5 MTT cell proliferation assays

For all MTT proliferation assays, 96-well microtiter plates were used. The wells of the 96-well plate were seeded at 1.0 x 10^4 cells/mL for both HL60 and HT29 cells at a final volume of 100 µL. The effects DMSO has above 0.5% were taken into consideration when selecting the top dose in the MTT assays, due to a minor calculation error early in the project the top dose of all drugs corresponded to a 1% DMSO concentration. As an example, the top dose of CHX and RBV was 500 µM, whereas the top dose of 4E1RCat was 40 µM. The two considerations when deriving the top dose for 4E1RCat were: the maximum achievable solubility in DMSO (4mM), and the maximum percentage of DMSO acceptable based on the literature. In HL60 cells a base proliferative decrease of ~3% is noticeable at 0.5% DMSO. All outer wells were filled with sterile distilled water to avoid evaporation affecting the

volume in the outer wells. Assays were generally spaced apart in terms of passaging. For example, cells were harvested from 3 separate passages from the same flask or the same origin cells over the course of 3 passages, instead of 3 biological replicate flasks being grown side by side and assays performed simultaneously. A half-log (3.16-fold) serial dilution scheme was used for all drugs (see Figure 6-1). A relevant DMSO control was included at concentrations where DMSO is expected to influence cell growth. A media only blank and cell-only control are also included. Assay data was collected from triplicate wells using a plate reader set at 570 nm.

3.5.1 HL60 cell line

For the MTT assays with suspension cells the final well volume was made up to 100 µL. The media used to maintain cell lines was used to dilute the drug stocks in preparation for treatment. Drug preparation was done in the 96-well microtiter plate prior to addition of cells. The top dose of drug was prepared in a single well if feasible (i.e. total volume does not exceed well volume of 300µL). The well containing the top dose was split into three equal volumes among the triplicate wells, enough was prepared to leave 50µL in the wells of the top dose. The media-drug mix was moved between the remaining triplicate wells containing 50 µL of media and mixed thoroughly to prepare a half-log (3.16-fold) serial dilution. Due to difficulty encountered culturing the HL60 cell line, the HT29 cell line became the focus of the proteomic analyses. Towards the end of this thesis the problems with the HL60 cell line was resolved, and a mirror experiment was carried out in this cell line, however, there was insufficient time remaining to accommodate analysing the HL60 samples on the MS.

3.5.2 HT29 cell line

Adherent cell lines were allowed 14 hours to adhere to the bottom of the MTT wells before treatment. Drug doses were prepared in a re-useable plastic container with a 96-well format, this was necessary for the HT29 cell line as the cells are allowed 14 hours to settle down in the 96 well plate prior to treatment. HL60 cells can have their drug doses prepared in a 96 well plate and have cells injected into the drug doses, this is possible as they are a suspension cell line. The top dose was made in a single well of the re-useable plastic container, then split into 3 equal volumes, enough liquid was prepared to have an excess of 50 µL in the wells in the 96-well mimic container as it is difficult to fully recover all the liquid from the container. The top dose triplicate wells are used to construct the half-log dilutions down the length of the container, the media cells were cultured in was used to dilute the drug in each assay. After all the doses were constructed in the plastic container, they were transferred to the 96-well plate and left for 2 days.

3.5.3 Collecting dose response data

The wells of a 96-well plates were seeded at 1.0 x 10^4 cells/mL of HL60 and HT29 cells at a final volume of 100 µL. A 20 µL aliquot of a 5 mg/mL MTT solution in PBS was pipetted into each well and the cells were given a 2-hour period to metabolise the MTT to formazan. After two hours the cells were lysed using the MTT solubiliser solution and left in an incubator overnight for the purple formazan crystals to dissolve. A (VERSAmax™) microplate reader set at 570 nm was used to read absorbance values. Excel was used to visualise general trends. Graphpad was used to generate graphs and get dose response values in the form of inhibitory concentration (IC) data.

3.6 Method of determining IC_{10} and IC_1 from experimental data

Two concentrations of drug were initially going to be explored, the IC_{10} and the IC_1. For practical purposes and in the interest of time the IC_{10} was selected. These were determined experimentally by MTT assay. In Prism, graphs were generated from the absorbances expressed as a percentage of untreated controls. A non-linear regression was fitted for each MTT assay replicate. To avoid determining IC_{10} and IC_1 by eye, 90% of the top asymptote value and 99% of the top asymptote values for each regression line on the graph were calculated and the corresponding $\log_{10}$(drug concentration) determined for all replicates individually. These values were combined and averaged to give the expected drug concentration to achieve 10% inhibition and 1% inhibition respectively.

3.7 Preparing cells for pharmacological challenge

Biological replicates were grown to sufficient concentration to seed enough flasks at $2x10^6$ cells. For example, HL60 cells were cultured to between 5-8.5 x 10^6 cells prior to treatment. T75 flasks were seeded at $2x10^6$ and in the case of HL60 cells were treated immediately, whereas the HT29 cells are given 14 hours to adhere to the bottom of the flask. A 48-hour drug challenge was then applied to cells at IC_{10} concentrations. HL60 and HT29 cells have a doubling time of about 24 hours under ideal conditions. The 48-hour treatment period was chosen to allow at least two mitotic divisions to occur. This treatment scheme was used to ensure the protein synthesis inhibitory effects of the drugs were given sufficient time to manifest. Inhibitory concentrations were determined by MTT proliferation assay described previously.

3.8 Sample preparation for use in LC-MS/MS

3.8.1 Cell lysis

Post-treatment cells were pelleted in a centrifuge at 300 x*g* for four minutes. The media was decanted, and cells were subsequently kept on ice. For the remainder of the lysis steps the cells were also kept on ice. The cell pellet was resuspended in 5-10 mL of ice-cold PBS and re-pelleted at 300 x*g* for a further four minutes, the PBS and all supernatant from this spin was discarded. Finally, 200 µL of the 8 M urea lysis solution was added to the cell pellet followed by vortexing. This combination of 8 M urea and the cell pellet was flash frozen at -80 °C three times, between freezes the pellet was allowed to defrost, followed by vortexing. The resulting lysate was transferred to 1.5 mL Eppendorf tubes.

3.8.2 Protein quantification

Protein quantification was necessary to assess how much trypsin would be used for tryptic digestion. Trypsin was added at a ratio of 1:50 of trypsin to protein. Two methods of protein quantification were explored.

3.8.2.1 NanoDrop (ThermoScientific)

The protein extracts were resuspended in a 50 µL solution of 8 M urea and quantified using a NanoDrop spectrophotometer. An 8 M urea blank was used to account for extraneous absorbance. 1 µL of sample proteins was placed on the contact point, the other contact was lowered into place with the sample between the two. The protein quantification A_{280} setting was used. Although the ratio of trypsin used to treat a given sample is 1:50 this can vary widely and still achieve successful digestion of proteins in a sample, however, the NanoDrop was exceptionally inaccurate with huge variation, even when analysing the same sample multiple times. The NanoDrop was considered too inaccurate for protein quantification and was dropped in favour of the DC protein assay.

3.8.2.2 DC™ Protein Assay (Bio-Rad)

Proteins were resuspended in 100 μL of 8 M urea or however much was necessary to fully re-dissolve the proteins. Proteins were quantified using the DC protein Assay (BioRad). Assays were performed in a 96-well microplate. A BSA standard was made at 40 mg/mL in dH_20 (40 μg/μL). Constructing a standard curve was achieved by performing 2-fold dilutions; 12 dilutions was sufficient to reach the lower end of the detection capacity of the assay. For each well containing standard or sample liquids were added in the order: 25 μL of reagent A → 5 μL sample/standard → 200 μL reagent B (yellow). The colour developed within 15 minutes and was stable for an hour. The standard generated a linear correlation between absorbance at 750 nm and protein concentration between 200 and 1500 μg/mL. Prism software from Graphpad was used to analyse the standard curve and sample data. For linear standard curves a simple linear regression function was fitted. A standard curve was generated with values outside the linear range, due to the small linear range of the assay this was extremely common. Due to the nature of tryptic digestion, often the amount of trypsin added is somewhat arbitrary and a 1:50 to 1:100 ratio of trypsin is more than sufficient to digest a protein sample.A sufficiently accurate result could be obtained by fitting a 2-phase decay non-linear regression to a standard curve starting at 40 μg/uL as the ratio of trypsin to protein will almost certainly be at a sufficient molar excess for digestion. Protein concentrations were interpolated based on the non-linear relationship between absorbance and protein concentration.

3.8.3 Protein precipitation

Chloroform-methanol precipitation

For every 100 μL of protein containing sample supernatant, 400 μL of methanol was added and agitated by vortexing. An aliquot of 100 μL chloroform was subsequently added, followed by agitation. 300 μL dH_2O was added, agitated and the lysate-solvent mixture centrifuged at 13,000 G for two minutes. The aqueous phase containing chloroform was carefully removed, and a further 400 μL of methanol added and vortexed. A second centrifugation pelleted the precipitated proteins. The remaining liquid was removed, and the protein precipitate was taken to near-dryness in the centrivap concentrator. Excessive drying caused issues with re-dissolving the protein pellet. The pellet was resuspended in an 8 M urea solution.

Acetone precipitation

To the protein sample, four-times the sample volume of acetone cooled to a temperature of -20 °C was added. The protein-acetone solution was vortexed and incubated at -20 °C for one hour. The solution was subsequently centrifuged at 13,000 x*g* for 10 minutes. The acetone was removed with a pipette with care being taken not to disturb the pellet, which was not always visible. The pellet was left to air-dry, then resuspended in 50 μL of an 8 M urea solution.

3.8.4 Protein pre-treatment and tryptic digestion

A 100 mM dithiothreitol (DTT) solution was used to reduce cysteine residues, removing disulfide bridges, and give the protease used in subsequent steps free access to the lysine/arginine residues of the fully unfolded protein. DTT solution was applied to each Eppendorf-contained protein extract at a working concentration of 5 mM and heated at 70 °C for 20 minutes. An iodoacetamide solution was added at 5 mM to prevent disulfide bond formation by alkylating the reduced cysteines with carbamidomethyl groups. Sample urea concentration was lowered to 2 M prior with dH_20 prior to trypsin addition. Trypsin was added to sample proteins at a 1:50 ratio and left to digest overnight at 37 °C.

3.8.5 Concentration, purification and desalting of peptides

Purification and desalting of the protein sample was achieved using a C-18 ZipTip®. A selection of solutions was made that filled the roles of conditioning the ZipTip column, rinsing the ZipTip column, binding the peptides to the C-18 resins, washing and desalting the peptides, and elution by a dilute solution of acetonitrile and neat acetonitrile.

Wetting solution – 100% acetonitrile
Cleaning solution – dH_20
Sample solution – peptides contained in a 2M urea solution
Wash solution – 0.5% formic acid
1st Extraction solution – 0.5% formic acid in 1:1 (v/v) water: acetonitrile
2nd Extraction solution – 100% acetonitrile

Where possible, 100µL amounts of all solutions relating to the ZipTip procedure were used. During aspirating and dispensing of solutions the ZipTip was kept wet, and air was not allowed to enter the pipette tip. The wetting solution was aspirated and dispensed into waste 7-8 times. The cleaning solution was aspirated and dispensed into waste a minimum of 10 times to remove the acetonitrile wetting solution. The sample solution was aspirated and dispensed within a given sample tube a minimum of 10 times. The sample loaded on the pipette tip's C-18 resins was washed by aspirating and dispensing the wash solution into the waste 10 times. A fresh LoBind tube was used in the following steps, the first extraction solution was aspirated and left within the pipette for 20 seconds then dispensed into the fresh tube. This action was repeated with the second extraction solution. The extraction solutions were evaporated to near dryness, using the centrivap concentrator. Peptides were resuspended in 0.1% formic acid, transferred to a liquid chromatography sample tube and submitted to the LC-MS/MS for analysis.

3.9 Matrix assisted laser desorption ionisation MS – time of flight (MALDI-TOF/MS)

Early in the optimisation phase of preparing proteins for MS analysis the presence of large amounts of polyethylene glycol (PEG) was noticed. Polyethylene glycol has a suppressive effect on the ionisation of molecules in electrospray MS. With this in mind MALDI-TOF/MS was used on samples to assay for PEG prior to transfer to the mass spectrometer. The main reason that MALDI-TOF was used is because PEG can be detected immediately after protein precipitation from the raw cell lysate. Tryptic digestion and the ZipTip processing are time consuming and being able to assay for PEG was a time-saving approach. Additionally, since proteins were re-dissolved in 8 M urea post precipitation and MALDI-TOF has a high salt tolerance it was a quick and easy way to detect PEG in samples and by a process of elimination identify the source of the PEG contamination. The Triton X-100 used in the RIPA lysis buffer used at the outset of this project is the suspected source of PEG contamination.

Matrix and MALDI

For mass spectrometry analysis, 1 µL of peptide-containing eluate was mixed with CHCA matrix in a 1:1 ratio and in a 1:10 ratio. Then 1 µL of each elution-matrix mixture was spotted onto a 384 well AB SCIEX Opti-Tof™ Cal Mix 5 plate and allowed to dry. The AB SCIEX TOF/TOF™ 5800 matrix-assisted laser desorption/ionisation time-of-flight tandem mass spectrometer (MALDI TOF/TOF) was calibrated using a 700-4000 m/z calibration mix. Many samples were in an 8 M urea solution when placed on a spot on the 384 well plate. These samples had high concentrations of urea salts present on the spot and often required the maximal laser setting of 4000 units.

3.10 LC-MS/MS settings and data analysis parameters

Peptides were separated using a flow rate of 0.2 µL/min and fractionated with a C18 column (Dionex, LC Packings, Netherlands). A 372 min buffer gradient was constructed from 0.1% formic acid (Buffer A) and 0.1% formic acid in 80% acetonitrile (Buffer B). The gradient was optimized to maximise the number of identified proteins using the gradient optimisation and analysis tool (GOAT) optimisation tool (Trudgian, Fischer, Guo, Kessler, & Mirzaei, 2014). The peptides in solution were ionised by electron spray ionisation with a silica tip emitter, with the voltage potential set at 2.2. Positive ion mode was used with the heated capillary temperature set at 200 °C and tube lens 160 V to permit entry of ions preferentially at 524.30 m/z. Ions with m/z range between 200 - 1850 m/z were analysed during the 372 min acquisition time using Fourier transform mass spectrometry (FTMS) in the Orbitrap, with data-dependent MS/MS on the top 6 intensity ions dynamically selected for collision-induced dissociation (CID) fragmentation and detection in the linear trap quadrupole (LTQ). The dynamic exclusion settings used were as follows: repeat count 1, repeat duration 30 s; exclusion list size 500; exclusion duration 90 s. A full-scan (500 ms maximum injection time) in the FTMS at a resolution of 30,000 identified the 6 highest abundance ions and selected them for CID (1.0 isolation width, normalised collision energy 35%, activation Q 0.25, activation time 30 ms) in the LTQ after accumulation of 500,000 ions with 10 ms maximum injection time. Between sample runs, the column was washed twice with a gradient from 2% Buffer B to 98% Buffer B across 30 min, the combination of washes used depended on how the chromatograms looked, if there was a lot of lipid at the end of the run a prolonged high %B wash was used. A minimum of two technical replicates were carried out on each of 3 or more biological replicate samples.

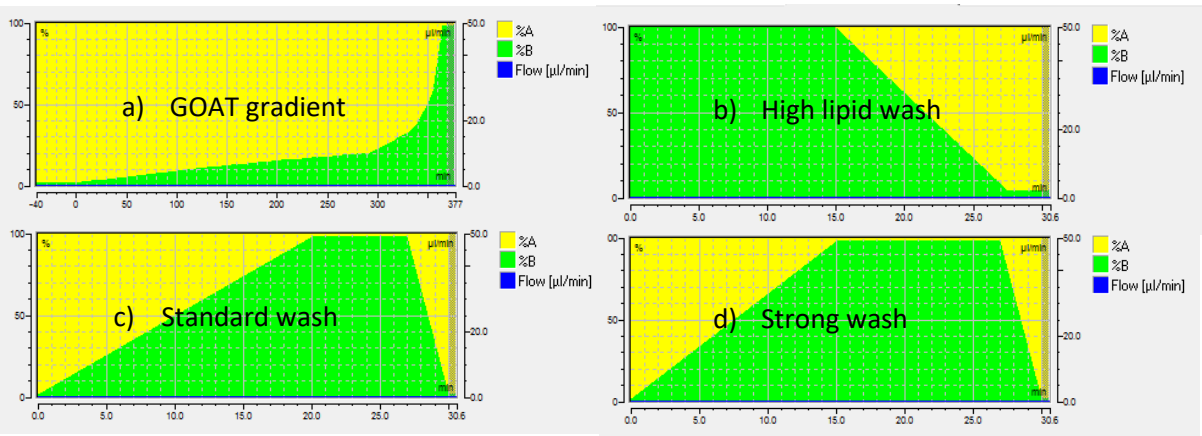

Figure 3-1 A selection of gradients used for LC-MS² analysis and column cleaning. The 100% max value on the y-axis corresponds to an 80% ACN solution. a) The GOAT gradient is an optimisation to spread the data evenly across a run. b) a high %B wash employed in the final sample processing to ensure lipids were removed from the column prior to starting a new run. c) a standard linear wash gradient. d) A stronger wash gradient.

3.10.1 Data analysis 1: Protein ID

Mass spectra were analysed with both Sequest HT and Mascot search methods using Proteome Discoverer 2.1 (Thermofisher) against the entire Uniprot human proteome database (reviewed 07/09/2017). To aid in comparability between the data generated in this thesis and previous data collected by our lab group, an older Uniprot review was used. Parameters were set to a maximum of 2 missed cleavages with peptide lengths ranging from 5 to 144 amino acids selected. A precursor mass tolerance of 10 ppm and fragment mass tolerance of 0.8 Da were allowed. Modifications were as follows – Static: carbamidomethylation and dynamic: oxidation (methionine) and carbamylation (both N-terminal and at lysine)

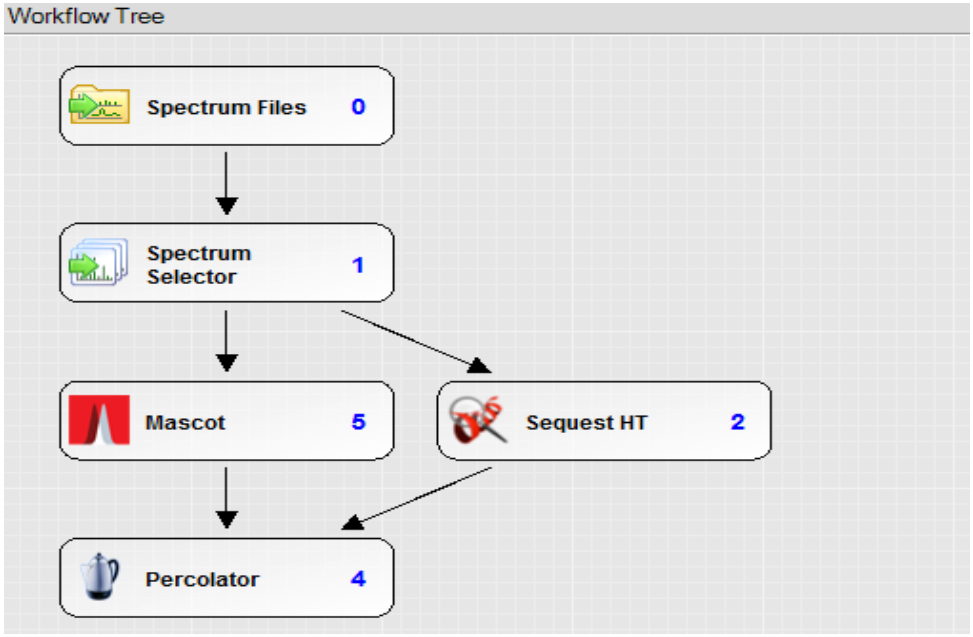

Figure 3-2 The Proteome Discoverer workflow showing sequence of nodes/modules used to analyse the RAW files from the LC-MS/MS. Static and dynamic modifications were set individually in Mascot and Sequest HT.

3.10.2 Data analysis 2: Protein quantification

Proteome Discoverer output files were then loaded into Scaffold Q+ (4.4.8) proteomics software for quantification analysis. Technical replicates were combined using MuDPIT processing (Kislinger, Gramolini, MacLennan, & Emili, 2005) and searches were again carried out against the Uniprot human proteome database (downloaded 07/08/2017). Protein abundance was quantified using the total TIC analysis method. Protein FDR thresholds were set to 1.0% and a peptide threshold of 0.1% FDR with proteins requiring at least 2 unique peptides to be identified. A protein abundance change, with a significance value less than 0.05 was considered significant.

The software converts the raw sequence files into potential peptide sequences. The peptide validator confirms whether the spectral data corresponds to a valid peptide. From this point, peptide sequences are matched against the Uniprot human proteome database for matches to defined protein sequences. The protein scorer assigns a quality score of the peptide sequence aligned with a known protein. Statistical due diligence from the FDR validator deals with false positives.

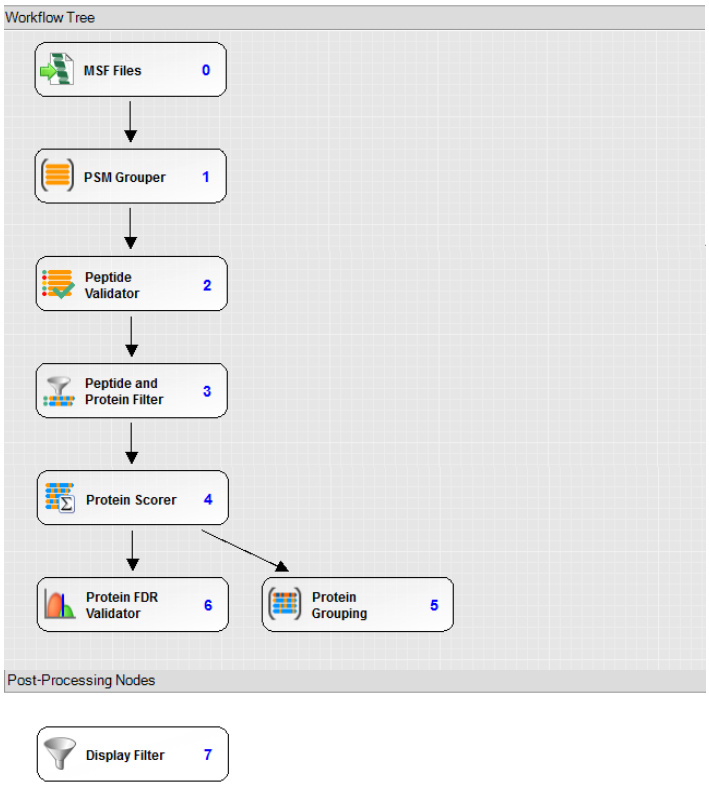

Figure 3-3 The processing workflow used to convert raw spectral data into peptide matches and ultimately to align sequences to known proteins to identify proteins from the spectral data. There are multiple nodes/modules used to perform statistics and validate findings

3.10.3 Analysis of proteome responses

Lists of proteins that changed in abundance to each treatment determined in Scaffold were compiled. The list of increasing, decreasing or combined change proteins were separately analysed for gene ontological (molecular function, cellular component, and biological process), pathway (KEGG and Reactome), and protein complexes (CORUM) enrichments through G:profiler (Reimand et al., 2016). Further analysis of clusters of proteins which had previously been found to be co-expressed was undertaken in STRING (Szklarczyk et al., 2019).

3.11 Gprofiler and STRING analysis pipeline

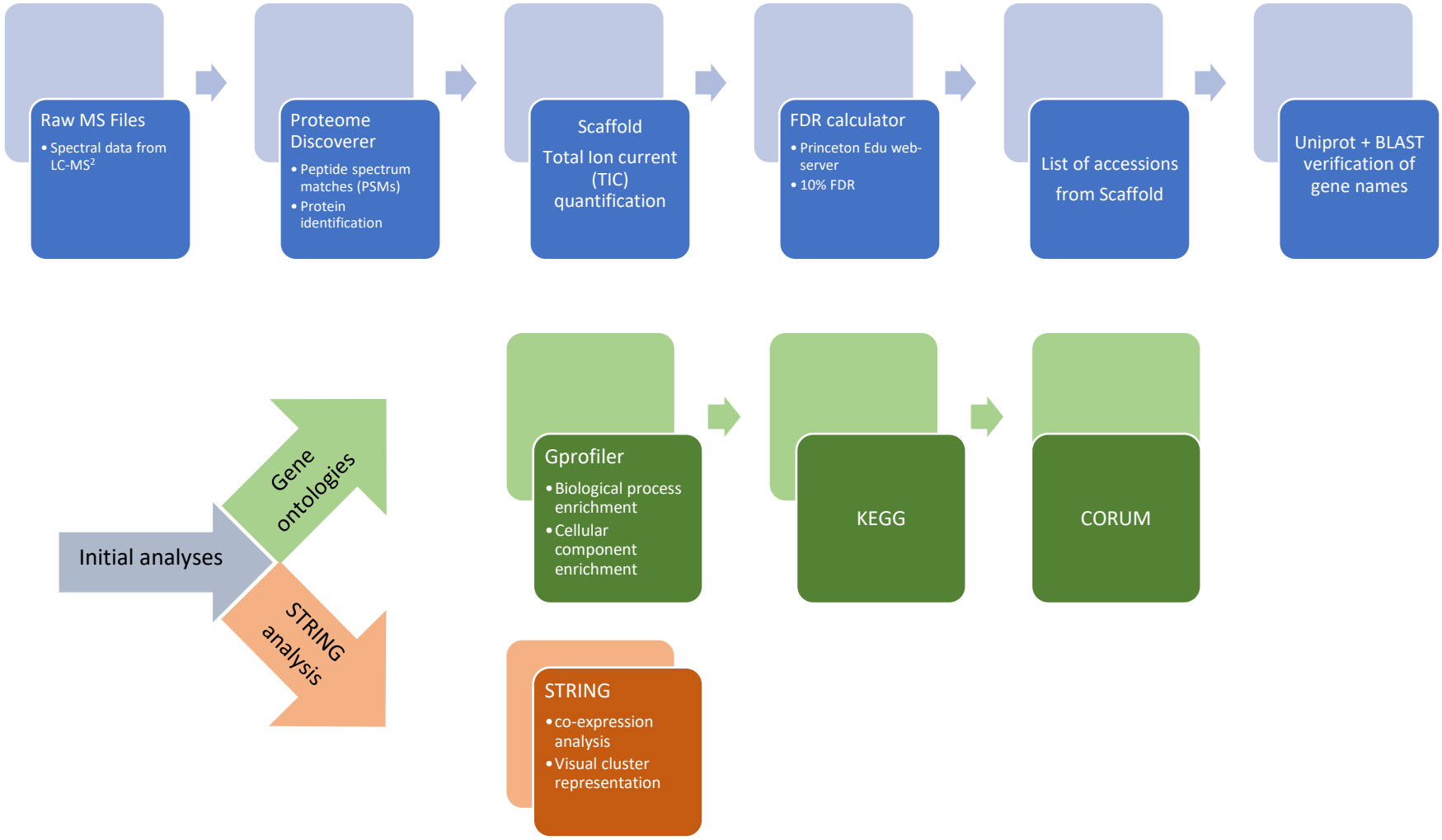

4 Results

4.1 IC_{10} and IC_1 treatment data

One main objective of this project is to mimic the low-doses (IC_{10} and IC_1) of drug used in a previous proteomics experiments using pateamine A. Obtaining growth inhibitory concentration (IC) data was achieved via MTT assay and non-linear regression analyses on data displayed in Figure 4-1, Figure 4-2, Figure 4-3, Figure 4-4, Figure 4-5, Figure 4-6, Figure 4-7. The MTT assays for ribavirin and cycloheximide generate excellent dose response curves in both cell lines, a key difference is the HT29 cell line not completely ceasing metabolism in response to treatment with the curves reaching their asymptotes well before zero. The 4E1RCat assay data displayed for the HT29 cell line demonstrate the impracticality of using a compound with low solubility and antiproliferative capacity. Below is a table containing the IC_{50}, IC_{10} and IC_1 data in HT29 and HL60 cells for the control protein synthesis inhibitor cycloheximide (CHX), the eIF4E inhibitors ribavirin (RBV) and 4E1RCat as well as for the vehicle, dimethyl sulfoxide (DMSO) displayed in % (v/v). A minimum of three biological replicates were used to obtain IC data for all drugs. The vehicle dose response data was done to ensure that the inhibitory effects of the vehicle were well established. For CHX and RBV treatment concentrations, the IC_{10} and IC_1 values did not include the effects of DMSO as the vehicle is diluted to beneath biological significance. For 4E1RCat this is not the case; the IC_{10} concentration was hard to establish in both cell lines, in this case the top dose of 40 µM was used as the IC_{10} concentration in both cell lines, indicated by a * in the table below.

*Table 1 Growth inhibitory concentration (IC) data at 3 levels, the IC_{10} values were the values used for further treatments. *4E1RCat: this compound was not sufficiently active to generate a full growth inhibition curve, and so IC values could not be modelled. The highest concentration used (40 µM) gave a growth reduction equivalent to the 10% growth reduction seen with other treatments. Displayed in brackets beneath the IC vlaues are the 95% confidence intervals. Note that curve fitting was not possible with all of the data and in some cases it was not possible to generate IC values in Prism despite having curves that superficially appeared model-able.*

Drug	***IC_1***		***IC_{10}***		***IC_{50}***	
	HT29	***HL60***	***HT29***	***HL60***	***HT29***	***HL60***
Cycloheximide (µM)	**0.004** (0.001 to 0.019)	**0.005** (0.002 to 0.0178)	**0.038** (0.020 to 0.071)	**0.048** (0.025 to 0.088)	**0.305** (0.226 to 0.412)	**0.349** (0.259 to 0.471)
Ribavirin (µM)	Not converged	Not converged	**11.9** (5.03 to 28.3)	**10.9** (5.15 to 22.9)	**81.4** (35.7 to 185)	**68.3** (39.1 to 119)
4E1RCat* (µM)	n/a	n/a	***40**	***40**	n/a	n/a
DMSO (%)	Not converged	**0.621** (0.421 to 0.917)	**0.390** (0.293 to 0.518)	**1.52** (1.31 to 1.76)	**1.46** (1.11 to 1.93)	**3.45** (2.87 to 4.15)

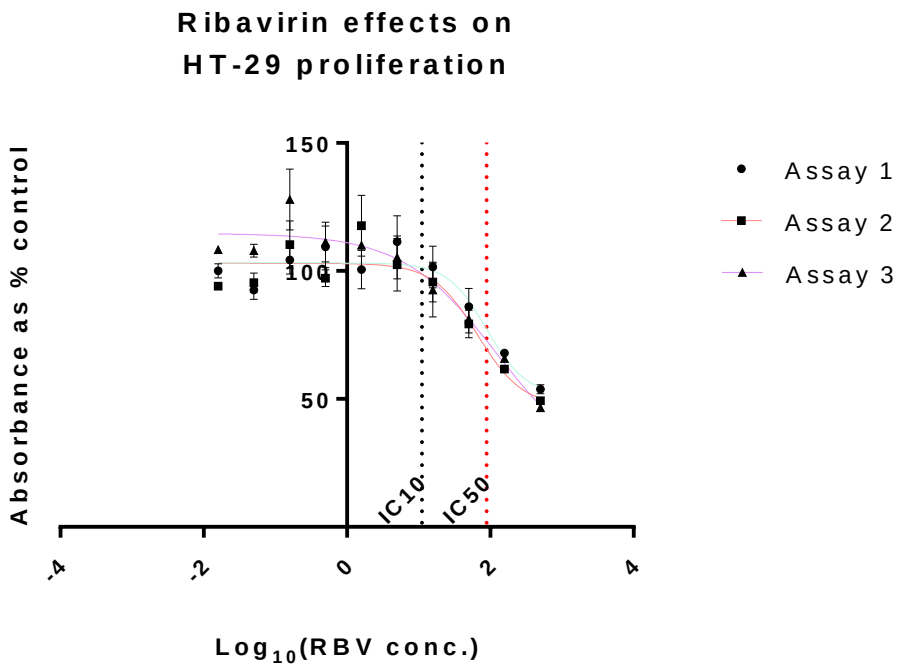

Figure 4-1 Absorbance changes reflect metabolic activity revealed by MTT treatment of 10^5 cells treated with increasing concentrations of ribavirin, with maximum inhibitor concentration limited to comfortably within the limit of solubility, with no more than 1% DMSO used in any dilution. Shown are the effects of ribavirin treatment on HT29 cell proliferation, graph generated in Prism. Note the failure to drop to total growth inhibition is not unusual in the HT29 cell line.

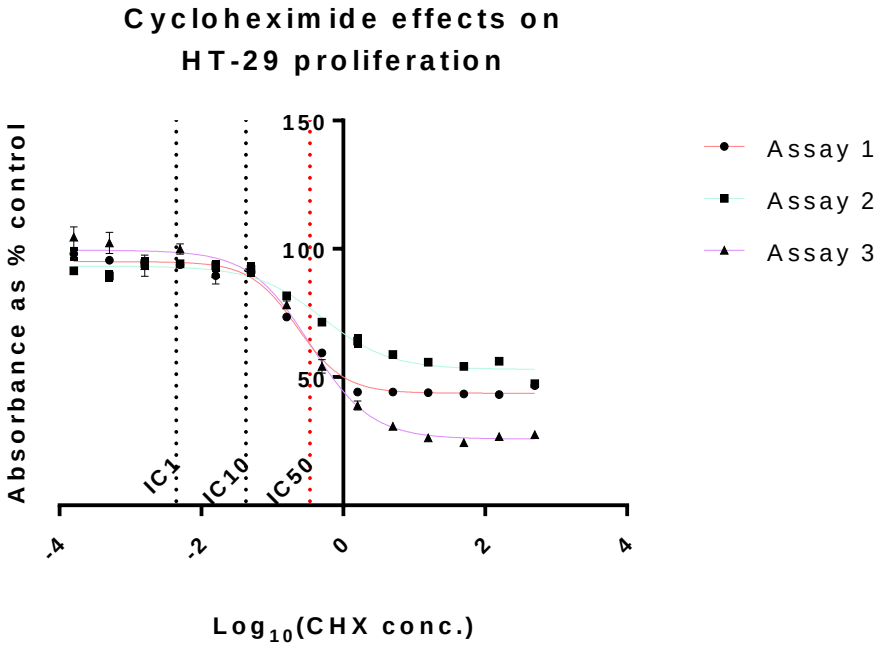

Figure 4-2 Absorbance changes reflect metabolic activity revealed by MTT treatment of 10^5 cells treated with increasing concentrations of cycloheximide, no more than 1% DMSO was used in any dilution. Shown are the effects of cycloheximide treatment on HT29 cell, graph generated in Prism.

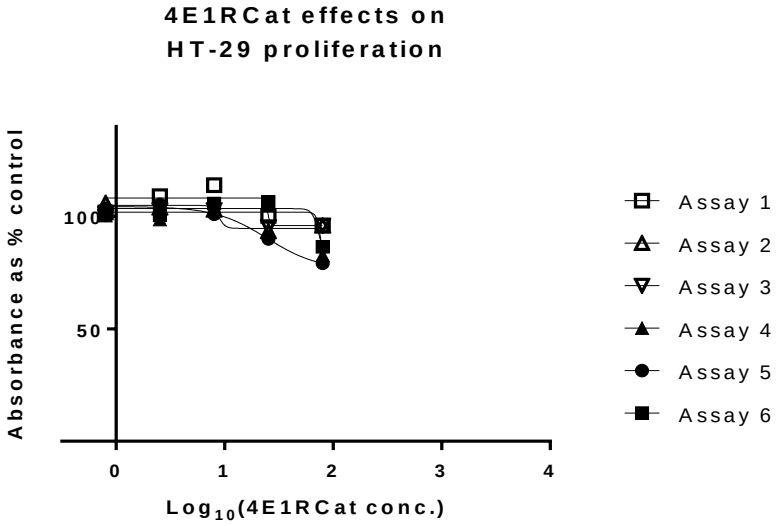

Figure 4-3 Absorbance changes reflect metabolic activity revealed by MTT treatment of 10^5 cells treated with increasing concentrations of 4E1RCat, with maximum inhibitor concentration limited by 4E1RCat solubility, with no more than 1% DMSO used in any dilution. Shown are the effects of 4E1RCat treatment on HT29 cell proliferation, graph generated in Prism. The DMSO vehicle at 1% v/v is likely to be partially contributing to the effects seen at the top dose of 40 µM.

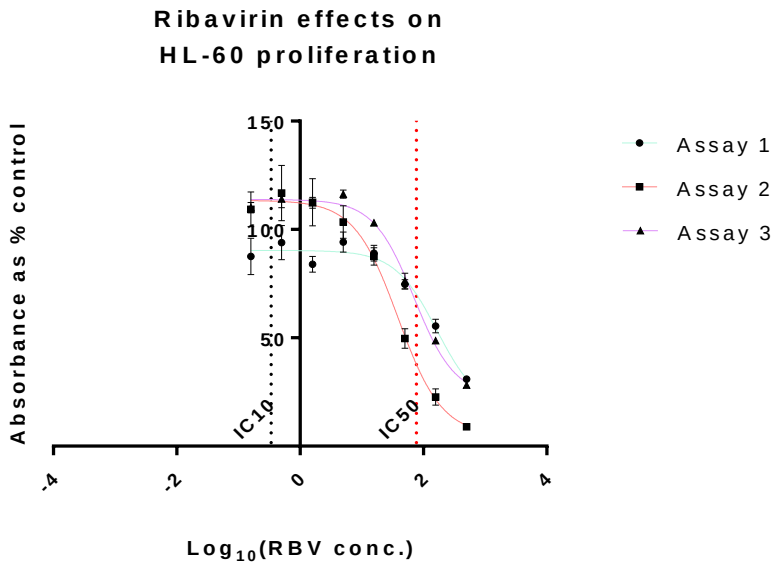

Figure 4-4 Absorbance changes reflect metabolic activity revealed by MTT treatment of 10^5 cells treated with increasing concentrations of ribavirin, with maximum inhibitor concentration limited to comfortably within the limit of solubility, with no more than 1% DMSO used in any dilution. Shown are the effects of ribavirin treatment on HL60 cell proliferation, graph generated in Prism. Note the drop to total growth inhibition is more noticeable in HL60 cells, presumably further increasing the ribavirin concentration would lead to total growth inhibition.

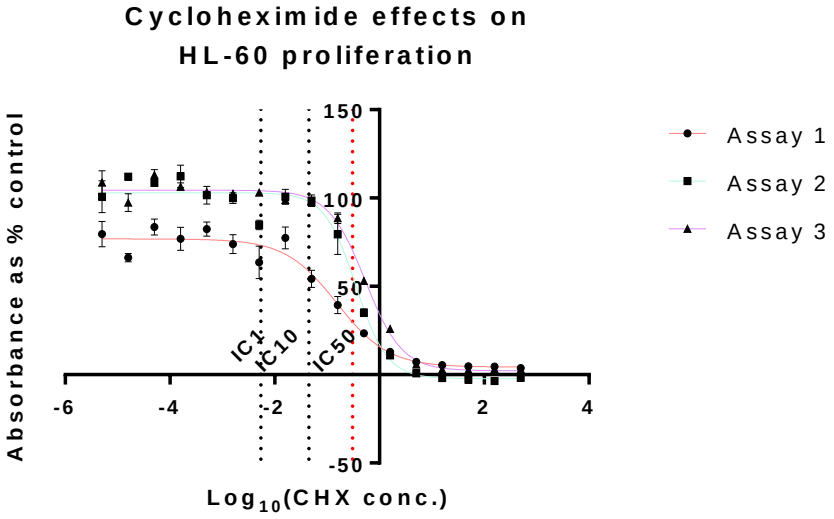

Figure 4-5 Absorbance changes reflect metabolic activity revealed by MTT treatment of 10^5 cells treated with increasing concentrations of cycloheximide, no more than 1% DMSO was used in any dilution. Shown are the effects of cycloheximide treatment on HL60 cell proliferation, graph generated in Prism. Note the drop to total growth inhibition.

4.2 Effects of DMSO

To establish the biologically relevant anti-proliferative effects of DMSO in the cell lines used in this project, MTT assays were used to generate a dose response between DMSO % in solution and proliferation. These graphs are shown below. The minimum of 3 biological replicates rule was waived as this was exploratory and was done partly out of curiosity to ensure that the effects of the vehicle on cell lines was well established. This became useful when it became apparent that a calculation error had occurred that established that the top dose of each drug in the MTT assays corresponded to 1% DMSO which is slightly above the well-accepted 0.5% DMSO cut-off.

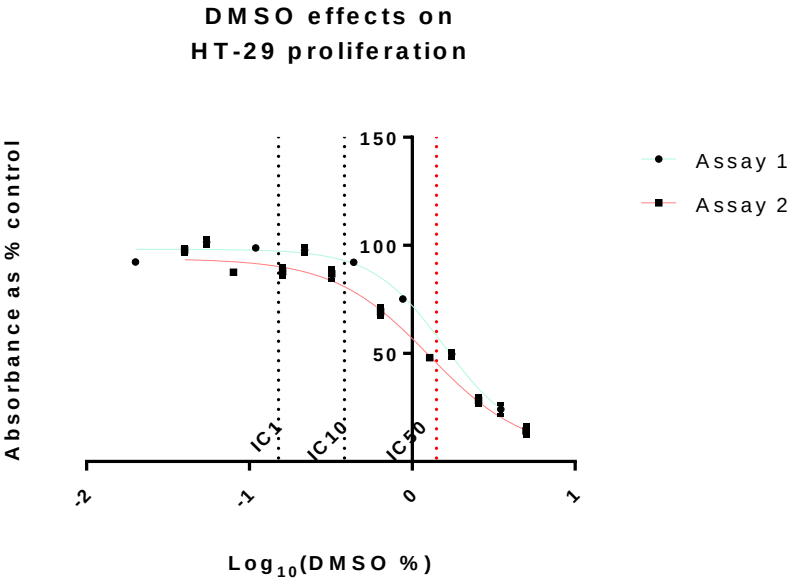

Figure 4-6 Effects of DMSO on HT29 cell proliferation, graph generated in Prism.

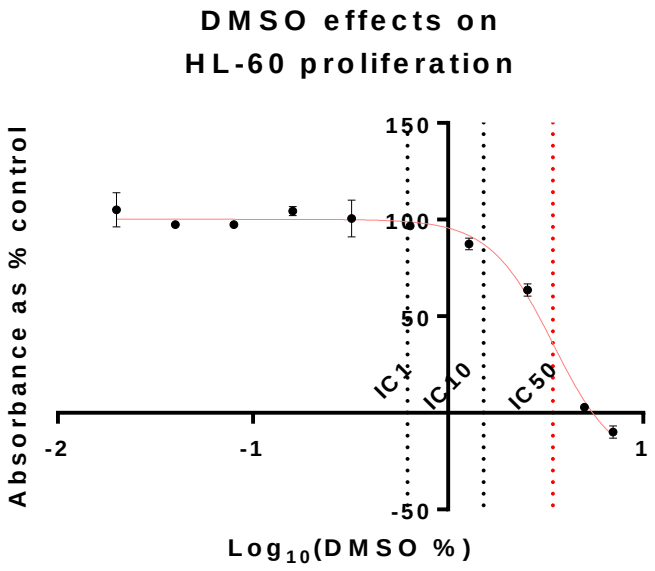

Figure 4-7 Effects of DMSO on HL60 cell proliferation, graph generated in Prism.

4.3 PEG contaminant detection by MALDI-TOF

Polyethylene glycol (PEG) is a polyether compound with an array of uses from medicine to plastics to molecular biology. It is commonly used as a plasticiser to change the thermal and mechanical properties of plastics to increase their pliability. Among its other uses, PEG is used in non-ionic detergents, often chemically added to the detergent molecule to increase its capacity to interact with water. In the mass spectrometry setting, PEG has the capacity to suppress ionisation of an analyte by competing for charge and lowering the capacity to generate peptide fragments, thus lowering the sensitivity of the analysis. Early in the course of this thesis it was discovered that PEG was present in test samples run on the LC-MS. A set of experiments were conducted to determine the source of PEG contamination. There were two expected sources of PEG contamination, the plastics used over the course of the experiment, and the non-ionic detergent Triton X-100 present in the RIPA buffer. Matrix assisted laser desorption/ionization – time of flight (MALDI-TOF) was used briefly in this thesis to detect PEG contamination. Due to most of the protein samples being dissolved in urea, and containing high salt concentrations the use of the maximum laser ablation setting was often necessary. The goal of this analysis was to achieve spectra containing peptide peaks without the characteristic series of peaks seen with PEG. These peaks differ by 44 mass units, and strongly resemble a statistical representation of a normal distribution. Figure 4-8, Figure 4-9 demonstrate spectra with only matrix peaks from the CHCA and peptide peaks respectively, these are placed here to give the reader an idea of what to expect from a MALDI-TOF spectra. (Figure 4-10, Figure 4-11, Figure 4-15, Figure 4-16) were all from samples processed using RIPA buffer and were evidence that RIPA buffer was the likely source of PEG. This was confirmed by samples processed using urea demonstrated in several of the figures below (Figure 4-10, Figure 4-11, Figure 4-15, Figure 4-16), these samples are free of PEG contamination and have clean peptide peaks free from the intrusion of the visually distinct PEG spectral motif

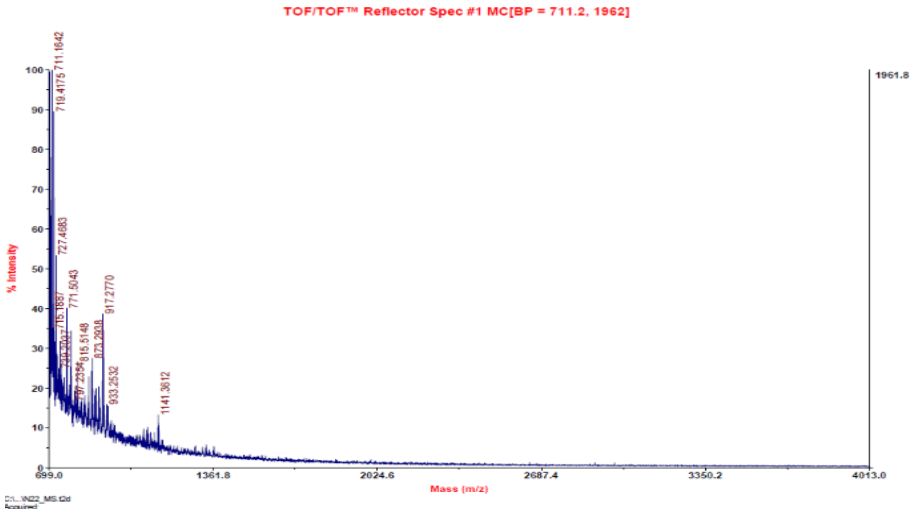

Figure 4-8 Spectra using maximum laser intensity where nothing of interest is visible, a few matrix peaks are visible near the Y-axis.

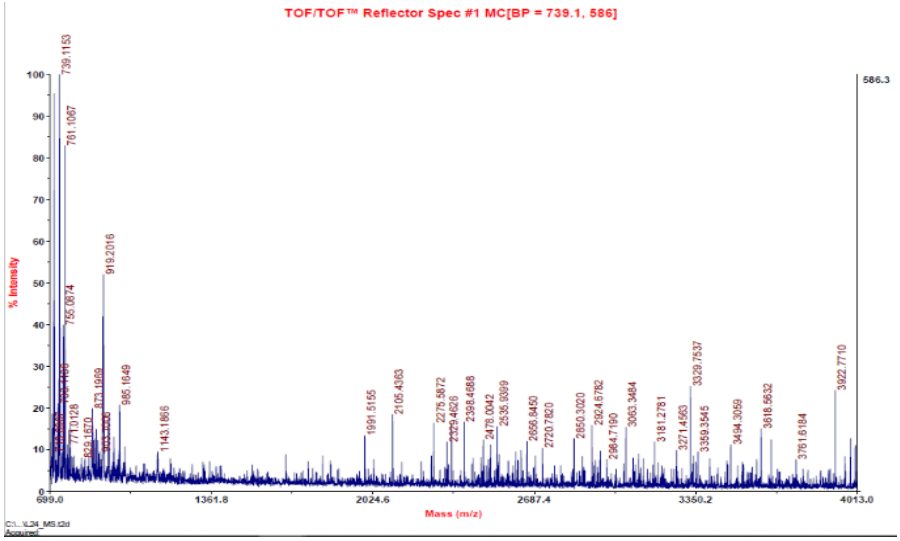

Figure 4-9 A spectrum showing matrix peaks near the Y-axis and demonstrating visible peptide peaks.

Pre-digestion, peptides in 2 M urea were mixed with CHCA at a 1:10 ratio. Laser ablation at the maximum of 7000 units was used. There was a noticeable decrease in PEG between the two methods of precipitation (Figure 4-10, Figure 4-11), however still abundant at concentrations too high to run on the LC-MS.

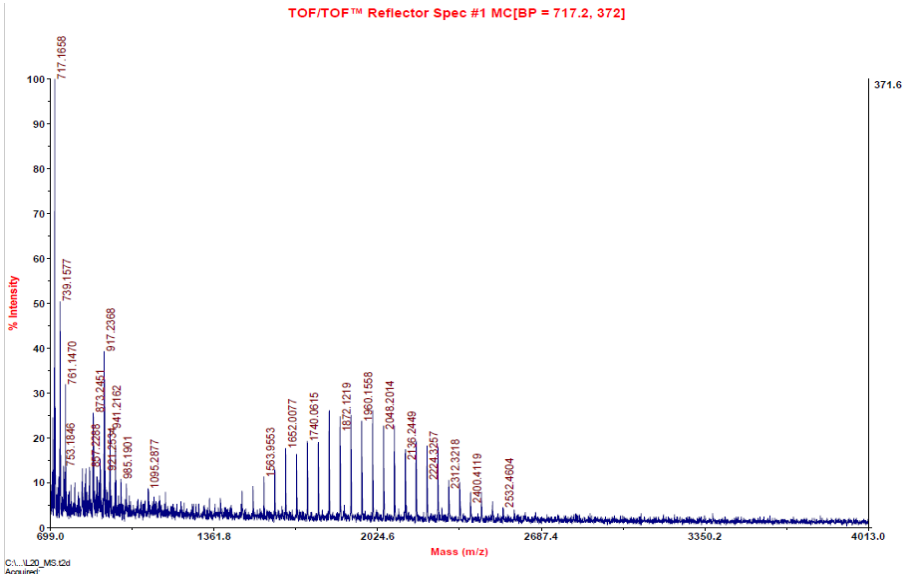

Figure 4-10 MALDI-MS/MS spectrum of a RIPA buffer precipitated PEG-contaminated sample following chloroform-methanol precipitation.

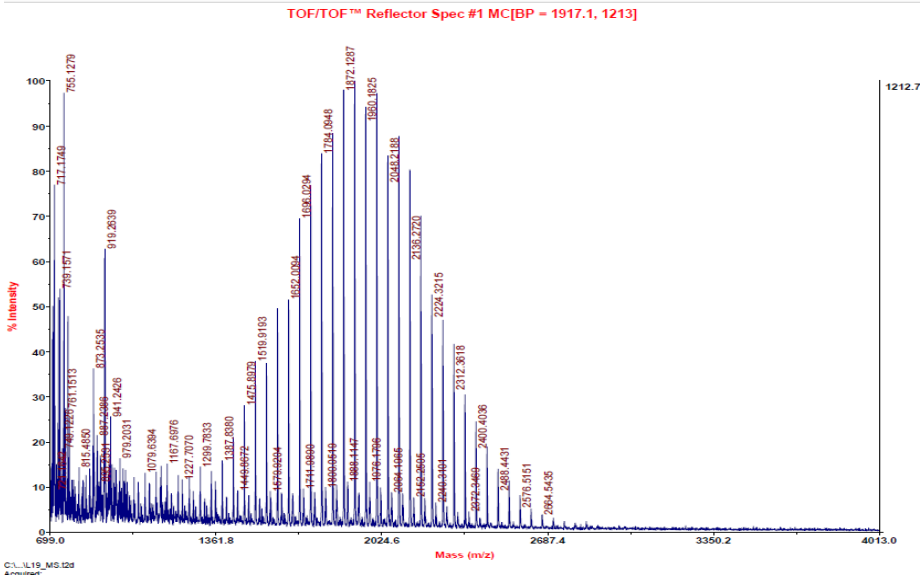

Figure 4-11 MALDI-MS/MS spectrum from a RIPA buffer precipitated sample showing particularly prominent PEG contamination in an acetone precipitated sample.

The figures below are post-digestion, ZipTipped peptides mixed with CHCA at a 1:10 ratio, Polyethylene glycol (PEG) is absent. They are a good demonstration of the spectrum expected from a complex protein sample without the presence of PEG.

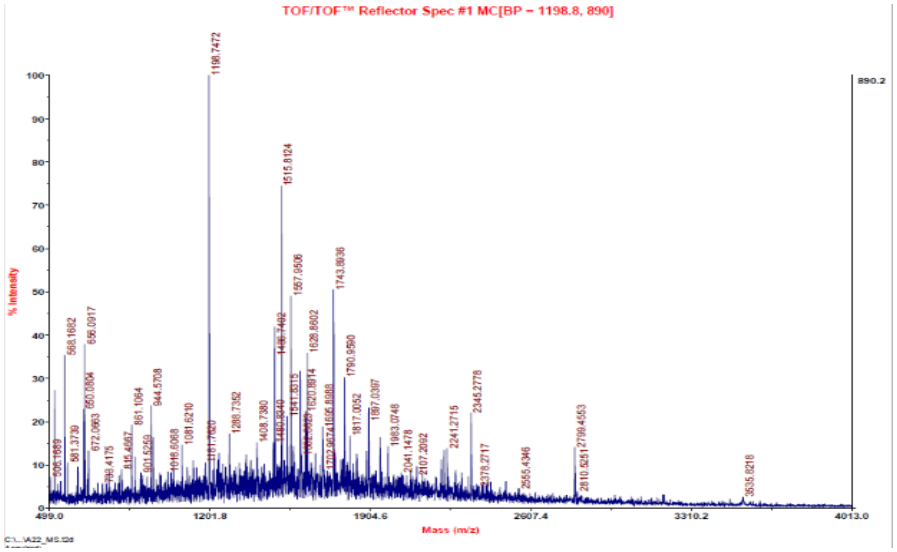

Figure 4-12 MALDI-MS/MS spectrum of a typical peptide sample (sample A22).

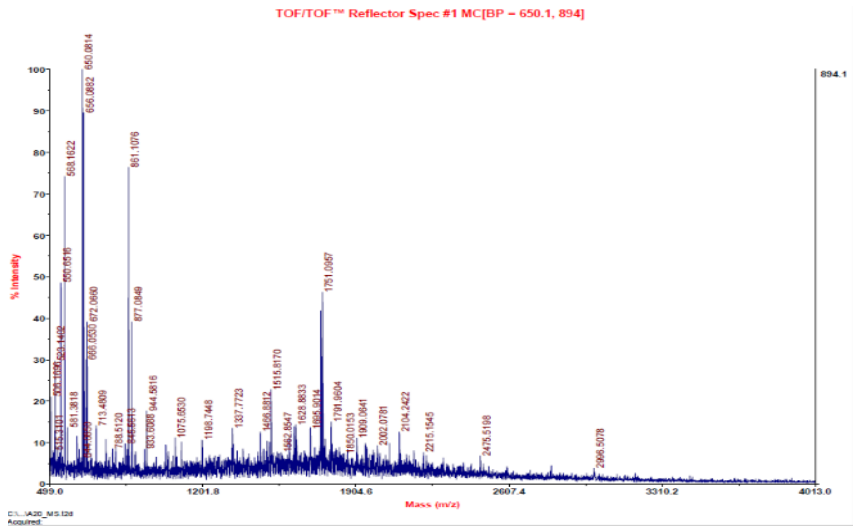

Figure 4-13 MALDI-MS/MS spectrum of a typical peptide sample (Sample A20).

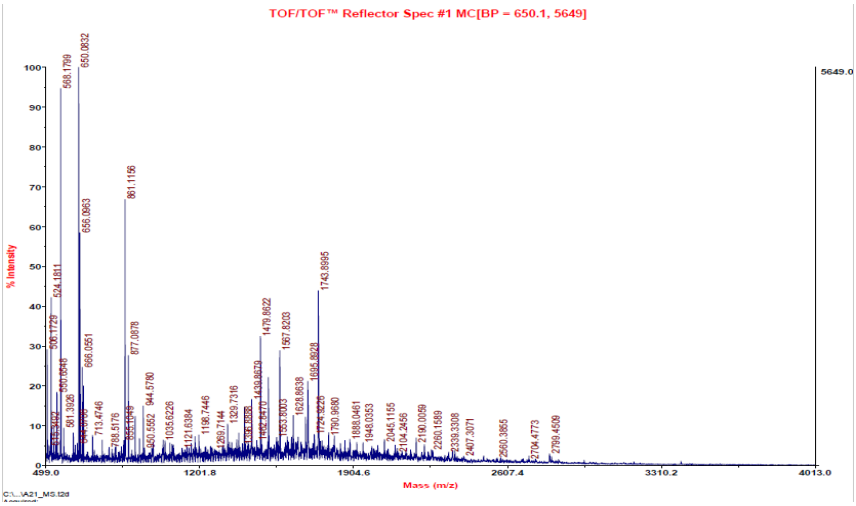

Figure 4-14 MALDI-MS/MS spectrum of a typical peptide sample (Sample A21).

The figures below show urea lysed, post-digestion, ZipTipped peptides mixed with CHCA at a 1:10 ratio. This is included as an example of polyethylene glycol that may come from another source, such as autoclaved pipette tips. Note the low abundance of PEG in comparison to peaks associated with the MS signal of the CHCA matrix on the left side of Figure 4-15.

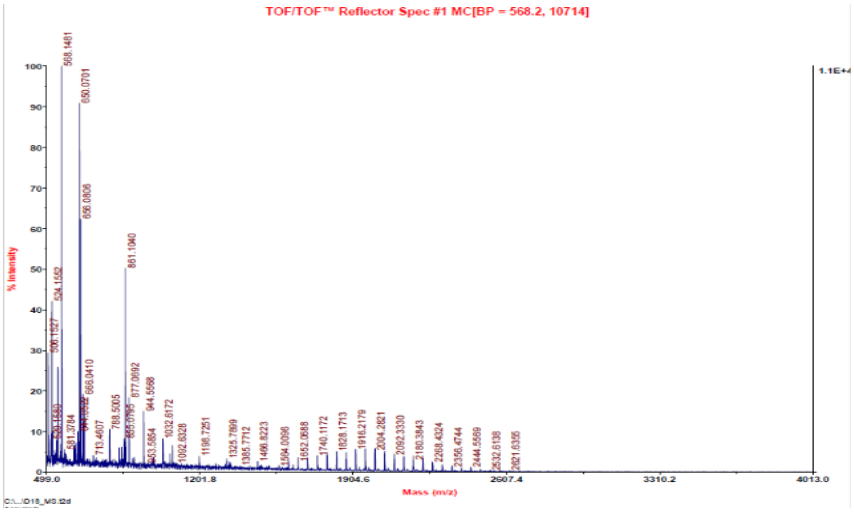

Figure 4-15 MALDI-MS/MS spectrum of a peptide sample (sample D18) with low peptide and PEG abundance in comparison to the matrix peaks on the far left.

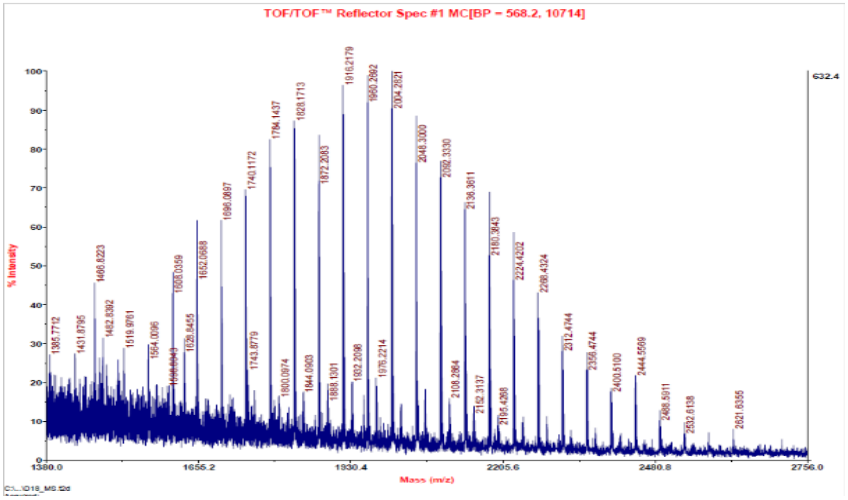

Figure 4-16 An expanded view of the PEG-containing region of the MALDI-MS/MS spectrum of sample D18.

4.4 A side-by-side comparison of protein precipitation methods

Side-by-side comparisons were made using the chloroform-methanol and acetone methods using known-protein standards (Bovine serum albumin) and HT29 raw-lysates to compare the efficiency and reproducibility of the two methods. The chloroform-methanol method produces an almost 'fluffy' pellet, which is useful for redissolving precipitated proteins. However, if sample proteins are not visible by eye, dislodging the pellet when removing the organic phase is a quick way to lose sample without realising it. As a result, although the chloroform-methanol method gave higher recovery in most cases, it occasionally lead to very low protein recovery. In contrast, the acetone precipitation method proved effective and robust and was adopted throughout this thesis.

4.5 Assessing the effectiveness of lysis solutions without non-ionic detergents

A core component of this thesis was the DC Protein Assay, it was used extensively to quantify protein concentrations (Figure 4-17). Although the assay recommends working in the linear range of the assay, it was noted that the working range of the assay was inconveniently small, in response to this a larger range of concentrations were used and a non-linear curve fitted.

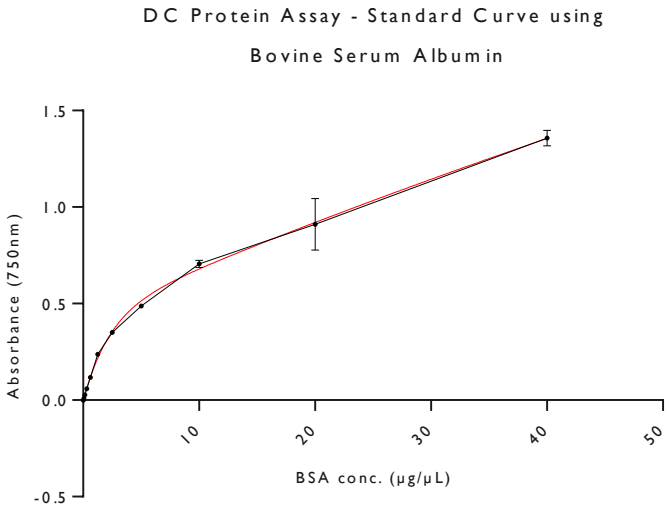

Figure 4-17 A standard curve of bovine serum albumin (BSA) was constructed using the DC protein assay, a portion of the graph between 200-1500µg/mL has a direct linear relationship between absorbance and BSA concentration. A non-linear regression is fitted to the curve.

To eliminate PEG contamination alternative buffers without non-ionic detergent (e.g. Triton-X100, NP40) were explored for protein extraction efficiency. $1x10^6$ cells were lysed using each buffer. Analysis was done using Prism, a non-linear 2-phase decay function was used to model the above standard curve to allow calculation of the protein concentrations in each sample.

Table 2 Lysis buffer versus protein concentration for several lysis methods. All buffers besides RIPA buffer were flash frozen at -80 °C three times to aid in the lysis process.

Lysis condition ($1x10^6$ cells)	**Protein concentration (µg/µL)**	**Efficiency relative to RIPA buffer (%)**	**Total extracted protein (µg)**
RIPA lysis buffer	2.10	100	420
8M urea	1.39	66.2	278
8M urea (replicate)	1.36	64.8	272
8M urea + 5% SDC	0.87	41.4	174
dH_20 + protease inhibitor	0.45	21.4	90

Although RIPA buffer was ~1/3 more effective than 8 M urea, it was significantly better than 8 M urea containing SDC and distilled water with protease inhibitor.

4.6 Mass spectrometry optimisation – chromatograms

Early attempts to generate spectra were largely unsuccessful, it was noted that samples from the earliest attempts were very low in protein content, comparable to the spectra for unrelated samples shown in figures Figure 4-18 and Figure 4-19. These have very few peaks in the middle of the gradient where most peptides would cluster and slightly more peaks corresponding to hydrophobic molecules, more than likely lipids. The change in the chromatograms between the exosome derived proteins and the proteins derived from a whole cell lysate with a comparatively high protein abundance is almost directly related to the protein concentration of the sample loaded on the MS. The exosome data show low protein abundances, toward the lower end of detection in the DC Protein Assay. It is used to demonstrate the relationship between loaded protein and the resulting chromatograms. Although visually assessing a chromatogram is not a reliable way of predicting the number of protein IDs generated in Proteome Discoverer, it is generally possible to determine the characteristic chromatograms of a low protein abundance sample (Figure 4-18, Figure 4-19). Note that the lysis method used in some samples of this section is a variation of the 8 M urea lysis solution containing 6 M urea and 2 M thiourea. This method was discontinued as the thiourea would crystallize at low temperatures which was inconvenient for later centrifugation steps.

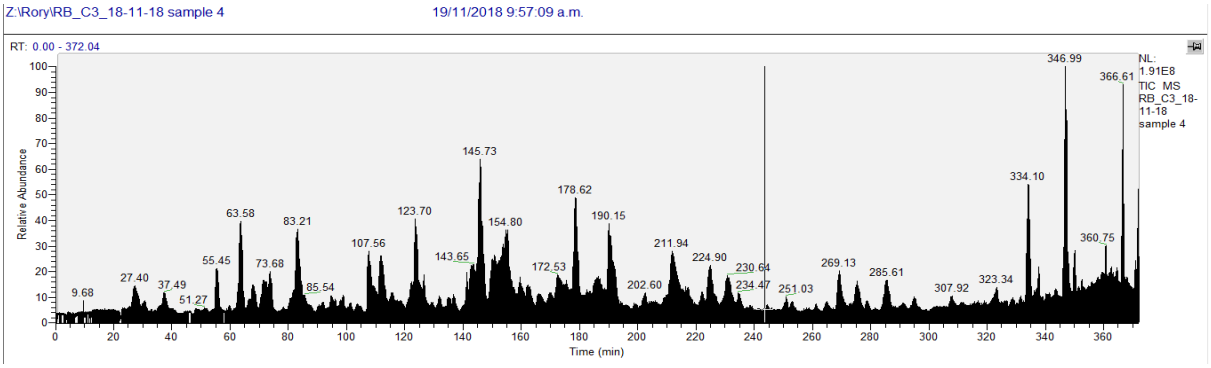

Figure 4-18 LC-MS/MS total ion count chromatogram of exosomes lysed using 6M urea + 2M thiourea. Number of recognised proteins: <50. The sample was obtained using 8 M urea lysis to replace the RIPA lysis buffer, exosomes prepared by Deanna Dupre. included to show the resulting spectra when peptide concentration is insufficient.

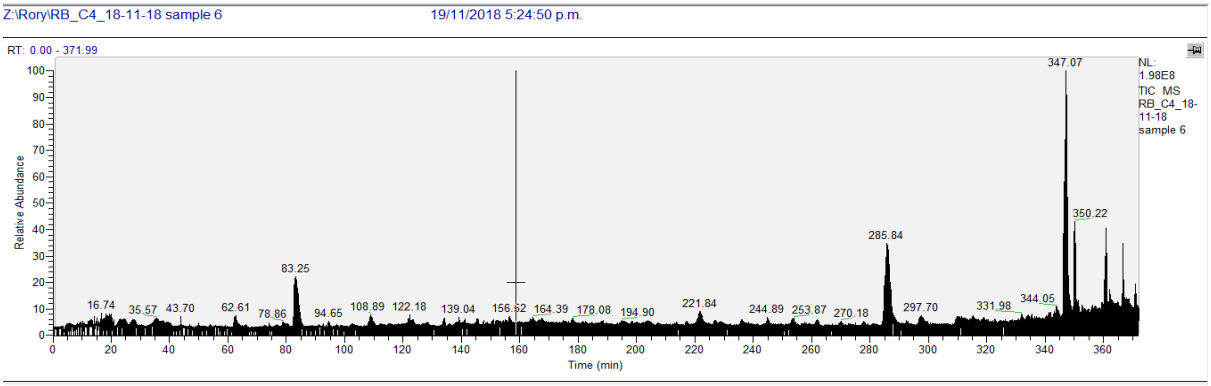

Figure 4-19 LC-MS/MS total ion count chromatogram of exosomes lysed using 6M urea + 2M thiourea. Number of recognised proteins: <10. The protocol I used to replace the RIPA lysis buffer, exosomes prepared by Deanna Dupre included to show the resulting spectra when peptide concentration is insufficient.

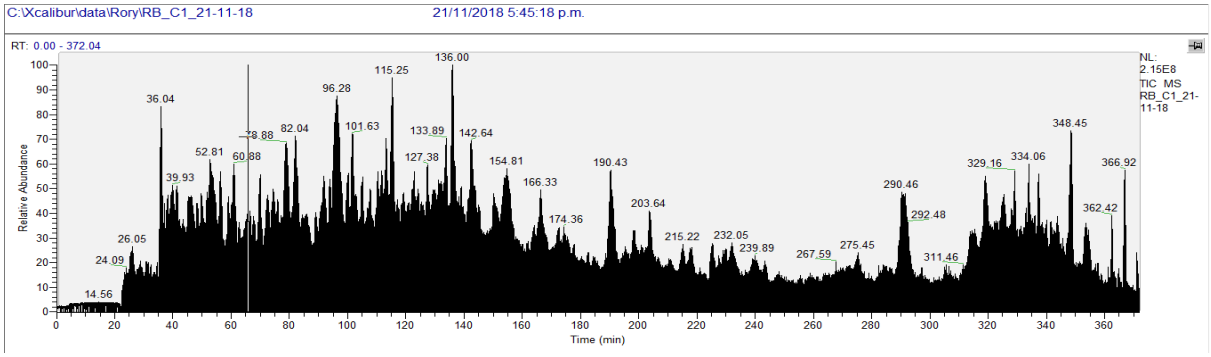

Figure 4-21 LC-MS/MS total ion count chromatogram of HT29 cells lysed using 6M urea + 2M thiourea. Number of proteins identified with a high level of confidence in proteome discoverer: 967

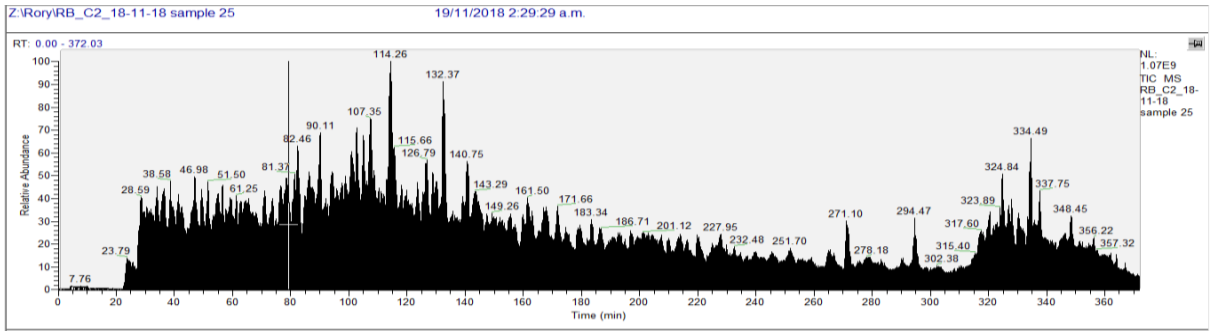

Figure 4-20 LC-MS/MS total ion count chromatogram of HT29 cells lysed using 6M urea + 2M thiourea. Number of proteins identified with a high level of confidence in proteome discoverer: 1234. Demonstrating the effectiveness of my digestion and processing protocol.

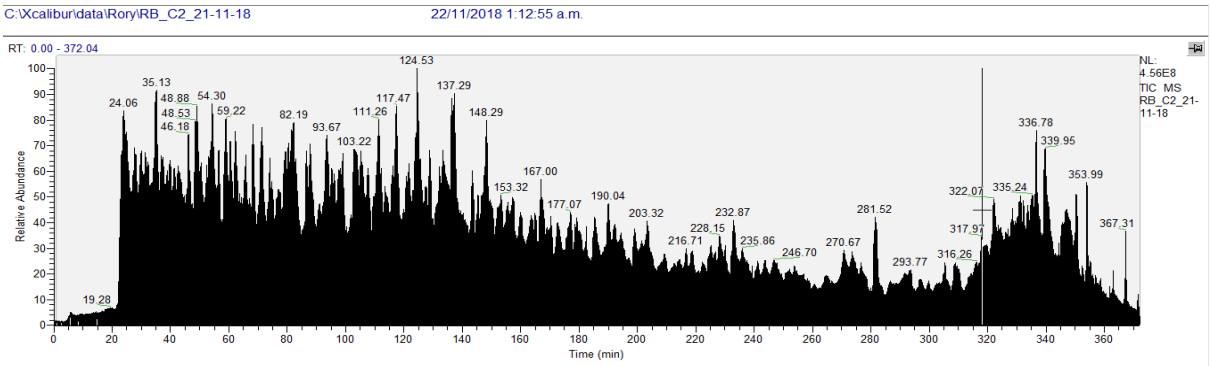

Figure 4-22 LC-MS/MS total ion count chromatogram of HT29 cells lysed using 6M urea + 2M thiourea. Number of proteins identified with a high level of confidence in proteome discoverer: 1286

4.7 Mass spectrometry results

It will become apparent in the MS results that data was only collected in the HT29 cell line. This was due in part to the difficulties encountered with culturing the HL60 cells and in part to availability of the mass spectrometer as it is a shared instrument with high usage and was unavailable for large periods of time whilst under repair. A mirror experiment was set up in the HL60 cell line and the cells processed to the point where they could be analysed on the mass spectrometer, however, in the interest of time and availability of the instrument, the HT29 cell data was the focus of the MS analyses.First Set of MS results: HT29 cells - 4E1RCat (3.2 µM) and DMSO at (0.4% v/v)
This set of data was not used to evaluate the effects of 4E1Rcat. It is provided as example of the effects of the protein loading concentration (total protein) on the number of protein hits in Proteome Discoverer. There is a correlation between total protein loaded and the number of proteins identified. In this preliminary experiment, a calculation error meant that the appropriate amount of 4E1RCat was not used, the target concentration of 40 µM was missed and cells were instead treated at 3.2 µM. The matching DMSO control data was obtained at the IC_{10} of DMSO, rather than at the DMSO concentration that corresponded to the 4E1RCat treatment. 8M Urea (instead of 6M urea + 2M thiourea) was used as the lysis buffer. Membranes were not pelleted after cell lysis, protein precipitation occurred in acetone with membranes still present, protein concentrations post-precipitation were highly variable.

Table 3: More proteins are identified in Proteome Discoverer in response to higher total protein run on the MS. Displayed are: Samples 1-3: DMSO (0.4% v/v), 4-6: 4E1RCat (3.2 µM)

Sample #	A_{750} (averaged triplicate)	Protein conc. (µg/µL)	Total protein (µg)	Protein IDs (Replicate 1; 2)
Control - 1	0.224	0.8	26.5	834; 783
Control - 2	0.267	1.2	41.4	781; 786
Control - 3	0.231	0.8	28.5	926; 849
4E1RCat - 4	0.354	2.5	87.3	1211; 1182
4E1RCat - 5	0.293	1.5	52.8	1040; 1039
4E1RCat - 6	0.271	1.2	43.1	985; 959

Samples were reconstituted in a final volume of 110 µL of 0.1% formic acid. The protein yield was sampled post acetone precipitation, and large amounts of variability between samples was observed. The correlation between protein yield and the number of proteins identified in Proteome Discover influenced the methods used for later experiments. Samples for subsequent experiments that had low initial concentrations were normalised by reconstituting the sample in a lower volume, thus increasing the concentration of protein. The mass spectrometer uses 25 µL for each replicate, and two technical replicates was considered enough. Therefore between 60 and 110 µL, there is room to adjust sample volume to increase the consistency of protein identification.

4.7.1 Second set of MS results: HT29 cells - Untreated, CHX (0.043 µM) and RBV (11.1 µM)

Table 4: Normalising protein abundance to 100 µg of total protein run on the MS leads to a large improvement in the number of proteins identified in Proteome Discoverer. Displayed: 1-3: Untreated cells, 3-6: Cycloheximide (0.043 µM), 7-9: Ribavirin (11.1 µM)

HT29 Sample #	A_{750} (averaged triplicate)	Protein Conc. (µg/µL)	Total protein (µg)	Dilution factor	Normalised protein abundance (µg)	Protein IDs (Replicate 1; 2)
Control - 1	0.484	3.9	290.6	2.9	100	1209; 1137
Control - 2	0.457	3.3	250.7	2.5	100	1171; 1169
Control - 3	0.392	2.2	168.1	1.7	100	1362; 1246
CHX - 4	0.460	3.4	255.0	2.6	100	1315; 1209
CHX - 5	0.476	3.7	278.5	2.8	100	1010; 1100
CHX - 6	0.311	1.2	93.5	n/a	93.5	1291; 1226
RBV - 7	0.402	2.4	179.5	1.8	100	1106;1096
RBV - 8	0.376	2.0	151.0	1.5	100	1264;1121
RBV - 9	0.296	1.1	82.7	n/a	82.7	1291;1149

4.7.2 Third set of results: HT29 cells – DMSO control (1%) and 4E1RCat (40 µM)

This data was used for subsequent analysis, and replaced data obtained from the first set of MS results.

Table 5: Normalising protein abundance leads to a consistent improvement in the number of identified proteins. Displayed are: Samples 1-3: DMSO (1% v/v), 3-6: 4E1RCat (40 µM)

HT29 Sample #	A_{750} (averaged triplicate)	Protein Conc. (µg/µL)	Total protein (µg)	Dilution factor	Normalised protein abundance (µg)	Protein IDs (Replicate 1; 2)
Control - 1	0.309	1.6	123.0	1.2	100	1120; 1172
Control - 2	0.354	2.2	167.3	1.7	100	1389; 1242
Control - 3	0.333	1.9	145.6	1.5	100	1218; n/a
4E1RCat - 4	0.357	2.3	170.6	1.7	100	1200; n/a
4E1RCat - 5	0.344	2.1	156.8	1.6	100	1040; 1395
4E1RCat - 6	0.301	1.5	116.0	1.2	100	1235; 1122

4.8 Further analysis of MS data post-protein identification

After processing in Proteome Discoverer, data was moved into Scaffold and four treatment conditions were constructed and analysed. Comparisons were as follows: untreated controls against the cycloheximide (CHX) treatment, untreated controls against ribavirin (RBV), a 1% DMSO control against 4E1RCat and lastly untreated controls versus the 1% DMSO control, essentially a DMSO treatment condition.

4.8.1 Gene ontological enrichment analysis using G profiler

Global proteome changes were computed in Scaffold prior to GO analysis in the G profiler online software. Inclusion as a significant change was managed internally by the Scaffold software, which uses a decoy generation strategy to manage the FDR. No formal cut-off was applied with respect to protein abundance in terms of fold-changes. Despite this, on closer inspection the Scaffold software appears to have imposed cut-off boundaries, the lower threshold for an upregulated protein based on the four analyses run in Scaffold is a fold-change of > 1.1 and the lower threshold for a downregulated protein appeared to be capped at a fold change of > 0.0002.

Table 6 gene ontology enrichment by biological process (BP) and cellular component (CC). The molecular function (MF) GO domain was included in one analysis. The top 5 BP and CC are displayed, the intention of the selection process was to pick the top 5 unique processes, components and MF if applicable. If 5 unique processes did not exist, the nested ontology terms were included, despite the smaller ontology contributing to the enrichment seen in the larger ontology. Ontological enrichments are reported separately for proteins that increase in abundance (UPs) in response to the treatment, and those that go down (DOWNs). Ontology term name, adjusted p-values from G:profiler and the number of proteins observed to change in abundance that are assoicated with the ontology (intersection size) are reported.

Cycloheximide UPs			
source	term name	adjusted p value	intersection size
GO:BP	RNA splicing, via transesterification reactions with bulged adenosine as nucleophile	4.57×10^{-2}	6
GO:BP	mRNA splicing, via spliceosome	4.57×10^{-2}	6
GO:BP	RNA splicing, via transesterification reactions	4.80×10^{-2}	6
GO:CC	ribonucleoprotein complex	1.53×10^{-5}	11
GO:CC	catalytic step 2 spliceosome	6.10×10^{-5}	5
GO:CC	spliceosomal complex	8.82×10^{-5}	6

Cycloheximide DOWNs			
source	term name	adjusted p value	intersection size
GO:BP	regulation of protein catabolic process	1.07×10^{-4}	9
GO:BP	positive regulation of protein modification by small protein conjugation or removal	4.63×10^{-4}	6
GO:BP	regulation of protein modification by small protein conjugation or removal	6.19×10^{-4}	7
GO:BP	proteolysis involved in cellular protein catabolic process	2.20×10^{-3}	10
GO:BP	proteasome-mediated ubiquitin-dependent protein catabolic process	2.80×10^{-2}	7

GO:CC	proteasome complex	2.10×10^{-3}	4
GO:CC	endopeptidase complex	2.23×10^{-3}	4
GO:CC	peptidase complex	6.80×10^{-3}	4
GO:CC	ubiquitin conjugating enzyme complex	3.16×10^{-2}	2
GO:CC	MCM complex	4.81×10^{-2}	2

Ribavirin UPs			
source	term name	adjusted p value	intersection size
GO:BP	nuclear-transcribed mRNA catabolic process, nonsense-mediated decay	1.41×10^{-4}	7
GO:BP	SRP-dependent cotranslational protein targeting to membrane	7.72×10^{-4}	6
GO:BP	RNA catabolic process	1.46×10^{-3}	9
GO:BP	ribosome biogenesis	3.79×10^{-2}	7
GO:BP	maturation of LSU-rRNA	3.14×10^{-2}	3
GO:CC	ribonucleoprotein complex	2.81×10^{-8}	17
GO:CC	cytosolic ribosome	2.73×10^{-4}	6
GO:CC	nucleolus	3.71×10^{-4}	13
GO:CC	polysome	5.82×10^{-4}	5
GO:CC	cytosolic part	1.42×10^{-3}	7

Ribavirin DOWNs			
source	term name	adjusted p value	intersection size
GO:MF	cadherin binding involved in cell-cell adhesion	1.34×10^{-3}	3
GO:MF	cadherin binding	4.30×10^{-3}	6
GO:MF	cell-cell adhesion mediator activity	2.62×10^{-2}	3
GO:MF	cell adhesion mediator activity	4.30×10^{-2}	3
GO:MF	cell adhesion molecule binding	4.35×10^{-2}	6
GO:CC	cell-cell adherens junction	5.65×10^{-3}	4

GO:CC	adherens junction	3.22×10^{-2}	6
GO:CC	proteasome complex	3.30×10^{-2}	3
GO:CC	endopeptidase complex	3.45×10^{-2}	3
GO:CC	anchoring junction	3.74×10^{-2}	6

4E1RCat UPs			
source	term name	adjusted p value	intersection size
GO:BP	SRP-dependent cotranslational protein targeting to membrane	2.46×10^{-7}	7
GO:BP	nuclear-transcribed mRNA catabolic process, nonsense-mediated decay	1.34×10^{-6}	7
GO:BP	translational initiation	1.13×10^{-6}	8
GO:BP	heterocycle catabolic process	3.03×10^{-5}	10
GO:BP	ribosomal large subunit biogenesis	9.21×10^{-3}	4
GO:CC	cytosolic large ribosomal subunit	1.26×10^{-9}	7
GO:CC	large ribosomal subunit	2.16×10^{-9}	8
GO:CC	ribonucleoprotein complex	4.62×10^{-7}	12
GO:CC	cytosolic part	1.57×10^{-5}	7
GO:CC	polysomal ribosome	2.72×10^{-5}	4

4E1RCat DOWNs			
source	term name	adjusted p value	intersection size
GO:CC	nucleoid	1.48×10^{-3}	3
GO:CC	mitochondrial nucleoid	1.48×10^{-3}	3
GO:CC	nuclear replisome	4.27×10^{-2}	2

DMSO UPs source	term name	adjusted p value	intersection size
GO:BP	SRP-dependent cotranslational protein targeting to membrane	3.20×10^{-25}	24
GO:BP	translational initiation	7.82×10^{-20}	26
GO:BP	nuclear-transcribed mRNA catabolic process, nonsens x 10-mediated decay	1.71×10^{-22}	24
GO:BP	nuclear-transcribed mRNA catabolic process	1.19×10^{-16}	24
GO:BP	ribosome biogenesis	9.87×10^{-6}	16
GO:CC	cytosolic ribosome	1.21×10^{-25}	25
GO:CC	cytosolic part	8.23×10^{-19}	26
GO:CC	mitochondrial matrix	4.27×10^{-10}	24
GO:CC	mitochondrial nucleoid	2.48×10^{-8}	9
GO:CC	cell-substrate adherens junction	5.69×10^{-7}	19

DMSO DOWNs			
source	term name	adjusted p value	intersection size
GO:BP	RNA splicing, via transesterification reactions	3.61×10^{-7}	21
GO:BP	protein folding	4.19×10^{-7}	17
GO:BP	translation	4.68×10^{-7}	30
GO:BP	negative regulation of mRNA metabolic process	5.71×10^{-7}	11
GO:BP	regulated exocytosis	2.10×10^{-6}	30
GO:CC	secretory granule lumen	1.58×10^{-11}	24
GO:CC	focal adhesion	1.09×10^{-7}	22
GO:CC	chaperone complex	7.91×10^{-6}	6
GO:CC	proteasome complex	1.23×10^{-5}	9
GO:CC	actin cytoskeleton	6.81×10^{-5}	20

The full tables generated from the GO analysis are provided in Appendix Table 11, Table 12, Table 13, Table 14. They are large and contain nested ontological terms, in which an ontological hierarchy is enriched by the ontologies nested below it. This table was constructed as a way to highlight the processes and cellular compartments in which our treatments seem to be generating the most significant enrichments in the HT29 cell line, revealing the major cellular response to the treatments.

5 Discussion

5.1.1 The research questions

The research performed in this thesis aims to gather more information surrounding the unknown consequences of inhibiting the eIF4E component of the eIF4F complex. Pateamine A has demonstrated the ability to selectively disturb protein expression at low doses, such that there is not a global lowering of translation in proportion to the disturbance, but rather has selective effects with interesting outcomes. Other eIF4A inhibitors, hippuristanol and silvestrol have mirrored these effects *in vitro* and the outcome of this selective lowering of protein expression has demonstrable therapeutics effects *in vivo,* namely the rescue of cachexia. Research has demonstrated that rocaglates can change the sequence selectivity of the 4A helicase with its mRNA target (Iwasaki, Floor, & Ingolia, 2016) – this selectivity is facilitated by motifs in the mRNA 5' UTR, and is one potential explanation for the non-uniform effects of Pateamine A on the proteome.
Previous research by our laboratory has demonstrated that at low dose treatment, equivalent to an IC_{10} or below in the cell lines treated, Pateamine A disturbs protein expression in a pattern across the global proteome. This in contrast to the selected control drug, cycloheximide which uniformly lowers global protein expression. This research was an extension of the proteomic work with Pateamine A. Treatment involved two main drugs, 4E1RCat and ribavirin, 4E1RCat acts at the eIF4E-eIF4G interface preventing interaction and so interfering with cap-recognition. Ribavirin acts as an m7G cap mimic and competes with mRNA vying for translation. This distinction may have functional outcomes as eIF4E interaction with eIF4G is likely to have a regulatory or stimulatory effect.

In this research, the eIF4F complex was perturbed by 4E1RCat and ribavirin treatment and the proteomic outcome investigated to see if a consistent pattern emerged. This research attempted to generate insight into inhibition of eIF4F in the context of cachexia. It is still uncertain how the cachexia rescuing effects of eIF4A inhibitors are mediated. The work was therefore designed to address a hypothesis that the selective anti-cachectic effects of inhibition of eIF4A are mediated by the eIF4F complex.

The structure of the experiments I undertook was chosen to attempt to answer a core set of questions:

1. Is there a pattern in the upregulation or downregulation of proteins in response to low dose eIF4E inhibition? Does this pattern mirror the effects seen with eIF4A inhibition?

2 Are there eIF4E dependent transcripts and what characteristics (e.g. motifs in the 5' UTR), if any, do they possess? Do these characteristics mirror those seen with eIF4A inhibition?

In answering these questions, I hoped to identify whether the anti-cachectic effects of inhibition of eIF4A is solely mediated by eIF4A itself, or whether there is a potential effector role for the eIF4F complex as a whole. Furthermore, the work should reveal whether there is a possibility of therapeutic intervention at eIF4E to ameliorate cachexia, much like eIF4A inhibition.

5.2 Practical work and technique focused discussion

5.2.1 Cell culture

5.2.1.1 Obtaining reproducible treatment data

Getting reproducible drug response data from multiple MTT assays was a challenge. The low solubility of 4E1Rcat in comparison to ribavirin and cycloheximide caused significant trouble when collecting treatment data. Low solubility combined with 4E1RCat's low toxicity and the cytotoxic effects of DMSO was a major challenge for data collection and made the task of fitting a non-linear regression open to interpretation. The variability of the data could be caused by several factors, one of them I addressed by the running an assay at two cell concentrations. Fig 6.6 shows the effects of cell number on the outcome of an MTT assay. I noticed early on that using the standard number of cells (10,000) appropriate for an HL-60 assay made the wells look exceptionally crowded when using the significantly larger HT-29 cells. In response to this, I ran an assay to check how cell number would affect the outcome of an assay. Decreasing the number of cells to 2,500 has a subtle, but noticeable effect at the lower drug concentrations, with a steeper drop in cell activity in comparison to the other three curves. Although the other three curves show significant variability at the high drug concentrations, they show a marked consistency at the lower doses.

In the MTT assay results of 4E1RCat in the HT29 cell line, there appeared to be limited absorbance changes, even at high concentration. This may be due low efficacy of the compound in this cell line. However, I wished to establish that it did not arise from the optical properties of the 4E1RCat treatment, as the compound has both a strong optical absorbance and low aqueous solubility, potentially leading to scattering effects. However, formazan crystals were formed during the MTT metabolism step of the assay in the treated HT29 cells, confirming that they remain metabolically active. Furthermore, the equivalent assay with HL60 cells does show a complete loss of metabolic activity showing that the 4E1RCat solution is unlikely to interfere with the absorbance readings from the MTT assay. This trend of cell quiescence was seen consistently across all the HT29 MTT assays.

5.2.1.2 Practicalities of cell maintenance

5.2.1.2.1 Growth characteristics relate to freezing methodology

The original stocks from which cells in this thesis were derived grew exceptionally well, despite being nearly 20 years old (frozen in 1998). HT29 cells grown over the course of this thesis were aggressively detached using a combination of trypsin and EDTA. When detaching cells from culture flasks, initially the goal was to separate the cells into individual 'colony forming units', however, cells thawed using this method tended to grow at a significantly slower rate than observed in the original stocks. Original liquid nitrogen stocks recovered from the thawing process with notable ease and rapidly adhered and begun to grow within 1-2 days. Closer inspection of the original stocks late in this thesis yielded some insights: cells from the original stocks were cryopreserved in clusters, which meant that cells must have been less aggressively detached from their cell culture flasks. These cells could have been frozen using a different method such as the 'Mr. Frosty' cryogenic isopropanol containers, the concentration of cryoprotectants or freezing media used may also have been optimised. Freezing cells in clusters is likely to be the main reason for the original stocks' excellent post-thaw growth.

5.2.1.2.2 HL60 cells

The HL60 suspension cells used in this thesis generally behaved well. However, growing cultures growing would frequently collapse, seemingly without explanation. It is unlikely that this is due to cells becoming over-confluent, as suggested by empirical evidence in the form experiments with

taking cells left in the incubator with the same media for >2 weeks and coaxing the cells back to a healthy state with fresh media. This was done out of an interest in understanding the cell line better. It seems to indicate that HL60 cells are robust to the effects of metabolic acids and high confluency. Another separate issue with HL60 cells that added to trouble in the tissue cell culture suite seemed to arise from cells that were frozen poorly or thawed poorly, leading to large numbers of dead cells. Unlike adherent cells, removing debris is a challenge when dealing with suspension cell lines. Attempts to slow-centrifuge cells in the hope that the cells which should have more mass than the debris surrounding them would be enriched showed little benefit. Even at the lowest speed settings, the centrifuged pellet would contain still contain significant quantities of debris.

5.2.1.2.3 **HT29 cells**

HT29 cells have peculiar growth patterns, distinct from most other cell lines observed over the course of this thesis. They tend to form pseudo-glandular structures and grow in an almost bacterial manner, with the colony expanding and even growing in a 3-D orientation rather than the traditional adherent cells which tend to form a monolayer, see Figure 6-2. The nature of HT29 cell growth made visual assessments of confluence challenging, a combination of observing the coverage of the flask's surface and the colour of phenol red in culture media was required to assess proximity to the confluence threshold. HT29 cells, much like the HL60 cells, suffered from the same issues seen where the culture seemed to collapse for no apparent reason. Similar experiments were done with HT29 cells regarding response to metabolic acid and high confluency, and the conclusion was again that HT29 cell culture collapse is unlikely to be due to these factors, refer to Figure 6-3, Figure 6-4, Figure 6-5.

5.2.1.2.4 **Rationale for removing PenStrep from media**

Cell culture was initially performed using a pre-made mix of penicillin and streptomycin. Use of antibiotics in cell culture media was discontinued prior to data collection using MTT assays and drug treatment regimens for several reasons. PenStrep was avoided primarily due to research demonstrating genome wide gene regulation and expression changes caused by anti-biotic use in cell culture implicating a molecular interaction within cells (Ryu, Eckalbar, Kreimer, Yosef, & Ahituv, 2017). Secondarily, bacteria can grow in media laden with antibiotics, with a sufficiently large bacterial or fungal load in a contamination event. Cell culture could be accurately described as a waiting game. Cultures where PenStrep is present will take longer for a contamination to become evident; removing PenStrep allowed mistakes to be rectified and new cultures to be started, generally within 24 hours of a contamination event.

5.2.1.2.5 **Problems with thawing, absence of glutamine and contamination**

Over the course of this thesis extensive trouble was encountered when culturing cells. The cause being three-fold. When attempting to start up cultures from freezer stocks, the recovery of cells from thaw, an unnoticed change to L-glutamine-free media, and periodic contamination compounded to make identifying the sources of problems difficult. Effectively caring for cells that have undergone sub-optimal freezing or thawing was a skill learned late in this thesis. Rinsing off dead cells was especially useful for adherent cells, as dead cells and debris can be selectively removed from the culture. Dead cells can acidify media inducing metabolic stress, and debris and secreted molecules from dying cells were also observed to inhibit the sustained, healthy growth of cells in culture. Initial orders of RPMI-1640 contained glutamine, the indicator of the presence or lack of glutamine is a small piece of text on the bottle. At various points during the year cells were dying for seemingly no reason, it is suspected that various orders of media with or without glutamine may explain this. The most useful approach was getting an experienced cell culture user to observe and criticise my technique in the cell culture environment, it became apparent that

assumptions about the sterility of pieces of equipment that had not been autoclaved had been made, this is likely to be a significant source of contamination across the course of this thesis. Trouble-shooting in the cell culture environment was an important component of this thesis, identifying the problem is the main issue and several simple tests were employed to quickly determine what was causing the problem. For contamination issues, the first step was to test potentially contaminated reagents by transferring an appropriate amount into uncontaminated media and incubating it for 1-2 days, to see if any bacteria or fungi grew. For cells that were not growing well, a different stock of the same cell line could be thawed to see if the problem was isolated at the individual level to the liquid nitrogen stock. It could also be checked if media was causing growth issues by seeing if an available HeLa cell line would grow in the media causing trouble. Alternatively, cells could be given more time to recuperate, and be given new media every few days to see if they could make a recovery.

It was noted that HT29 cells grow slowly in media without glutamine, but HL60 cells start to die and refuse to grow, this may have been a fourth confounding factor that made identifying the problem more difficult, this was realised late in the thesis.

5.2.1.2.6 **A criticism of cell counting**

Cell counting was an important component of this project. However, it was also something that seemed to be a ballpark measure at times. The variability is likely to be a result of three phenomena, firstly, although the samples were thoroughly mixed by pipette prior to sampling, after a sample had been removed and placed on the glass adjacent to the hemocytometer squares, cells would have a chance to settle to the bottom within the globule of media. The second source of variability was the inconsistent pattern of capillary-like uptake of media between the glass coverslip and the glass of the hemocytometer. This inconsistency of can lead to some regions of the hemocytometer having significantly more or less cells. Lastly, small volumes were used, typically 2 µL was diluted in 18 µL, a 10-fold dilution, if the settling of cells in the globule of media is occurring then sampling using small volumes could encounter a problem when sampling of regions of lower or higher cell density. Prior to treatment with compounds, roughly 2 million HT29 or HL60 cells were plated. Whether 2 million cells were plated or 1.5 million cells or 2.5 million matters, see fig 6.6. There are also carry-over effects when it comes to sample processing on the mass spectrometer. Ideally there should be a comparable number of cells between treatment conditions and minimal normalisation towards the later stages, where the volume that peptides are reconstituted in can be varied to ensure consistent concentrations are run on the mass spectrometer. In this sense errors in cell counting could carry through all the way to mass spectrometry stage. There are two points in this project where an accurate cell count will have the most effect on experimental data, the cell counting required to plate 10,000 cells in an MTT well and the cell counting prior to plating up for drug treatment. Although we control for variability between MTT assays by taking absorbance as a percentage of a given control, accurately plating 10,000 cells per well every time improves the comparability of assays. The same principle applies to plating for drug treatment. Cell counting is time consuming and extends the hours spent in the tissue culture suite with every sample that requires counting. Increased consumable used in the form of plastic falcon tubes for the centrifugation process, and pipette tips for the counting are generally necessary, the extra handling can also occasionally result in contamination events, and the mental burden of doing mundane basic mathematics where mental energy could best be applied elsewhere. Cell counting using a hemocytometer is still an important skill in the wet-lab scientists' arsenal, however, it is 2019 and automated tools have existed for several years now, perhaps it is time to put away the archaic technology and move into the future.

5.2.1.3 Defining a biological replicate in the context of this study

Biological replicates were defined as a culture that had spent at least one passage in its own flask before being seeded and used for either an MTT assay or a treatment at a selected concentration of drug. Technical replicates are defined as either two cultures seeded from the same initial cell culture and used as part of an MTT assay or drug treatment or, in the case of MS data collection, peptide solutions were sampled twice, and thus two technical replicates were combined for later analysis.

5.2.2 Cell lysis and protein handling optimisation

The preparatory steps prior to mass spectrometry involved cell lysis, protein precipitation, disulfide bridge removal, subsequent capping of cysteines with carbamidomethyl moieties, tryptic digestion, desalting and concentration of peptides. This process required extensive optimisation to improve the spectral data abundance and quality. The methodologies for cell lysis and protein precipitation were evaluated, and steps taken to increase peptide abundances as described below.

5.2.2.1 Protein extraction/precipitation methodology choice

Plastics used for protein-related work were not autoclaved to lower the risk of plasticiser leaching into samples. LoBind Tubes were also used as a precaution, reducing the risk of peptides bonding with the plastic when drying in the centrivap concentrator.

5.2.2.1.1 **Cell lysis/protein extraction optimisation**

Following recognition of PEG contamination, the lysis solution needed to be changed to one not containing non-ionic detergents as these are a source of PEG. The efficiency of several lysis solutions was assessed - RIPA buffer, 8M urea, 8M urea + SDC, and dH_20 with added protease inhibitor. The lysis solutions were also combined with 3 quick freeze/thaw cycles in a -80°C freezer, with vortexing of lysate in between. This was an added step to increase the extraction efficiency. RIPA buffer is a purpose-designed lysis buffer and the most aggressive solution, liberating a total of 420 µg of protein this is likely to be the maximum amount that can be extracted. Due to losses during the acetone precipitation a solution as close to the RIPA buffer efficiency as possible was desirable. Human cell lines are generally easy to lyse and don't require an aggressive lysis procedure for protein liberation; 8M urea is used as a solubilising agent in later steps in the protein extraction protocol, thus it was logical to test it as a lysis solution. The 8M urea lysis was simple and deemed efficient enough to be used extensively.

5.2.2.1.2 **Protein precipitation**

Two methods were investigated for protein precipitation – acetone, and chloroform-methanol (C-M). I found the acetone precipitation to be simpler, more consistent, and predictable in its ability to precipitate proteins from cell lysates. Previous research performed by our laboratory using C-M suggested that it was the more effective of the two precipitation methods. The slightly more complex C-M precipitation outperformed the acetone precipitation in raw protein yield, but results were more variable overall. Ultimately, the reliability and utility of acetone precipitation were the deciding factors and this method was employed for the data acquisition phase of this project.

5.2.2.1.3 **Protein loading optimisation for LC-MS/MS**

A need for optimising protein loading concentration by normalising became apparent after the first round of mass spectrometry data was collected. This need came to light after the first round of data of 4E1RCat and DMSO treated HT29 cells was captured. A large discrepancy between protein abundance between samples 1-6 was noted, with some as low as ~25 µg and some as high as ~90 µg. This could have been a consequence of seeding density due to poor cell counting, loss of cells when aspirating media, or an error in the estimation of protein abundance using the DC assay. The

analysis in graphpad was done using a non-linear regression to extract protein concentration using a standard curve of known protein abundances, this strategy may also have contributed to some of the variability. However, the incredibly strong correlation between post-precipitation protein concentration and the number of identified proteins in Proteome Discoverer suggest that the DC assay and non-linear regression are not at fault. The above observations are evidence that protein concentration in a sample and the number of protein IDs are strongly linked, indicating that using around 80-100 µg is likely to give a high number of protein IDs.

5.2.2.2 The polyethylene glycol saga

5.2.2.2.1 **Rationale for exhaustive removal of PEG from samples**

The reason PEG contamination became an issue is two-fold. Another student doing affinity pull-down of a low abundance protein initially used RIPA buffer for cell lysis, the RIPA recipe includes Triton X-100 a non-ionic PEG containing detergent. This became an issue as PEG tends to lead to ion suppression of sample peptides. This becomes a significant issue when working with low abundance proteins where the sensitivity decrease caused by PEG ion suppression manifests as an inability to detect peptides from a sample. The second issue is that the mass spectrometer is a shared instrument and the PEG takes significant washing to remove from the LC column, another user interested in low-abundance proteins was concerned that the presence of PEG was lowering the sensitivity of the mass spectrometer, although later recognised as a contamination within their own samples. Previous research done by our lab group did not run into the problem of PEG contamination despite the use of RIPA buffer, this is likely because these experiments were observing a whole proteome and the protein abundances were well in excess of the PEG present. The work performed in this thesis is likewise a whole proteome approach with high protein abundances, and so should not theoretically have run into any issues, however, it was noted that a good run from the previous research was expected to yield ~800 protein IDs, and a bad run about ~600. In contrast, an excellent run over the course of this thesis would yield up to 1400 proteins and a bad run was expected to yield 800 or below protein IDs. This discrepancy of protein yields could come as direct consequence of ion suppression by PEG that may never have been addressed had such stringency in identifying and removing the source of PEG been implemented.

5.2.2.2.2 **MALDI-TOF use for PEG detection**

The MALDI-TOF was used as a tool for analysing samples because it is quick, simple and samples require less processing (desalting, tryptic digestion) before a sample can be analysed as MALDI is more tolerant to high salt concentrations. This allows PEG contamination to be detected more rapidly in comparison to the LC-MS/MS. For a given MALDI experiment the matrix, generally CHCA is combined with a few microlitres of sample at ratios of 1:10 and 1:100, a single microlitre is spotted and dried, this drying period can be very brief or, in the case of high urea concentrations can take up to an hour. Polyethylene glycol has a characteristic fragmentation pattern, with a difference of 44 mass units which closely resembles the shape of a normal distribution (Figure 4-11). In summary, MALDI-TOF is quick, simple, salt-tolerant and has low preparatory time, the 44-repeating pattern of PEG is easy to spot. Using this technique, samples were verified to be free of PEG to identify the ideal methodology for sample preparation for LC-MS/MS analysis.

5.2.3 Mass spectrometry

5.2.3.1 Mass spectrometry interpretation software

Proteome Discoverer (Mascot, Sequest databases), Scaffold and the Princeton Edu FDR calculator were used to identify peptides and protein matches.

5.2.3.1.1 Rationale of static and dynamic modification settings

There are settings within Proteome Discoverer to address peptide modifications in a given proteomics experiment. A static modification refers to those modifications which have been intentionally imposed on the sample peptides, in this case cysteine residues were capped with carbamidomethyl groups from the iodoacetamide treatment to prevent disulfide bridges from reforming. Dynamic modifications refer to modifications that may arise non-uniformly to the sample imposed intentionally or unintentionally because of sample handling. Urea was used extensively as a lysis buffer and a means to re-dissolve proteins. At times the urea/sample solutions would reach as high as 56 °C, increasing the likelihood of carbamylation at the N-terminus and at lysine residues. Oxidation at lysine residues, and deamidation of amide sidechains were also considered as dynamic modifications. Tryptic digestion occurs at lysine and arginine residues, and extensive carbamylation and oxidation can lead to poorly digested polypeptides, this did not become a problem during this thesis. Below is an example of protein ID numbers improving in response to addition of modifications. In addition, a readout has been added from the Proteome Discoverer interface showing a selection of heavily modified peptides some with multiple modifications per peptide chain. It is important to note that most peptides identified have no modifications, with a small proportion having 1 modification, usually carbamidomethylation at a cysteine residue, and an even smaller minority having 1 or more dynamic modification. Adjusting the dynamic modification settings resulted in a slight improvement to the number of proteins identified. Overall the processing methodologies used to prepare samples for LC-MS/MS analysis worked well, samples were not degrading and the effect of using urea was relatively minor.

1. Only fixed carbamidomethylation (no dynamic)
Total high-quality proteins: 1225
Total PSMs (peptide sequence matches): 22271

2. +oxidation (only)
Total high-quality proteins: 1234
Total PSMs (peptide sequence matches): 22655

3. +carbamoylation (only)
Total high-quality proteins: 1246
Total PSMs (peptide sequence matches): 22421

4. +oxidation +carbamoylation
Total high-quality proteins: 1249
Total PSMs (peptide sequence matches): 22811

5. +carbamoylation +deamidation
Total high-quality proteins: 1249
Total PSMs (peptide sequence matches): 21711

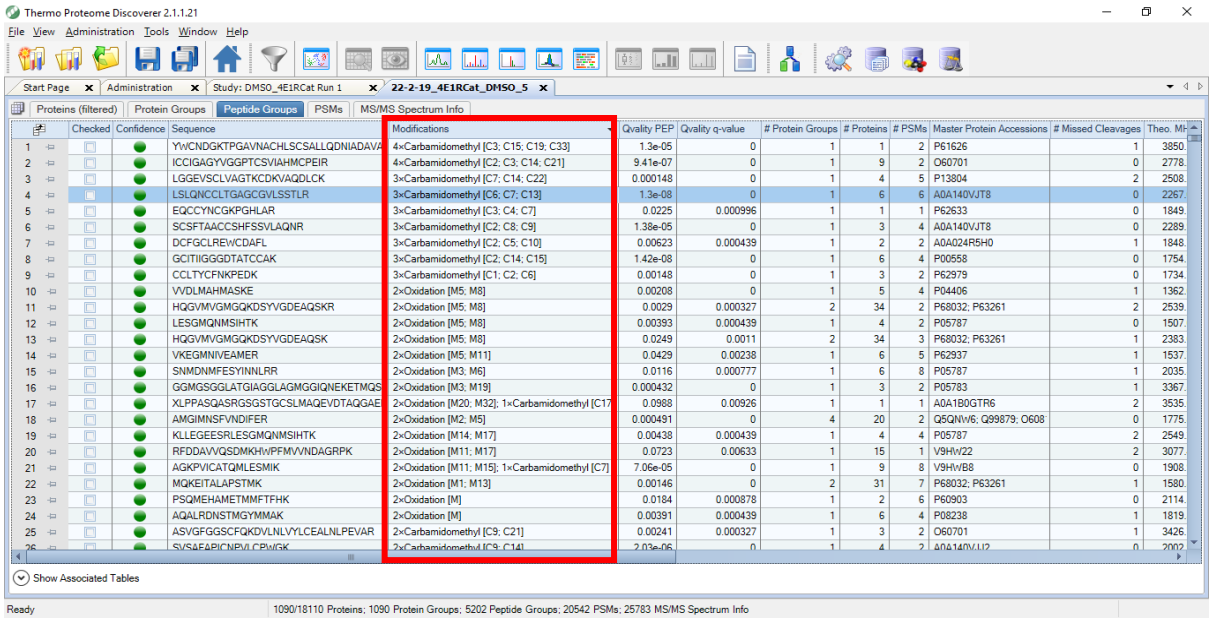

Figure 5-1 A readout from Proteome Discover. Outlined in red is a selection of heavily modified peptides identified in an MS experiment. Note this readout is from a separate analysis than the modifications and values reported above.

5.2.3.2 Label-free protein quantification from MS/MS spectra

The desire to use label-free tools for protein quantification offers benefits that include limited manipulation of the original biological sample over the course of an experiment, saving time and reagents. The techniques for quantification based on MS spectra have expanded and many of these are available with their own strengths and weaknesses depending on the nature of the experiment. MS Spectra were analysed using licensed software (Scaffold 4) using in-built label-free methods of quantification. Total ion current (TIC) is a no-nonsense method that is very robust, however, iBAQ which has been developed with an ability to correct for proteolytic fragments from a given protein also looks to be an effective method. Spectral counting employs a similar alignment method as used for calculating mRNA abundance in an RNA-seq experiment, where the 'reads', in this case validated peptides are aligned with a known protein sequence. This method was ignored as there are well known biases, as larger proteins will generate more peptides and it is affected by how the machine is running on a given day. This research follows on from previous research performed by our group in which TIC and iBAQ were both used, and thus both techniques were used for protein quantification from the MS spectra. If a significant difference became apparent between the two quantification methods, it was noted and assessed.

5.2.3.2.1 TIC - Total ion current quantification

TIC is a label-free quantification tool and an extension of spectral counting. It is reliable and more robust to some of the problems that plague spectral counting as a quantification technique. For a TIC quantification the average of the TIC for all of the MS/MS spectra that identify a protein is used as a quantitative measure. With the TIC method each spectral count is assigned a unique abundance value (Asara, Christofk, Freimark, & Cantley, 2008).

5.2.3.2.2 iBAQ - Intensity based absolute quantification

iBAQ is a relatively new quantification tool that works very well for protein quantification with various methods of correcting for bias. The central concept of iBAQ is taking the sum of peak intensities of all peptides matching to a specific protein this value is taken and divided by the number of theoretically observable peptides. This process is corrective and aims to control for the capacity of larger proteins to have their peptides overrepresented in a sample. The process of

figuring out which peptide fragments are theoretically possible is aided by knowing the digestion enzyme, in this case trypsin cutting at lysine/arginine (unless followed by proline). The values from this iBAQ method are an accurate proxy for protein levels (Schwanhäusser et al., 2011).

5.2.3.3 Statistical techniques for dealing with false positives

Multiple testing correction with Bonferroni usually makes all results insignificant. False discovery rate algorithms are necessary to figure out what is worth exploring further, FDR as a concept is interesting, it invites the possibility of encountering false positives (e.g. discovering a protein not present in a sample) while attempting to minimise false negatives (e.g. not recognising a correctly identified protein as significant). As an example, below in the first treatment data run through the mass spectrometer. Aiming to identify a change in protein expression between the 4E1RCat treated cells and the DMSO treated cells a list of 1052 proteins was identified. Of these, at 5% FDR no significant change was noted, at 10% FDR, 2 protein changes became significant, at 15% 20 protein changes became significant (18 proteins increasing in expression and 2 decreasing) and at 20% FDR 22 changes were identified as significant. At an FDR of 15%, it would be expected that 15% of the changes identified as significant are erroneous, corresponding to 3 insignificant changes being falsely identified.

pi0:	0.566902				pi0:	0.566902419		
	FDR: 5%					**FDR: 10%**		
	p-value	q-value	lfdr	significant		p-value	q-value	lfdr	significant
	1.00E-04	0.056387	0.065952	0		1.00E-04	0.056387	0.065952	1
	1.90E-04	0.056387	0.087095	0		0.00019	0.056387	0.087095	1
	0.00034	0.067269	0.1094	0		0.00034	0.0672686	0.1094	1
	0.001	0.141792	0.135618	0		0.001	0.1417917	0.135618	0
	0.0014	0.141792	0.143506	0		0.0014	0.1417917	0.143506	0
	0.0022	0.141792	0.159851	0		0.0022	0.1417917	0.159851	0
	0.0022	0.141792	0.159851	0		0.0022	0.1417917	0.159851	0
	0.0022	0.141792	0.159851	0		0.0022	0.1417917	0.159851	0
	0.0025	0.141792	0.166078	0		0.0025	0.1417917	0.166078	0
	0.0029	0.141792	0.17428	0		0.0029	0.1417917	0.17428	0
	0.0037	0.141792	0.18997	0		0.0037	0.1417917	0.18997	0
	0.0039	0.141792	0.193705	0		0.0039	0.1417917	0.193705	0
	0.0043	0.141792	0.200917	0		0.0043	0.1417917	0.200917	0
	0.0043	0.141792	0.200917	0		0.0043	0.1417917	0.200917	0
	0.0043	0.141792	0.200917	0		0.0043	0.1417917	0.200917	0
	0.0043	0.141792	0.200917	0		0.0043	0.1417917	0.200917	0
	0.0047	0.145419	0.207779	0		0.0047	0.145419	0.207779	0
	0.0049	0.145419	0.211079	0		0.0049	0.145419	0.211079	0
	0.0059	0.166758	0.226306	0		0.0059	0.1667584	0.226306	0
	0.0067	0.180762	0.237036	0		0.0067	0.180762	0.237036	0
	0.0025	0.141792	0.166078	0		0.0025	0.1417917	0.166078	0
	0.0028	0.141792	0.172245	0		0.0028	0.1417917	0.172245	0

pi0:	0.566902419				pi0:	0.566902419			
	FDR: 15%					**FDR: 20%**			
	p-value	q-value	lfdr	significant		p-value	q-value	lfdr	significan
	1.00E-04	0.056387	0.065952	1		1.00E-04	0.056387	0.065952	1
	0.00019	0.056387	0.087095	1		0.00019	0.056387	0.087095	1
	0.00034	0.067269	0.1094	1		0.00034	0.067269	0.1094	1
	0.001	0.141792	0.135618	1		0.001	0.141792	0.135618	1
	0.0014	0.141792	0.143506	1		0.0014	0.141792	0.143506	1
	0.0022	0.141792	0.159851	1		0.0022	0.141792	0.159851	1
	0.0022	0.141792	0.159851	1		0.0022	0.141792	0.159851	1
	0.0022	0.141792	0.159851	1		0.0022	0.141792	0.159851	1
	0.0025	0.141792	0.166078	1		0.0025	0.141792	0.166078	1
	0.0029	0.141792	0.17428	1		0.0029	0.141792	0.17428	1
	0.0037	0.141792	0.18997	1		0.0037	0.141792	0.18997	1
	0.0039	0.141792	0.193705	1		0.0039	0.141792	0.193705	1
	0.0043	0.141792	0.200917	1		0.0043	0.141792	0.200917	1
	0.0043	0.141792	0.200917	1		0.0043	0.141792	0.200917	1
	0.0043	0.141792	0.200917	1		0.0043	0.141792	0.200917	1
	0.0043	0.141792	0.200917	1		0.0043	0.141792	0.200917	1
	0.0047	0.145419	0.207779	1		0.0047	0.145419	0.207779	1
	0.0049	0.145419	0.211079	1		0.0049	0.145419	0.211079	1
	0.0059	0.166758	0.226306	0		0.0059	0.166758	0.226306	1
	0.0067	0.180762	0.237036	0		0.0067	0.180762	0.237036	1
	0.0025	0.141792	0.166078	1		0.0025	0.141792	0.166078	1
	0.0028	0.141792	0.172245	1		0.0028	0.141792	0.172245	1

Figure 5-2 A table of 1052 proteins identified between the 4E1RCat and DMSO treatment conditions (only showing the top 22). Four FDR stringencies, 5,10,15,20% were applied. Cells highlighted in blue were scored as significant by the FDR calculation. FDR calculations were run through a web service retrieved from http://qvalue.princeton.edu/

5.2.3.3.1 Multiple testing correction

With the rise of computational biology and the mountains of data modern biologists are capable of generating, the use of multiple testing correction is essential. High-throughput experiments, including RNA-seq studies and proteomics aimed at identifying global protein expression changes between treatments, are examples of molecular biology experiments where multiple testing correction is used. The problem being solved by multiple hypothesis testing is that when tests are done enough, chance plays a part in determining whether significant findings will be deemed insignificant and vice versa. As an example, if 100 proteins from experimental data are known to be unaffected by a treatment, i.e. levels don't change between a treatment and a control, at a defined statistical confidence cut-off, of $\alpha = 0.05$, five of these 100 by pure chance will have p-values that would encourage rejection of the null hypothesis (i.e. give a response that would be assumed to indicate a change, or a failure to change, between treatments). The risk of falsely discovering a protein is something accepted as part of a proteomics experiment, as the goal is to generate leads which can be validated by molecular biology techniques. The problem with this is that t-tests

individually are frequently undertaken at an α = 0.05, generally speaking. However, as the number of tested outcomes gets higher the absolute number of false positives increases. The t-tests performed for a given protein are a comparison between the untreated control and the treatment condition, if the distributions of peptide 'counts' or another quantitative measure between control and treatment are the same, the p-values would be uniformly distributed (Figure 5-3A). Conversely, if there are changes in a quantitative measure between treatment and control, the distributions would overlap less and thus in terms of p-values the distribution would be skewed towards lower values (figure 5-3B). As an example, in a case where most protein levels are unaffected by drug treatment, and a small proportion are affected, statistically you have a case where the affected proteins which will have p-values skewed and closer to 0 and the p-values from the unaffected proteins which will have uniformly distributed p-values between 0 and 1 comingling in the same analysis. Multiple testing corrections like the Benjamini-Hochberg attempt to address this by essentially overlaying the histograms by summation of the p-value distributions of treated and untreated conditions. Then drawing a line across the uniform portion of the distribution crossing into the affected and unaffected proteins the p-values above the line are true-positives. Based on the general FDR of 0.05, less than 5% of the significant results will be false positives (figure 5-3C). The False Discovery Rate (FDR) approach attempts to control the *proportion* of false discoveries in the results. A decision is made beforehand to accept a proportion 'α' of false discoveries, then a threshold is calculated in a way that ensures that the global FDR is expected to be at worst equal to α.

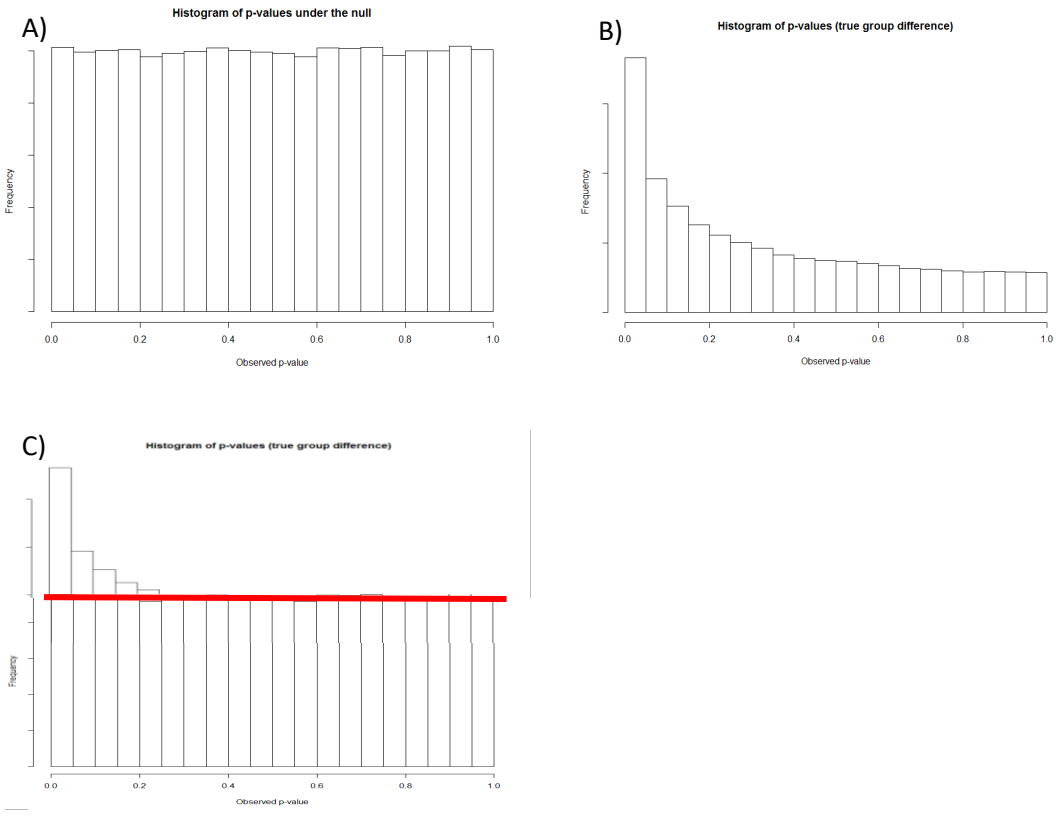

Figure 5-3 A) An example of an even statistical distribution, if peptide 'counts' or another quantitative measure between control and treatment are the same, the p-values would be spread uniformly. B) If there are changes in a quantitative measure between treatment and control, the distributions would overlap less, and p-value distribution would be skewed towards lower values. C) An example of a distribution in which both A) and B) are present in the same analysis, a Benjamini-Hochberg-type correction is applied by the red-line across the uniform portion of the graph.

5.2.3.3.2 False discovery rates (FDR)

False discovery is a statistical concept that involves accepting an erroneous outcome or 'false positive' as a true positive outcome. In statistical analyses, there is an inherent risk that a type 1 error, a false positive, or a type 2 error in which a statistically significant result is discounted as insignificant, a false negative. The goal of FDR is to minimise false negatives, at the cost of introducing false positives into an analysis at an unspecified rate, in this study the FDR is set at 10%. While the analysis now captures most if not all of the potentially significant findings, they are now interspersed with erroneous results which cannot readily be separated from correctly identified results.

http://qvalue.princeton.edu/ - is a web-based server that performs a Benjamini-Hochberg-like multiple testing correction in which the FDR rate can be specified.

5.2.3.3.3 Decoy protein database strategies for FDR estimation

Decoy protein databases are an empirical strategy for estimating FDR, the basic concept involves generating sets of 'decoys' which are a set of distinct generated peptide/protein sequences that don't correspond to actual peptides/proteins. These decoys are seeded among experimentally identified peptides and the final number of decoys that make it through in the list of identified peptide spectrum matches (PSMs) is an accurate way of empirically determining FDR. Generated decoys are generally beholden to criteria that try to ensure:

1. Similar amino acid distributions as target protein sequences.

2. Similar protein length distribution as target protein sequence list.

3. Similar numbers of proteins as target protein list.

4. Similar numbers of predicted peptides as target protein list.

5. No predicted peptides in common between target and decoy sequence lists.

(Speicher, 2010)

There are two core strategies for generating decoys that can satisfy the above criteria, the first and simplest is a 'reversal' strategy that involves reversing the sequence of a peptide/protein to obtain a new entity with the exact constituent amino acids but a non-existent (typically) counterpart in the realm of protein/peptide sequences. The second, a 'stochastic' strategy employed by search engines like Mascot, one of the primary protein validation search engines used for protein identification in this thesis. This involves the generation of proteins in a pseudorandom manner, proteins are random in some aspects while following amino acid bias patterns or even using a Markov chain model to better imitate real proteins by mimicking micro-patterns such as single or double amino acid repeats or highly basic/acidic regions (Speicher, 2010).

Multiple testing is a fundamental component of modern biology, and statistical-mathematical and empirical-computational methods in the proteomics field are used to ensure that the number of false-positives and false-negatives are minimised within a given statistical analysis. Corrections like the Bonferroni and Benjamini-Hochberg adjustments are common in this space, modern proteomics also uses an empirical-computational approach to false discovery that involves seeding an analysis with known decoys to model the FDR rate. These two approaches are fundamental to this thesis and have been employed extensively on the path from raw LC-MS^2 through to PSM identification, to lists of identified and quantified proteins and finally to lists of proteins up or downregulated in response to a treatment.

5.3 Insights from gene ontology and STRING analysis

The FDR adjustment used alongside Scaffold's existing multiple testing corrections was deemed too stringent as it removed all significant hits from the three main treatment conditions, cycloheximide, ribavirin and 4E1RCat. The DMSO condition however, gained an additional 163 hits at a 10% FDR adjustment through the Princeton Edu web server (Migliaccio, Rotondi, & Auricchio, 2006). In response to this, it was decided that on the whole, the 10% FDR adjustment was too stringent for the main treatments, where the focus on a concentration that produced a small growth defect resulted in few hits. In contrast, it was too generous for use in the DMSO control analysis, which had many hits and accepting a 10% FDR would mean including a large number of false positives. Therefore, the analyses discussed here use the up and downregulated hit list from the Scaffold software, depending only on its multiple testing corrections to limit false positives. Gene ontologies (GOs) are categories of processes, functions, and locations that use standard terms to describe the characteristics of biological systems. An ontology analysis moves the analytics away from what the individual protein or gene specifically does in a molecular sense and attempts to generate new insights by contextualising the specific molecular mechanisms of each individual protein responding to a treatment into more general processes. For example, a DNA helicase specifically unwinds DNA, but is in a more general sense involved in replication. Although at the molecular level the DNA helicase melts and annuls complementary base pairing, its function as a helicase is in the context of providing access to polymerases and other DNA replication proteins to the now single stranded DNA which is important for the replicative process. The use of standard GO terminology ensures it is possible to group proteins together under common ontological terms, and therefore also to analyse protein changes under the three GO domains – Biological Process, Molecular Function, and Cellular Component. Ontological analyses are useful for understanding what processes, functions and cellular locations are associated with a proteome response to a treatment. There are additional ways of analysing proteome responses, beyond the GO terms. These include investigation of changes in sets of proteins that relate to specific pathways, which can be obtained through pathway databases, such as KEGG (Tanabe & Kanehisa, 2012). There are also databases, such as the CORUM database, which can be interrogated to identify whether responding proteins are found in the same complex. Another analysis tool used is STRING (Szklarczyk et al., 2017), this is a visualisation tool that constructs a network of protein nodes based on the confidence with which the nodes interact. Interaction networks can be based on a range of features, including appearance in the same publications, correlation in databases (such as GO and KEGG) and co-expression. This latter analysis reveals clusters of proteins in a set that have been shown to be co-transcriptionally regulated. Proteins in a co-expression network are generally involved in the same biological responses, and these networks can be a useful tool, in addition to GO term analysis, to understand the proteins that appear in the proteome response data. In our analyses, due the small number of hits, in the form of upregulated and downregulated proteins, analyses were sometimes done with a combination of up and downregulated hits to improve the confidence relating to affected processes. The STRING analyses were constructed in this manner, with the exception of the up and downregulated proteins in the DMSO condition, where no benefit was achieved by doing analyses on the combined hits. It is important to note that the apperance of a protein in the GO analysis does not indicate that it will form part of a cluster in the STRING diagrams. All the hits from the Scaffold analysis were included in the GO and STRING analyses. However, in the STRING analyses if the protein did not have partners from the same analysis the node was not included in the STRING output.

5.3.1 Cycloheximide (69 hits)

In the work presented here, cycloheximide is used as a control to evaluate which changes are occurring due to general translational stress, and which are specific to the compound under study. Cycloheximide is expected to decrease protein synthesis uniformly across the protein expression profile of the cells treated at IC_{10}. We may also see a stress response signal due to stalled translation at the ribosome.

GO term enrichment analysis reveals that spliceosomal process and ribonucleoproteins are upregulated in the cycloheximide treatment (Table 7). This assessment is supported by the STRING analysis of the combined up and downregulated proteins (Figure 5-4). This shows a spliceosome-related protein cluster as well as a ribosomal protein cluster. The upregulation of the ribonucleoproteins by cycloheximide is expected as it directly affects protein synthesis at the level of the ribosome. It is likely that cycloheximide is removing a portion of the protein output capacity of the cells and the cellular response is to produce more ribosomes to counteract the loss. The spliceosomal process could also be explained by this observation as new ribosomes will need to be built by the remaining functional ribosomes in the cell and mRNA is the precursor to both the rRNA and ribonucleoproteins.

Proteins involved in ubiquitination and protein degradation via the proteasomal process are downregulated.

Interestingly, associated with the proteosomal components in the cluster diagram are proteins involved in ubiquitination and energy metabolism in the form of enzymes involved in the production of NADPH and ATP. The proteosome is energy dependent and requires a ubiquitination signal for degradation of proteins.
The CORUM and KEGG analyses showed no changes in the upregulated hits condition. In the downregulated hits condition, three complexes showed up in the CORUM analysis: PA28-20S proteasome, the OTUB1-UBC13-MMS2 complex and the MCM4-MCM6-MCM7 complex. These are involved in proteasomal degradation, ubiquitination and DNA replication respectively. These three processes being downregulated in response to protein synthesis inhibition is logical. The balance of protein synthesis is disturbed, and the cells are responding by downregulating the degradation of proteins via ubiquitination and the proteasome. Under normal circumstances proteins will be replaced by protein synthesis. Since cycloheximide has perturbed protein synthesis, downregulating the turnover of proteins is a necessary adaptation to preserve remaining functional proteins. The decrease in DNA replication may be a generalised stress response to the toxicity of cycloheximide, an instruction to cease or lower replicative efforts. In the combined analysis of up and downregulated proteins the CORUM analysis pulled out an additional complex that is not involved in proteasomal degradation that didn't show up in either of the separate analyses, the SF3b complex which recognises the branch point adenosine of pre-MRNA as part of the splicing process (Rakesh, Joseph, Bhaskara, & Srinivasan, 2016). In the combined condition, the KEGG analysis showed two pathways termed proteasome (as expected from the GO and STRING analyses) but also arginine biosynthesis. Response of the arginine biosynthetic pathway to translational stress has been observed previously (Venturi et al., 2018).

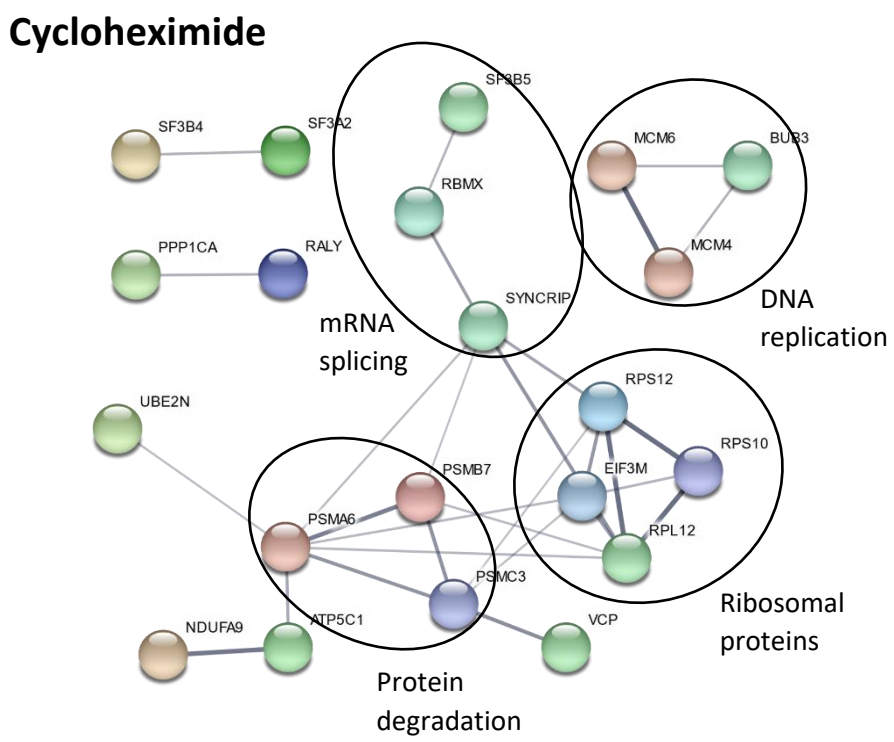

Figure 5-4 STRING diagram of proteins expression change in response to low-dose treatment with cycloheximide

5.3.2 Ribavirin (83 hits)

The two main processes seen in the upregulated hits are cell adhesion/cadherin and proteasomal proteins involved in protein degradation.

Interestingly far more proteins seem to be downregulated in response to ribavirin treatment, and subsequently more processes are affected. Three main processes seem to be ribosome biogenesis, protein targeting to the endoplasmic reticulum (ER), and RNA metabolism. The CORUM analysis of the downregulated hits showed two complexes, the Nop56p-associated pre-rRNA complex presumably a complex involved in ribosomal biogenesis (Hayano et al., 2003), and cytoplasmic ribosome. The KEGG analysis also notes that the ribosome is downregulated. Taken together these results suggest that ribavirin is influencing the ribosome and its biogenesis.

No new clusters or processes appeared in the combined analysis. The enrichment for ontologies relating to cell-cell adhesion and cadherin binding is unique to the results found with ribavirin and points to a function of ribavirin that is not related to translational inhibition. This is not unexpected, as ribavirin has been noted to have multiple cellular targets. The observation of a downregulation in cadherin binding proteins is consistent with a recent publication which suggests this may be part of the mechanism through which ribavirin can protect against viral infections, at least in combination with an interferon treatment (Rendón-Huerta et al., 2013).

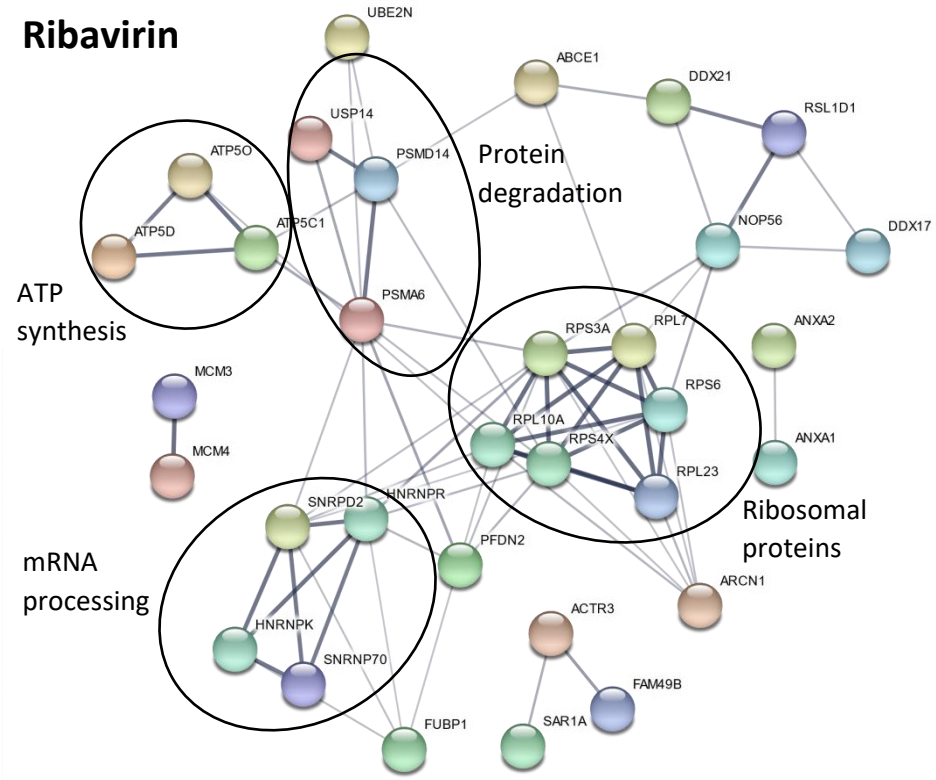

Figure 5-5 STRING diagram of proteins expression change in response to low-dose treatment with ribavirin

5.3.3 4E1RCat (47 hits)

Upregulated proteins and processes in response to 4E1RCat involve ribosome biogenesis, protein targeting to the ER, and RNA metabolism.

The downregulation change in response to 4E1RCat seems to be minimal, the affected processes involve the mitochondrial proteins HADHB (involved in beta-oxidation) (Naiki et al., 2014), ATAD3A (a heavily expressed mitochondrial membrane protein involved in nucleoid organisation, and various aspects of growth and metabolism) (Li & Rousseau, 2012), and TFAM (a mitochondrial transcription factor) (Litonin et al., 2010). Also affected is the eukaryotic replisome, a complex required for rapid and accurate chromosome replication (Yeeles, Janska, Early, & Diffley, 2017).

The CORUM analysis pulls out three clusters of which the cytoplasmic ribosome and 60S ribosomal subunit clusters are nested ontological terms. This means that the 60S ribosomal cluster term contributes to the significance of the cytoplasmic ribosome term. Also, in this analysis is the Nop56p-associated pre-rRNA complex, as noted for ribavarin. The CORUM analysis indicates effects on ribosome biogenesis. The KEGG analysis confirms this with ribosome being the only process identified. The effects on mitochondrial proteins and processes and effects on eukaryotic replication were unexpected. No additional insights were obtained through the combined analysis.

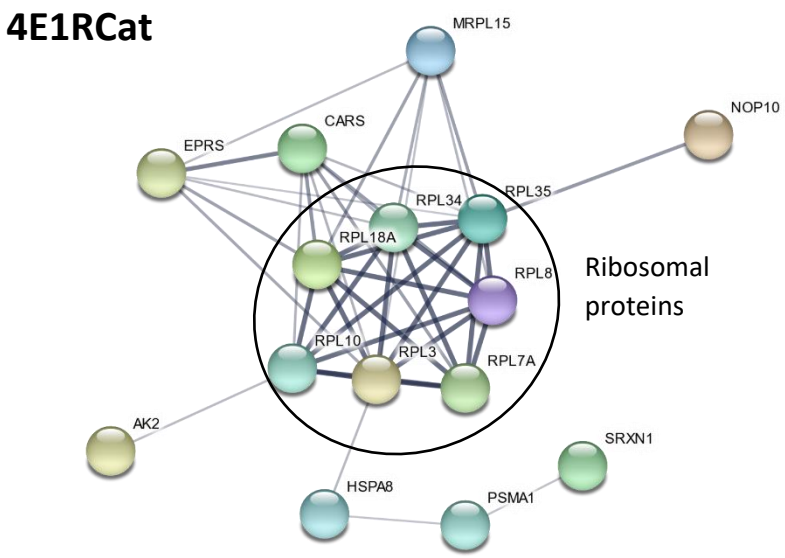

Figure 5-6 STRING diagram of proteins expression change in response to low-dose treatment with 4E1RCat

5.3.4 Comparisons between treatments

The number of hits aligns with the expectations from the drugs in terms of molecular specificity within the cell. Ribavirin, the drug with the most expected interactions within the cell (1.2.4.2), has the largest number of hits, whereas 4E1RCat, with only two molecular interactions (1.2.4.1), has the least hits. cycloheximide is middling. This may be superficial, but it is interesting to note, nonetheless. Unique to the 4E1RCat treatment is the downregulation of mitochondrial nucleoid proteins and the eukaryotic replisome. For the ribavirin treatment, upregulation of cell adhesion molecules and proteins associated with the cell adhesion process is also unique. It is noticable that responses to ribavarin are in the opposite direction to those observed in other treatments. For example, the decrease in ribosome and ribosome biogenesis is in contrast to the increase in proteins associated with these ontologies found for cycloheximide and 4E1Rcat. A trend of converse regulation between ribavirin and 4E1RCat, protein targeting to the ER is a downregulated process in the RBV treatment and an upregulated process in the 4E1RCat treatment. In the same vein proteasomal proteins and processes are seen in the cycloheximide and RBV, however in cycloheximide they are downregulated and upregulated in ribavirin this process is upregulated. Finally, RNA metabolism is another process that is downregulated in the RBV treatment but upregulated in the 4E1RCat treatment.

5.3.5 DMSO (364 hits)

The intention of the DMSO treatment was as a control, and so it is not a treatment aligned with the aims and objectives of this thesis. It was required, due to the low solubility and low activity of 4E1Rcat, which combined to require a high DMSO concentration in its treatment. However, the sheer strength of the response to 1% DMSO in the HT29 cells is intriguing. The 1% DMSO treatment condition roughly corresponds to a growth inhibition of between 30-40%. In the context of this study this would be considered a medium-high dose treatment, which explains the magnitude of hits seen in the DMSO condition. I strongly think that 4E1RCat is having a molecular effect on the cells. Observation of cell pellet sizes post-drug treatment indicates that 4E1RCat is contributing to lowering proliferation, as cells in the DMSO control run alongside 4E1RCat had noticeably smaller pellets, which were stained red interestingly (4E1RCat is red in solution). Although appropriate DMSO controls were run in tandem with the 4E1RCat treatment it may not be possible to de-convolute the effects that DMSO is exerting on the proteome, it may be possible that effects we see in the 4E1RCat condition have been tweaked by the action of DMSO. Although it is possible to overlay the proteomic effects of the treatment and control and subtract the DMSO controls' proteomic effects from those exerted by 4E1RCat. However, this might not be convincingly possible, it may be that some of the effects seen in the 4E1RCat treatment are a result of the combined efforts of the two compounds. The decision to analyse the DMSO condition proved worthwhile as some of the processes affected by such a general toxic agent appeared in the treatment conditions by compounds that were expected to be far more selective comparatively.

DMSO has wide-ranging effects on cells, upregulated processes ranked by significance include targeting to the ER (localisation and targeting), translation (initiation, peptide biosynthesis and ribosome biogenesis), RNA catabolism (cellular nitrogen catabolism, aromatic compound catabolism, nuclear base-containing compound catabolism and heterocycle catabolism). Some minor upregulated processes include DNA conformation change and energy metabolism.

The processes that respond to DMSO through protein downregulation include RNA metabolism, translation, splicing, protein folding and exocytosis.

DMSO is likely to have general toxic effects on the cell, perhaps interestingly in the context of the other treatments, a high proportion of the processes seen in the other treatments are also seen in the DMSO condition. Localisation to the ER, effects on translation, RNA metabolism and catabolism, splicing and minor effects on energy metabolism are seen on aggregate in the three treatment conditions. In this sense, DMSO appears to be delivering responses typical of a translation inhibitor. This was an unexpected finding, and not anticipated at the outset of the study. However, investigation of the literature revealed a 2019 paper which investigates the effects of DMSO on cells (Verheijen et al., 2018). The study included a proteomic analysis, for which data (presented in the supplementary information Tables 3 and 4) is consistent with the results presented here. Although analysed through a different process, focusing on pathways from the ConsensusPathDB with the Reactome database, the proteomic data shows exceptional q-values (down to 10^{-49}) associated with translation and the ribosome, making these the strongest pathway hits in their proteomic study.

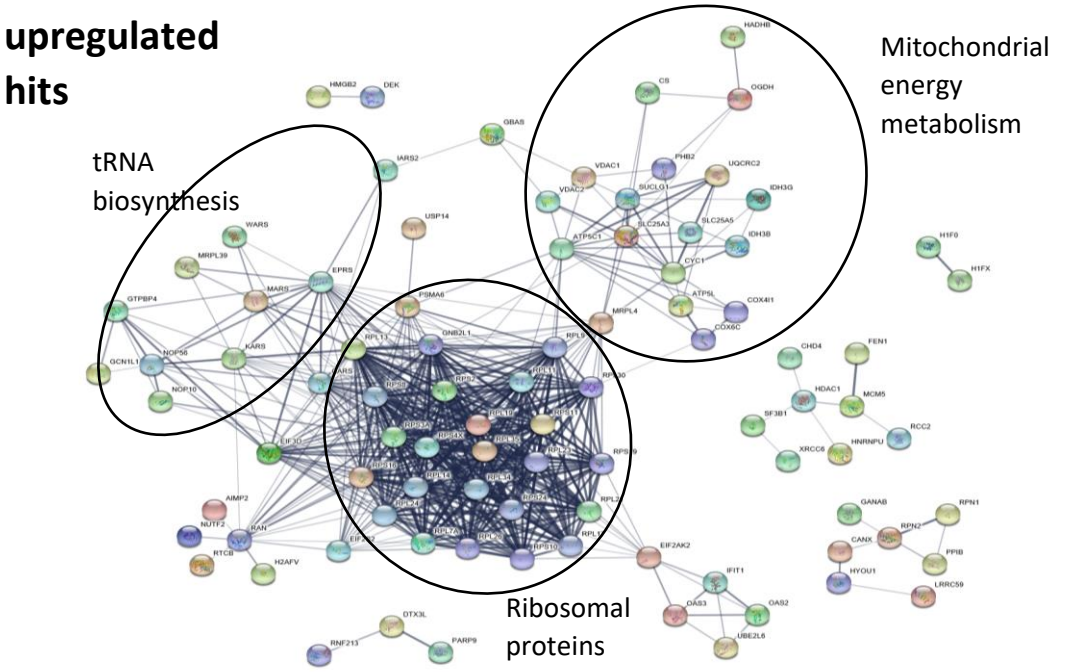

Figure 5-7 STRING diagram of upregulated proteins expression change in response to treatment with DMSO at 1%, equivalent the concentration in the 4E1RCat top

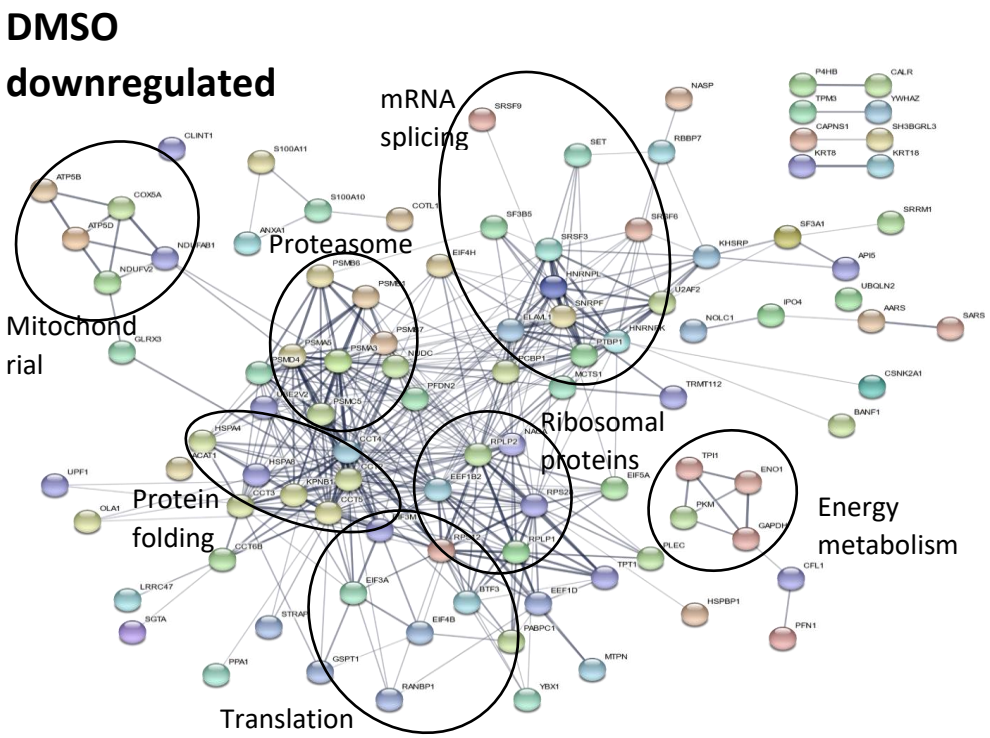

Figure 5-8 STRING diagram of downregulated proteins expression change in response to treatment with DMSO at 1%, equivalent the concentration in the 4E1RCat top dose

5.3.6 Summary of insights from GO and STRING analysis of treatments

In summary, the drug treatment effects on the HT29 cells largely result in ontological enrichments related to processes that they are the directly targets of the treatments. In terms of named processes, the treatments caused many of the same effects, which include ribosomal processes, splicing, protein degradation, targeting to the ER and energy metabolism. It seems highly likely that proteomic outcomes in response to each compound are a direct result of the perturbation of the molecular process in combination with general toxic responses to treatment and the subsequent effects on the cell. Some unique responses do appear in the ribavirin treatment in the form of effects on cell adhesion and expression of cadherins in ribavirin. Likewise, in the 4E1RCat treatment condition mitochondrial nucleoid and the appearance of the eukaryotic replisome are unique. The revelation that DMSO causes cellular responses that are consistent with protein synthesis was unexpected. Furthermore, it brings into doubt the proteome responses observed in response to 4E1Rcat. This compound required high concentrations of DMSO to solubilise it at a concentration of 1% (v/v) DMSO sufficient to cause a growth defect in the HT29 cells at. Even though the up-and down-regulated proteins associated with the 4E1Rcat treatment have been determined in relation to the DMSO control, it is difficult to confidently rule out that noted enrichments might arise from experimental artifacts. Conversely, the low number of varying proteins and enriched proteins found with the 4E1Rcat treatment may arise simply because 4E1Rcat-induced changes are being masked by the cellular response to DMSO.

5.4 General discussion

5.4.1 The purpose and power of a whole-proteome experiment

Mass spectrometry is an excellent tool for investigating protein expression at a global level and prospecting for interesting biological outcomes and generation of hypotheses to further explore and validate using molecular biology techniques. Generally, biases and enrichment from sample handling and data analysis are minimised to ensure that any enrichment noticed in a given proteomics experiment are a consequence of biological activities and processes, rather than a consequence of a given method of protein isolation and analysis. Proteomics often begins without a prior hypothesis in mind and is a prospective analysis tool. Therefore, the software we use to analyse our spectral data and the methods of cell lysis and protein precipitation are likely to bias the analysis. However, these biases can be mitigated by a thorough understanding of the analytical tools, and the enrichment outcomes of a given wet-lab methodology. An example of a false enrichment discovery by members of our lab group involved noticing that treatments from HT29 and HL60 cells treated at IC_{10} values with PatA were heavily enriched for extracellular exosomes. Although initially interesting, retrospectively the extraction methods removed many membrane-bound proteins and enriched for cytosolic proteins; extracellular exosomes are derived from the membrane and cytosolic components, which could explain this enrichment.

5.4.2 The significance of ‘low dose’

Previous research suggests that PatA has its anti-cachectic effects at low doses, well below anti-tumour dosing. Since the nature of PatA’s anti-cachectic effects are still poorly understood and may involve the eIF4F complex, it is appropriate when targeting another component of the same complex to treat it at the same dosing scheme as this will help clarify whether it is low dose eIF4A inhibition mediating the effects, or whether the complex as a whole plays a role in cachectic reversal.

5.4.3 4E1RCat and separating the DMSO effects from drug treatment effects

The effects of compounds on proliferative or metabolic activity of human cancer cell lines is a way to establish the potency of a drug. Cell lines have variable responses to the anti-proliferative effects of

a given treatment. The MTT assay is a mainstay in drug discovery, the principle of this assay is the conversion of 3-(4,5-dimethylthiazol-2-yl)-2,5-diphenyltetrazolium bromide (yellow) to its corresponding formazan (purple) by actively metabolising cells. This assay was used extensively in this thesis as a tool to assay the anti-proliferative effects of compounds selected for this study. Dimethyl sulfoxide (DMSO), the solvent used to reconstitute the drugs used in this thesis has demonstrable anti-proliferative effects. Data was collected to establish the effects of the vehicle on the cell lines used. DMSO alone was shown to have an IC_1 of 0.151% (v/v in buffer) in HT29 cells and 0.621% (v/v in buffer) in HL60 cells. DMSO controls were included in the analysis to address the effects DMSO has on cells. A concentration of 0.1% (v/v in buffer) has been established as having negligible cytotoxic effects, evidenced by the literature (Timm, Saaby, Moesby, & Hansen, 2013) and backed by MTT assays performed over the course of this thesis. DMSO controls were only relevant to the 4E1RCat treatment conditions, where the 100-fold drop in concentration from the stock concentration in 100% DMSO to 1% DMSO in the top dose, which corresponds to a ~IC_{10} treatment, is not enough of a dilution to avoid the cytotoxic effects of DMSO. For CYCLOHEXIMIDE and ribavirin, the ability to dissolve these drugs at 50 mM and their cytotoxicity being significantly higher than 4E1RCat mean that in the process of diluting the drugs to their appropriate IC_{10} values in treatment conditions, the DMSO concentration is low enough to not warrant controlling for the effects of DMSO. As an example, the IC_{10} of ribavirin in HT29 cells of 11.1 µM is more than 1000-fold lower than the 50 mM starting stock concentration. Cycloheximide with an IC_{10} of 0.0427 µM (42.7 nM) is also below 1000-fold more dilute than the starting stock. The IC_{10} of DMSO generated from an assay of HT29 cells treated with DMSO was 0.4% by volume. This contrasts with the top dose of 4E1RCat treatment, which was selected as the ~IC_{10} treatment value which has a DMSO concentration of 1%. These findings conflict, as by my treatment data an IC_{10} for DMSO treatment is at a lower percentage than used in the top dose in the 4E1RCat treatment condition used as an IC_{10}. One could interpret this as 4E1RCat being protective against the effects of DMSO, however, this is unlikely. Another interpretation is that since the 4E1RCat data was assayed on six separate occasions, that it is the more reliable collection of data. Whereas the dose response to DMSO, was initially completed as an exploratory experiment and subsequently an IC_{10} was generated. The assay was only replicated two times, if replicated a few more times the IC_{10} may shift. Over the course of this project, it has been repeatedly noted that 4E1RCat is not particularly cytotoxic to cells (see Figure 4-3). When dissolving 4E1RCat, significant solubility issues were encountered, consistent with some online resources which showed conflicting solubility values for dissolution in DMSO. Efforts to dissolve the drug by sonication were unsuccessful, the drug eventually became soluble at a concentration of 4 mM, about 10-fold lower than the 50 mM stocks of RBV and CYCLOHEXIMIDE. Early attempts to solubilise at higher concentrations were motivated by the low cytotoxicity expected from 4E1RCat. These concerns manifested in the form of a struggle to get 4E1RCat to kill cells even at the top dose of 40 µM, at this dose the DMSO concentration is 1% making it hard to determine whether 4E1RCat is having any effects or whether the effects of DMSO are being observed. RBV by contrast was soluble up to 180 mM and demonstrated by dose response curves to be significantly more cytotoxic by comparison. As mentioned in the introduction 4E1RCat only has 2 molecular interactions, with 4EBP and eIF4E, in this sense it is pharmacologically 'clean' (1.2.4.1). However, due to its low cytotoxicity (see Table 1) and low solubility (see 4.2), the approximate IC_{10} value is influenced by the DMSO vehicle which is at 1%, this may confound results. The appropriate DMSO controls have been generated in response to the conditions necessary for 4E1RCat to be useable as a treatment. Despite this, we may expect that 4E1RCat will have a small uniform lowering effect on protein synthesis in line with its molecular function as an eIF4E inhibitor.

5.4.4 Ribavirin, a 'dirty' drug with multiple interactions

It has been noted in the literature that Ribavirin, a commercially available clinical drug, has a suite of molecular interactions at a range of concentrations. Ribavirin mainly targets enzymes involved in metabolism, but also polymerases, consistent with its status as a guanosine mimic. This is further

evidenced by its ability to be misincorporated into viral mRNA at millimiolar concentrations by viral RNA-dependent RNA polymerases, Crotty et al suggest that the effect of this on viral replication is an increase in mutation rates in response to misincorporation of ribavirin into the viral genome to a catastrophic level, however a caveat to this is that the researchers used ribavirin at 20 times higher a concentration than clinically relevant doses, at 100 µM (Crotty, Cameron, & Andino, 2001). This interaction with RNA-dependent RNA polymerase is not the central mediator of its broad anti-viral activity. This has been attributed to inhibitory effects on inosine monophosphate dehydrogenase (IMPDH) by ribavirin 5'-monophosphate, leading to depletion of intracellular pools of GTP (Leyssen, Clercq, & Neyts, 2006). Strong evidence for this model of interfering with viral replication, is that treatment with ribavirin results in a 4-log reduction in viral RNAs which can be partially reversed by the addition of guanosine. Researchers noted, interestingly, that despite suspected involvement of IMPDH in ribavirin's anti-viral activity, mycophenolic acid, another IMPDH inhibitor had no anti-viral effect (Lanford et al., 2002). As mentioned previously (1.2.4.2), despite conflicting findings (Westman et al., 2005; Yan et al., 2005), ribavirin has been confirmed to interact with eIF4E at micromolar concentrations (Kentsis et al., 2005, 2004). The conflicting results were suggested to be a result of free-eIF4E (often referred to as apo-eIF4E) being sensitive to structural changes at pH changes between 7.5-8. Some backing for this is the observation by Westman et al (Westman et al., 2005) that ribavirin bound to eIF4E at 2-4 orders of magnitude lower than originally reported by Kentsis et al (Westman et al., 2005), suggesting that buffer conditions in the conflicting papers could be lowering the capacity of eIF4E to bind ribavirin. Ribavirin is unlikely to exert its molecular effects in its unmetabolized form, ribavirin is metabolised in the liver and intracellularly. Since the intracellular metabolism is the form relevant to a cell culture, this will be the focus. Ribavirin is the substrate of adenosine kinase which converts ribavirin into ribavirin monophosphate (RMP), which in turn is the substrate of monophosphate and diphosphate kinases which respectively dephosphorylate, and triphosphorylate RMP into ribavirin triphosphate (RTP). In most cell types RTP dominates at concentrations 20-100 times that of RMP (T. Page & Connor, 1990). Viruses function within the cell and the cellular machinery is co-opted for their replicative processes, thus the relevance of such an in-depth assessment of ribavirin's mode of action in an anti-viral setting is relevant to the effects it may have on cellular processes. With such a wide variety of molecular targets at a variety of concentrations, it is important to acknowledge this when treating cells, as the effects on the proteome may be confounded by the other interactions within the cell. The effects of ribavirin are slightly less certain in comparison to cycloheximide or 4E1RCat due to the variety of molecular targets it is known to interact with, refer to section 1.2.4.2. We expected that there would be a general lowering effect on protein synthesis as some proportion of eIF4E will be competitively inhibited by ribavirin. There may be other effects as ribavirin lowers the GTP pool within the cell which may lead to a cellular response for guanosine producing enzymes or enzymes involved in generating or using GTP.Although other processes, such as those associated with cell-cell adhesion, were found, the relatively clean ontological enrichment profile of ribavirin for processes associated with translation validate its potential for studies of this kind.

5.4.5 Cycloheximide – control protein synthesis inhibitor

Cycloheximide is a eukaryotic protein synthesis inhibitor used extensively in molecular biology to stop the cellular production of protein. Cycloheximide was selected as a control compound due to its known protein synthesis inhibition by blocking translation at the ribosome (Schneider-Poetsch et al., 2010). More importantly cycloheximide inhibits all protein synthesis in a non-selective manner, thus it was an appropriate tool to use as a positive control in these experiments as the goal is to tease out any specific effects of eIF4E inhibitors from the change in the proteome that could be a result of a biological response to translation stress, giving a skewed or selective effect on protein expression.

5.4.6 Regulatory network influence on translational output

It is not apparent that the magnitude of change any individual protein can make to a cell is in proportion to its abundance. In fact, the opposite can be true. If you take a set of 100 proteins randomly selected from a proteome, it is likely that some of these proteins will have structural, enzymatic, or regulatory roles within the cell. However, the majority of the proteins in which change is detected are likely to be high abundance structural and enzymatic proteins. Transcription factors are the most extreme example of a proteins with extremely low abundance but correspondingly extreme effects on gene expression and protein synthesis in the cell in response to growth factors and the cellular stresses within an environment. Transcription factors, despite being encoded by 6% of the genome (Barabási, Gulbahce, & Loscalzo, 2011) and so the second largest group of genes, are generally the lowest in abundance by far. Evidence of this being that only 5% of all TFs have been purified and characterised (Ngagore et al., 2013).

Whilst transcription factors provide one example of how an abundance change in a protein can cause broad change within a cell, they are not alone in having this property. Barabási etl al describe non-transcription factor related abnormalities in an insightful way - “The impact of a specific genetic abnormality is not restricted to the activity of the gene product that carries it, but can spread along the links of the network and alter the activity of gene products that otherwise carry no defects.” (Barabási, Gulbahce, & Loscalzo, 2011). This insight can be extended to the outcome of translational inhibition. For example, pateamine A is suspected to give selective translation inhibition of transcripts with specific 5’ UTR structures in a manner similar to rocaglates (Iwasaki et al., 2016). Due to the nature of cellular regulatory networks, if the translationally repressed gene product is part of a network – and especially if it is a key regulator – its down-regulation can have flow on effects on protein expression lower down in the pathway. This observation can be used to potentially trace the effects of a treatment and its effects on proteins that are identified through a proteomics experiment and potentially finding a regulator, such as a transcription factor, or set of processes responsible for the changes seen in protein expression between treated and untreated cells.

5.4.7 The search for 5’ UTR motifs

It has been observed that motifs in the 5’ UTR sequences are often involved in mRNA regulation. This can happen in two ways. In the first, the sequence itself is a recognisable element that can be bound by a regulatory protein that can either increase or decrease some aspect of expression of these mRNAs. An example of this is the 5’-Terminal Oligopyrimidine tracts (TOP) motif present in 30% of transcripts in actively growing mammalian cells (Pichon et al., 2012), the TCT motif is also a requirement for transcription for the majority of the TOP containing mRNAs (Pichon et al., 2012). The second way is by the motif generating a higher order secondary structure that indirectly interferes with translation by enforcing a requirement for helicase activity prior to expression, as mentioned in the introduction (see 1.2.1). Even for a transcript with a 5’ UTR with minimal secondary structure, translation can be severely inhibited if eIF4A is not present. Although the intention initially was to explore 5’ UTR motifs to see if there were transcripts that respond to eIF4E treatment in the manner observed with pateamine A (previous work by our lab group) and presumably part of the puzzle that explains why pateamine A can rescue cachexia at low doses. We have not ruled out that there are eIF4E responsive transcripts. At a glance our eIF4E treatment data does not present enough proteins that cannot be explained by a direct biological response effects of ribavirin and 4E1RCat treatment. In terms of running motif enrichment analyses, statistically speaking small numbers of proteins, and their transcripts are likely to generate false leads by way of randomness. We have not been exhaustive in our separation of biological responder transcripts and eIF4E inhibitor sensitive transcripts on the current analyses approach in the interest of time.

However, it is in many ways justified as a replacement drug for 4E1RCat would need to be found and a higher dose of ribavirin will need to be used to elicit a greater proteome response to justify running a series of motif enrichment analyses. As it currently stands, we do not have enough data to deny or confirm the existence of eIF4E inhibition sensitive transcripts.

5.5 Conclusion

The findings in this thesis are unable to meaningfully test the notion that low dose eIF4E inhibition has selective effects that mirror outcomes from pateamine A treatment. This arises because the eIF4E inhibitors used in this study each have problems associated with their use. Ribavirin has a suite of molecular interactions within the cell which can cloud the interpretation of the proteomic outcome in response to treatment. The major problem was the low efficacy of 4E1Rcat and its overlapping proteome response with the DMSO vehicle. The 4E1Rcat was chosen due to its reported selectivity for eIF4E inhibition, and it was intended to use this to aid abstraction of eIF4E-mediated effects from the proteome response of the polypharmacological ribavirin. Together, these create uncertainty in interpreting the proteome responses observed as being specific to eIF4E inhibition. However, the ontological enrichments observed with ribavirin do support its use in ongoing studies. Furthermore, many of the proteins observed to decrease in abundance in response to eIF4E inhibitors appear to be associated with the direct biological response to the known effects of the inhibitors, such as their effect on translation, as revealed by GO term and co-expression analysis. Relatively few protein changes are left to be explained in terms of translational repression based solely on a 5' UTR sequence motif. This small number coupled with the uncertainty of the origin of their translational repression led to the conclusion that sequence motif analysis would not be meaningful. The major outcomes of this work are, cycloheximide, ribavirin and 4E1RCat exert effects on the proteome consistent with their classification as translation inhibitors. An interesting finding comes in the form of DMSO our solvent of choices' effects on translation, seemingly consistent with a translation inhibitor at a growth inhibition of 30-40%. Although there are a few examples of proteins and protein and protein clusters that may not be easily explained by a direct biological response of the cell line to perturbation by the treatments applied in this thesis. There is not enough information to ruled out the existence of eIF4E sensitive transcripts. This study has paved the way for future experimentation with higher doses of ribavirin and a replacement inhibitor for 4E1RCat or another strategy to disentangle the effects of 4E1RCat from the DMSO vehicle it is dissolved in.

5.6 Future directions

Due to time restraints treatment data was obtained only in the HT29 cell line. The continuation of this project would involve confirming whether the observations seen in HT29 cells in response to treatment are mirrored in other cell lines. A mirror experiment in the HL60 cell line has been performed and these cells will be processed and run on the mass spectrometer to see if the data supports the findings seen in the HT29 cells, an experiment that unfortunately could not be accommodated in the timeline of this thesis due to instrumental down-time. Although initially the intention was to quantify proteins using both TIC and iBAQ, in the interest of time TIC was used exclusively for protein quantification. Further research could make use of the robust iBAQ method and see if any new proteins appear in the analyses or other proteins disappear. The use of more potent or selective eIF4E inhibitors would be an ideal way to confirm these results, especially if this allows avoidance of a solvent vehicle control such as DMSO. This may not be possible however, as 4E1RCat and another commonly used inhibitor, 4EGI-1, have comparable solubility. In fact, 4E1RCat seems to have the edge in this department. Based on the literature, 4E1RCat is the more frequently used of the two, and unfortunately alternative direct eIF4E inhibitors may not yet exist. Another possibility, if it is impossible to find a stronger eIF4E inhibitor would be to repeat the IC_{10} treatments with DMSO added to the cycloheximide and ribavirin treatments and perhaps pateamine A as well to

see if the proteomic effects of DMSO can be convincingly subtracted from a treatment. It would be worthwhile investigating the effects of ribavirin at a higher concentration to see if sufficient proteins can be downregulated, which fall outside the direct biological response to the translational stress, to investigate 5' UTR motifs associated with reduction in protein expression. Future research could also test the effects of hippuristanol or other available eIF4A inhibitors on the proteome response to see if it matches the proteomic effects of pateamine A in HT29 and HL60 cells. Another possible avenue to explore could involve replicating the effects on muscle fibers, the muscle fibers responding to pateamine A could be subjected to a proteomic analysis to gather more information about the specific effects of pateamine A on the proteome of muscle cells, ideally from *in vivo* studies, and compared to the effect of ribavirin or another eIF4E inhibitor.

6 Appendices

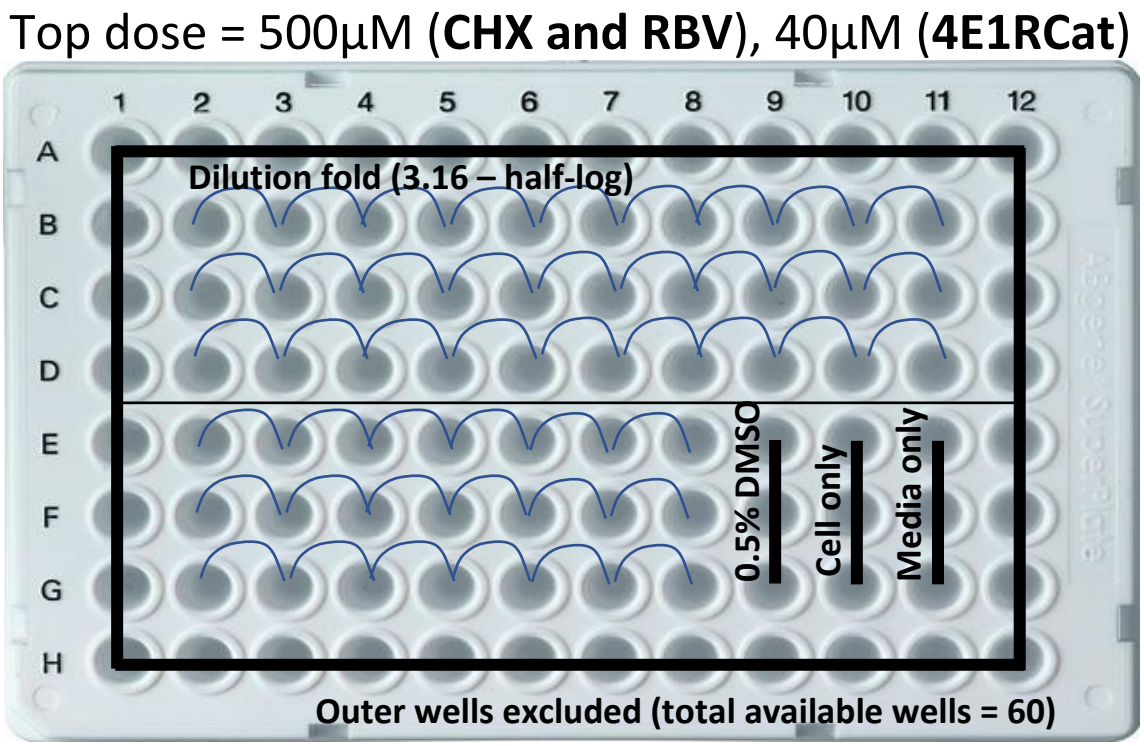

Figure 6-1 Plate plan example done in triplicate following a half-log (3.16) serial dilution scheme. DMSO controls were included at concentrations where DMSO is expected to influence cell growth. A media only blank and cell-only control are also included.

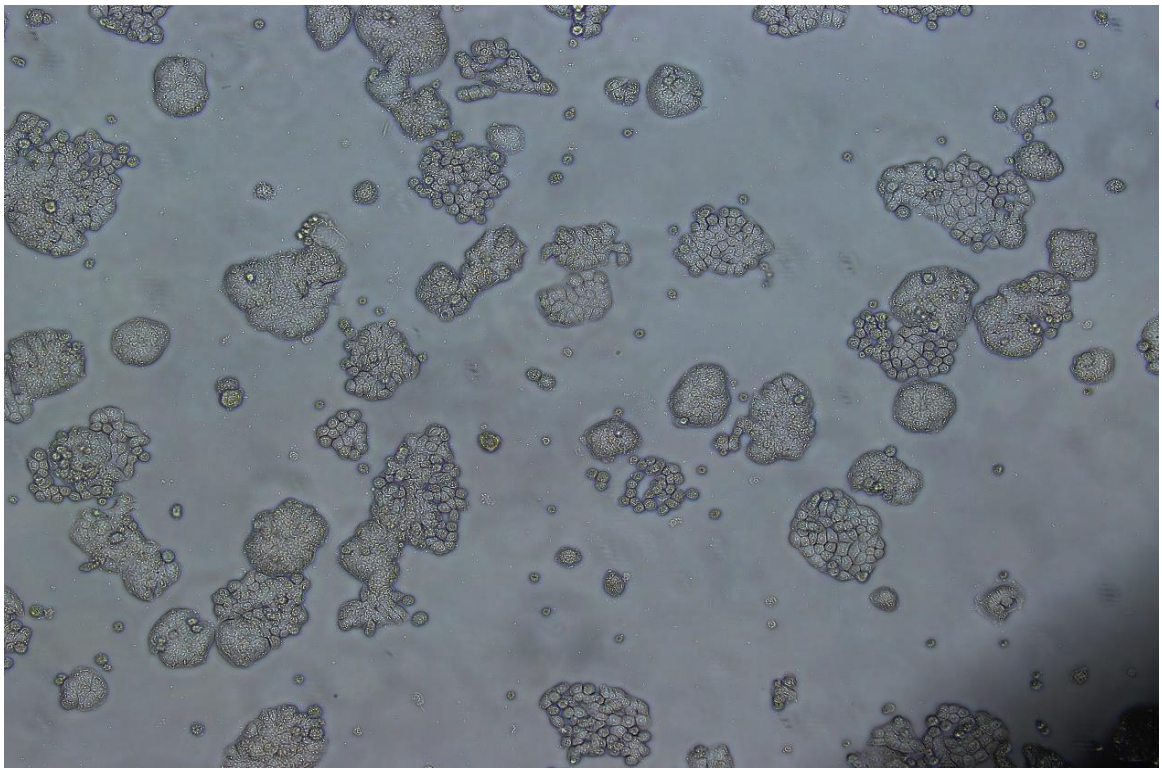

Figure 6-2 Shown at 10x magnification. Healthy cells from the original stock from 1999, after 1 passage. Note the the propensity of the cell line to form colonies, also note the healthy look and regularity of the glandular structures

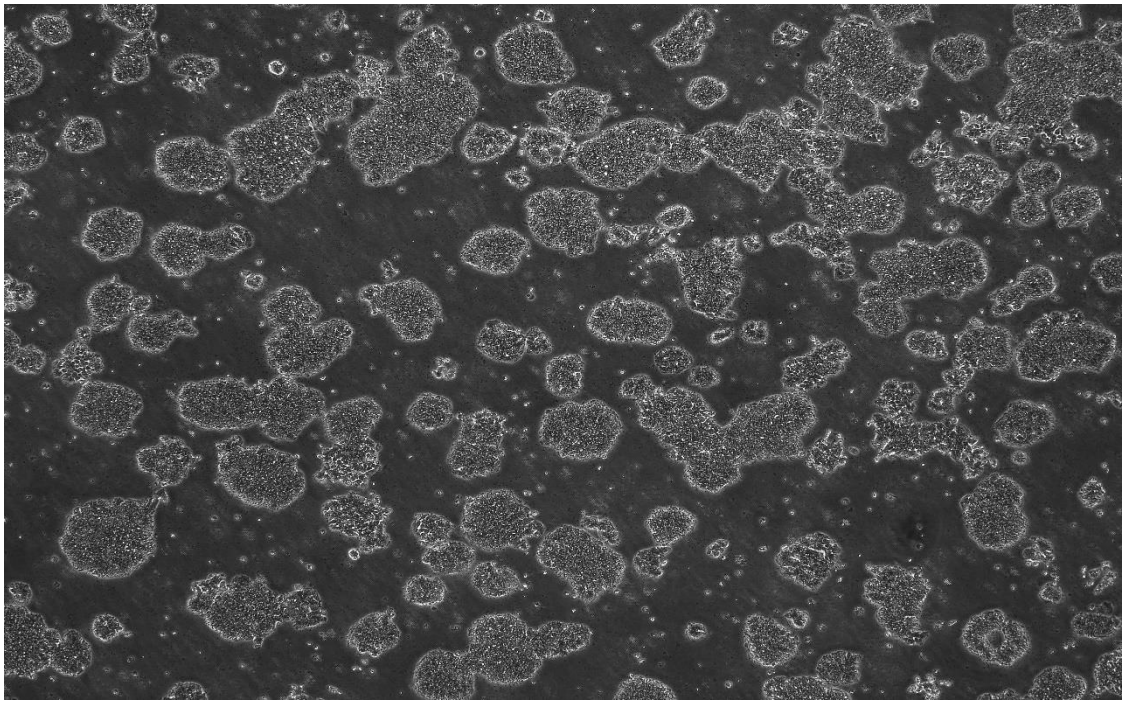

Figure 6-3 Shown at 10x magnification, HT29 cells grown in depleted acidic media at high confluence for ~1 week. Note, that the glandualar structures are becoming jagged looking and the dead cells in suspension.

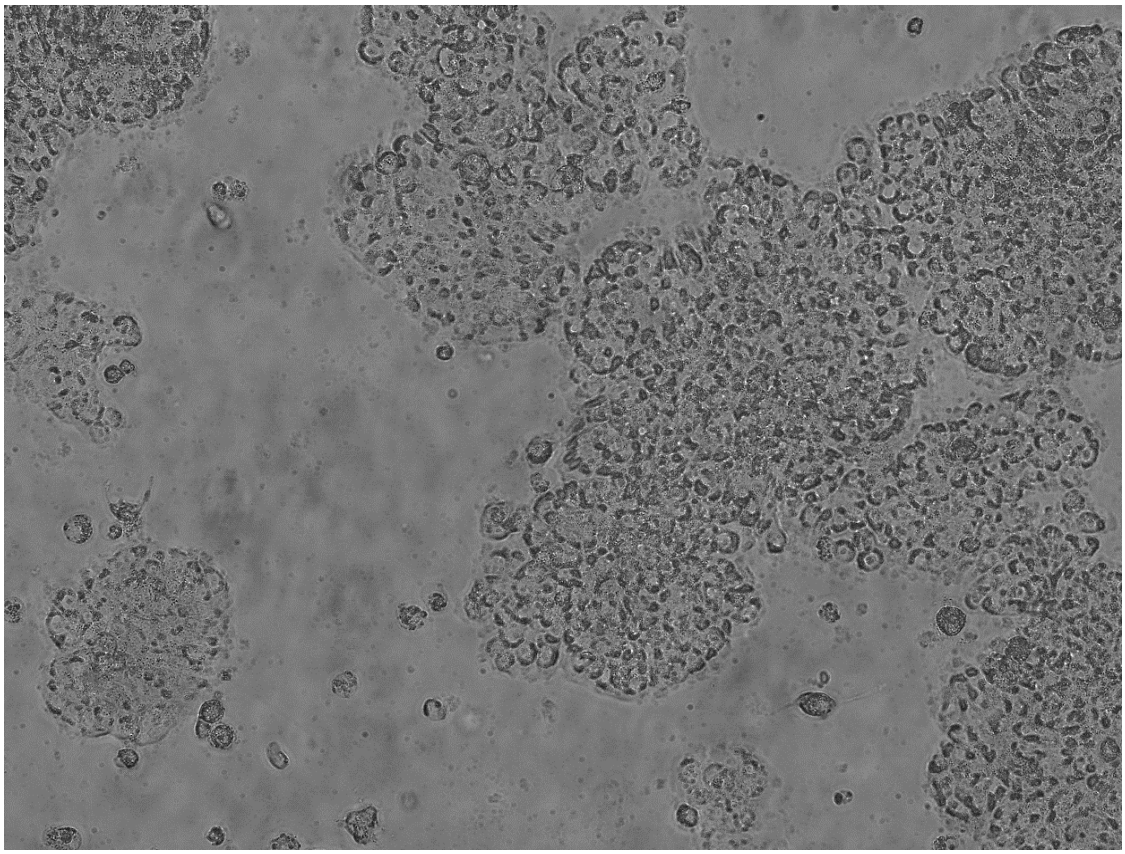

Figure 6-4 40x magnification - a closer look at cells from the same flask as figure 6-3. Note the debris and apoptotic blebs in the environment surrounding the cells

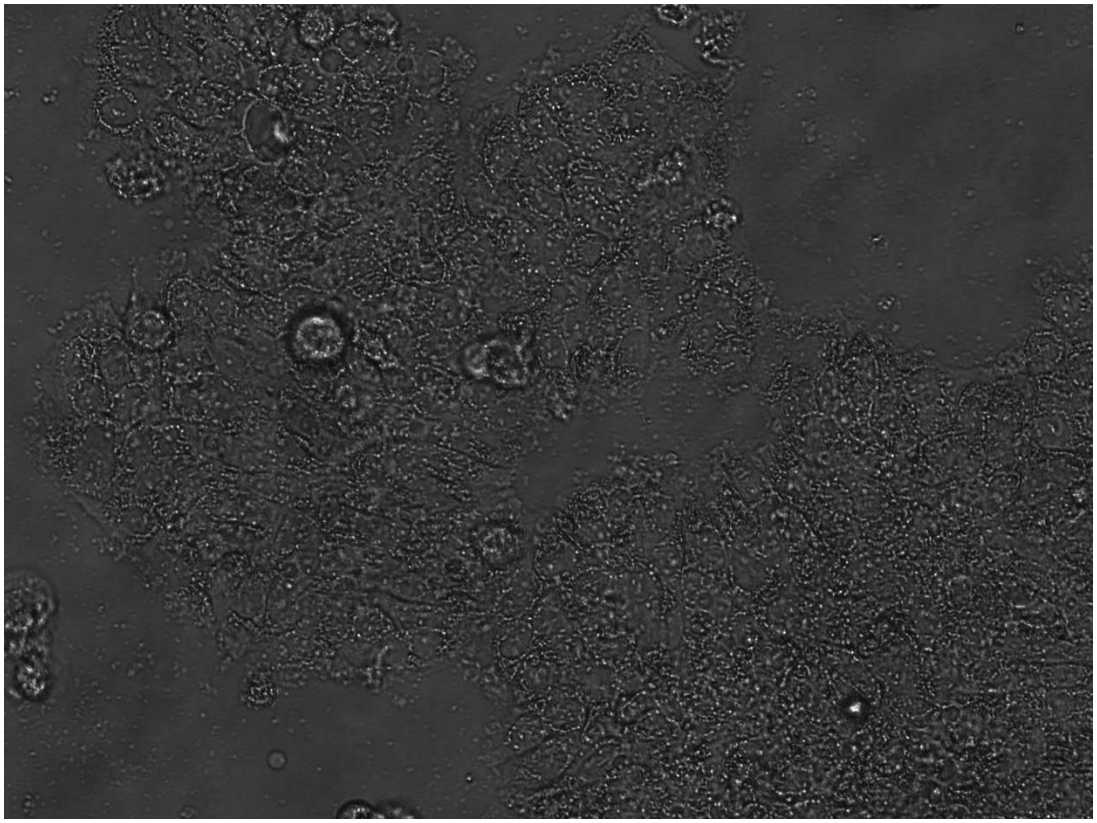

Figure 6-5 100x magnification - a closer look at cells from the same flask as figure 6-3. Note the number of apoptotic blebs in the environment surrounding the cells

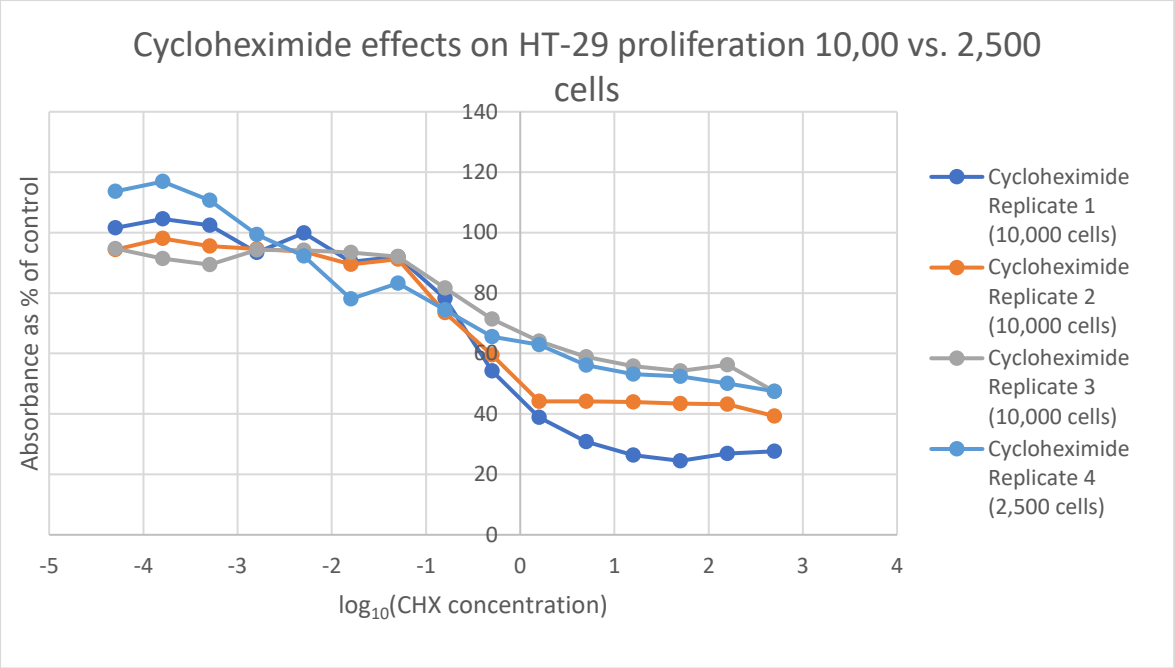

Figure 6-7 The effects of cell seeding density on proliferative signal from the MTT assay.

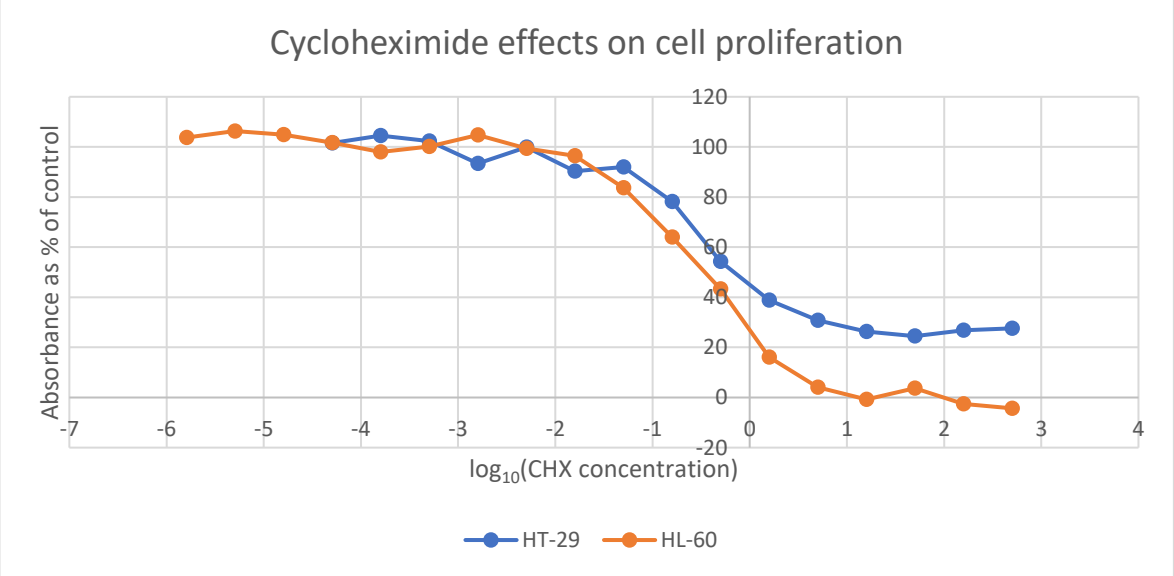

Figure 6-6 A comparison of the proliferative effects of cycloheximide on HT29 and HL60 cells. Note how in HT29 cells the graph does not level out at 0, whereas the HL60 cells do.

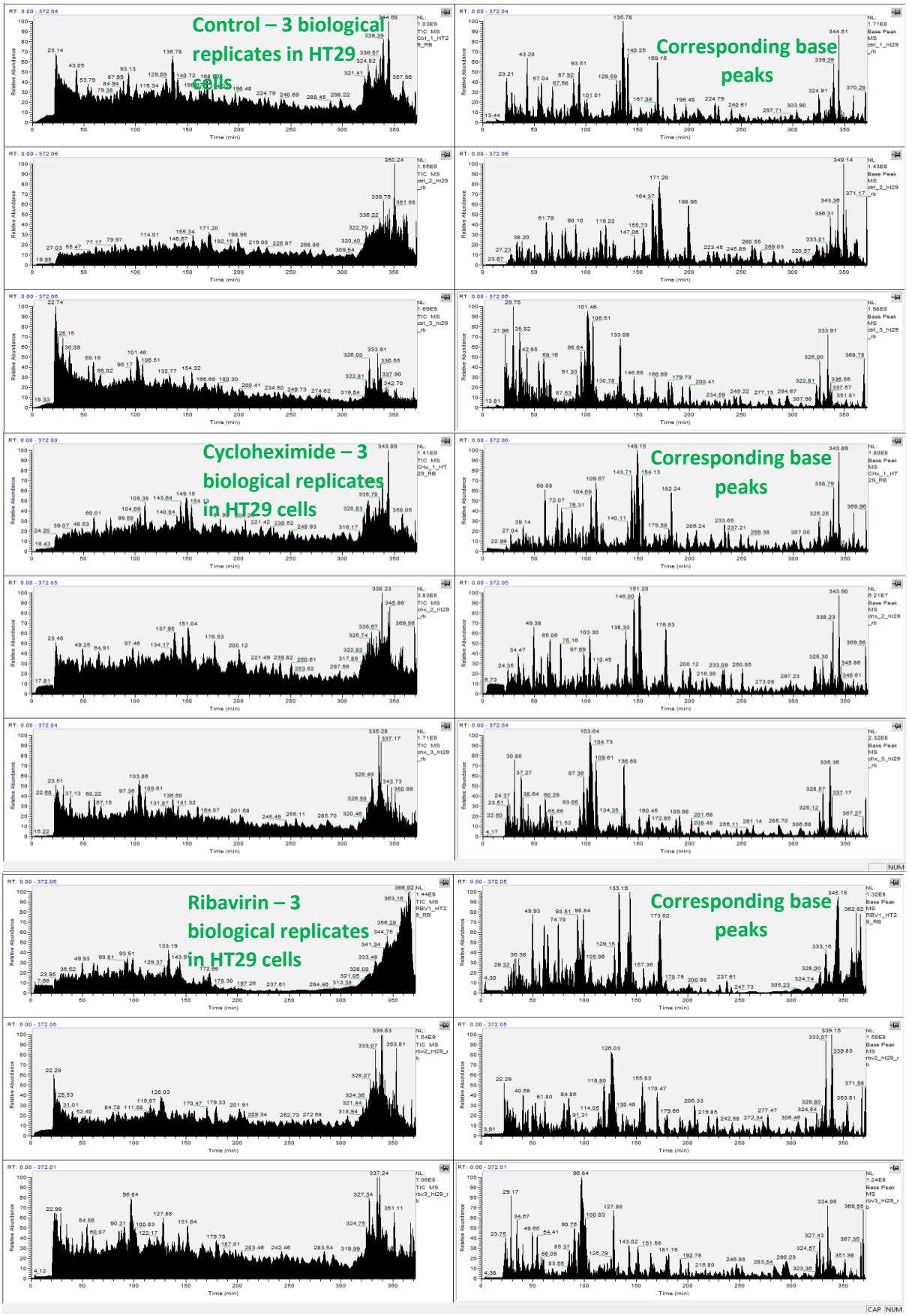

Figure 6-8 Relating to section 4.7.2, three biological replicates are displayed for the untreated controls, cycloheximide and ribavirin. Displayed in the left panels is the unfiltered LC-MS^2 chromatogram, in the right panels the base peaks are isolated from the unfiltered data.

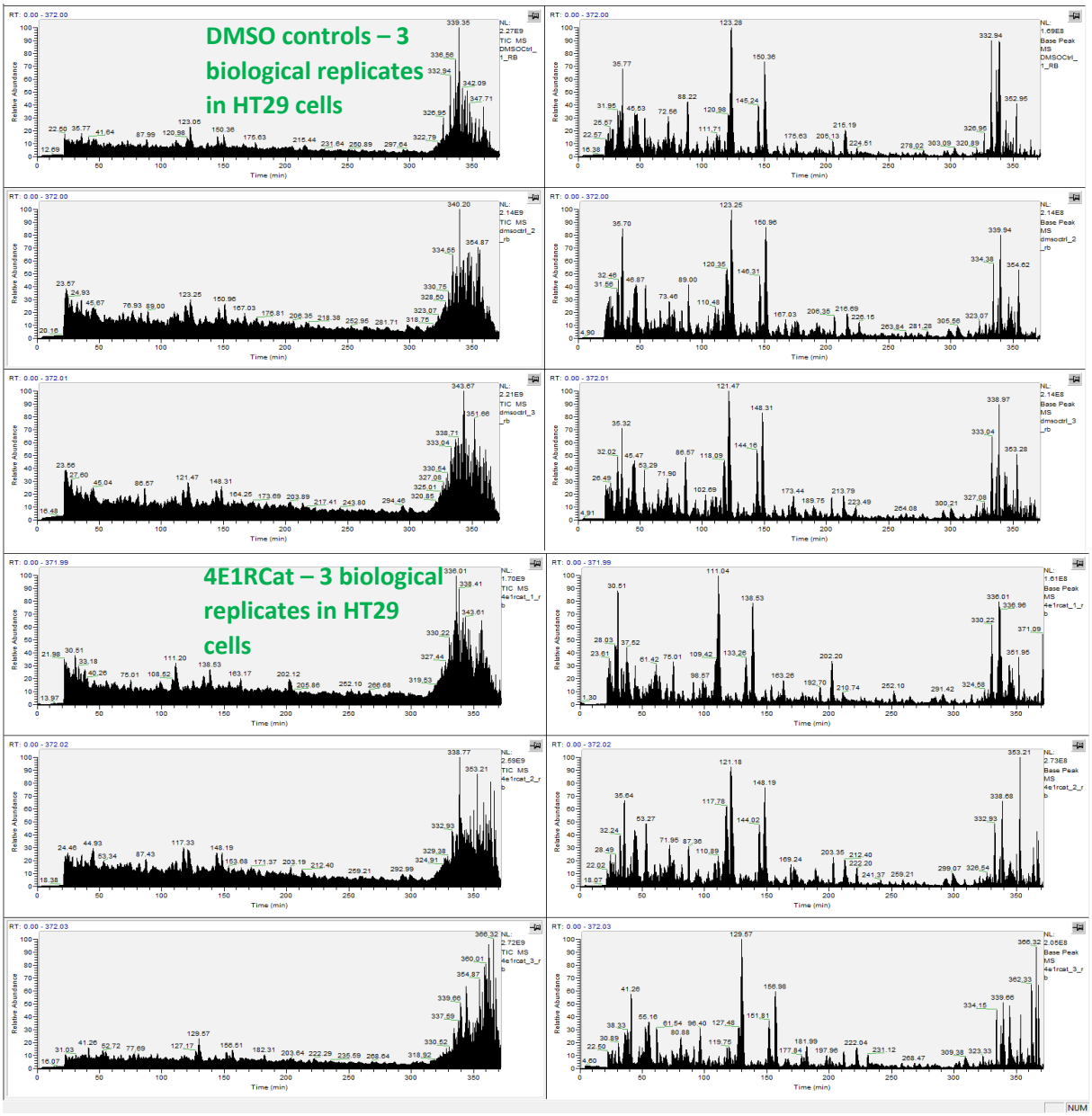

Figure 6-9 Relating to section 4.7.3, three biological replicates are displayed for 4E1RCat and the DMSO control. Ddisplayed in the left panels is the unfiltered LC-MS^2 chromatogram, in the right panels the base peaks are isolated from the unfiltered data.

Table 7 Proteins responding to treatment with cycloheximide.

Identified Proteins	T-Test (p-Value)	Up or Down regulated		Identified Proteins	T-Test (p-Value)	Up or Down regulated
PSME2 protein OS=Homo sapiens GN=PSME2 PE=2 SV=1	0.048	Down		Cluster of Sialic acid synthase OS=Homo sapiens GN=NANS PE=1 SV=2 (SIAS_HUMAN)	0.045	Up
Cluster of cDNA FLJ54047, highly similar to Alpha-1 catenin (Cadherin-associated protein) OS=Homo sapiens PE=2 SV=1 (B4E2G8_HUMAN)	0.048	Down		Testicular tissue protein Li 27 OS=Homo sapiens PE=2 SV=1	0.039	Up
SUMO-conjugating enzyme OS=Homo sapiens PE=2 SV=1	0.047	Down		cDNA FLJ76092, highly similar to Homo sapiens 5'-nucleotidase, cytosolic II-like 1 (NT5C2L1), mRNA OS=Homo sapiens PE=2 SV=1	0.034	Up
Endoribonuclease LACTB2 OS=Homo sapiens GN=LACTB2 PE=1 SV=2	0.046	Down		Cluster of 26S protease regulatory subunit 6A OS=Homo sapiens GN=PSMC3 PE=1 SV=1 (E9PM69_HUMAN)	0.033	Up
Ubiquitin-conjugating enzyme E2 K OS=Homo sapiens GN=UBE2K PE=1 SV=3	0.046	Down		Cluster of Epididymis secretory protein Li 21 OS=Homo sapiens GN=HEL-S-21 PE=2 SV=1 (V9HWG9_HUMAN)	0.032	Up
Cluster of Ubiquitin thioesterase OS=Homo sapiens PE=2 SV=1 (B4DPD5_HUMAN)	0.044	Down		Vacuolar protein sorting-associated protein 29 OS=Homo sapiens GN=VPS29 PE=1 SV=1	0.03	Up
MARCKS-related protein OS=Homo sapiens GN=MARCKSL1 PE=1 SV=2	0.036	Down		39S ribosomal protein L39, mitochondrial OS=Homo sapiens GN=MRPL39 PE=1 SV=3	0.028	Up
Cluster of cDNA PSEC0016 fis, clone NT2RM1001076, highly similar to Procollagen-lysine,2-oxoglutarate 5-dioxygenase 3 (EC 1.14.11.4) OS=Homo	0.036	Down		Cluster of Serine/threonine-protein phosphatase PP1-alpha catalytic subunit OS=Homo sapiens GN=PPP1CA PE=1 SV=1 (PP1A_HUMAN)	0.028	Up

sapiens PE=2 SV=1 (B3KQQ3_HUMAN)						
Cluster of cDNA FLJ55694, highly similar to Dipeptidyl-peptidase 1 (EC 3.4.14.1) OS=Homo sapiens PE=2 SV=1 (B4DJQ8_HUMAN)	0.034	Down		RNA binding protein (Autoantigenic, hnRNP-associated with lethal yellow) long isoform variant (Fragment) OS=Homo sapiens GN=RALY PE=1 SV=1	0.027	Up
Splicing factor 3B subunit 3 OS=Homo sapiens GN=SF3B3 PE=1 SV=4	0.031	Down		Cluster of Small nuclear ribonucleoprotein-associated protein N OS=Homo sapiens GN=SNRPN PE=1 SV=1 (RSMN_HUMAN)	0.026	Up
Synaptic vesicle membrane protein VAT-1 homolog OS=Homo sapiens GN=VAT1 PE=1 SV=2	0.031	Down		Cluster of Protein canopy homolog 2 OS=Homo sapiens GN=CNPY2 PE=1 SV=1 (CNPY2_HUMAN)	0.025	Up
Cluster of Spermine synthase OS=Homo sapiens GN=SMS PE=1 SV=2 (SPSY_HUMAN)	0.03	Down		Serpin B6 OS=Homo sapiens GN=SERPINB6 PE=1 SV=1	0.017	Up
L-aminoadipate-semialdehyde dehydrogenase-phosphopantetheinyl transferase OS=Homo sapiens GN=AASDHPPT PE=1 SV=2	0.026	Down		40S ribosomal protein S12 OS=Homo sapiens GN=RPS12 PE=1 SV=3	0.017	Up
Cluster of Proteasome subunit alpha type OS=Homo sapiens GN=PSMA6 PE=1 SV=1 (G3V295_HUMAN)	0.026	Down		ATP synthase subunit gamma OS=Homo sapiens PE=2 SV=1	0.015	Up
Cluster of DNA replication licensing factor MCM4 OS=Homo sapiens GN=MCM4 PE=1 SV=5 (MCM4_HUMAN)	0.024	Down		cDNA FLJ39996 fis, clone STOMA2002166, highly similar to Splicing factor 3B subunit 4 OS=Homo sapiens PE=2 SV=1	0.015	Up
Cluster of Epididymis secretory protein Li 71 OS=Homo sapiens GN=HEL-S-71 PE=2 SV=1 (V9HW41_HUMAN)	0.022	Down		Stathmin OS=Homo sapiens GN=STMN1 PE=2 SV=1	0.014	Up
Cluster of cDNA FLJ76962, highly similar	0.021	Down		Eukaryotic translation initiation factor 3 subunit	0.013	Up

to Homo sapiens nucleolar protein 5A (56kDa with KKE/D repeat) (NOL5A), mRNA OS=Homo sapiens PE=2 SV=1 (A8K9K6_HUMAN)				M OS=Homo sapiens GN=EIF3M PE=1 SV=1		
Similar to NADH dehydrogenase (Ubiquinone) 1 alpha subcomplex, 9 (39kD) (Fragment) OS=Homo sapiens PE=2 SV=1	0.02	Down		UPF0160 protein MYG1, mitochondrial OS=Homo sapiens GN=C12orf10 PE=1 SV=2	0.012	Up
Peptidyl-prolyl cis-trans isomerase NIMA-interacting 1 OS=Homo sapiens GN=PIN1 PE=1 SV=1	0.016	Down		SF3A2 protein (Fragment) OS=Homo sapiens GN=SF3A2 PE=2 SV=1	0.012	Up
Hsp70-binding protein 1 OS=Homo sapiens GN=HSPBP1 PE=1 SV=1	0.015	Down		Cluster of cDNA, FLJ94136, highly similar to Homo sapiens synaptotagmin binding, cytoplasmic RNA interacting protein (SYNCRIP), mRNA OS=Homo sapiens PE=2 SV=1 (B2R8Z8_HUMAN)	0.011	Up
Cluster of DDAH2 OS=Homo sapiens GN=HEL-S-277 PE=1 SV=1 (V9HW53_HUMAN)	0.015	Down		60S ribosomal protein L12 OS=Homo sapiens GN=RPL12 PE=1 SV=1	0.0087	Up
Cluster of Elongation factor 1-alpha 2 OS=Homo sapiens GN=EEF1A2 PE=1 SV=1 (EF1A2_HUMAN)	0.015	Down		7-alpha-hydroxycholest-4-en-3-one 12-alpha-hydroxylase OS=Homo sapiens GN=CYP8B1 PE=1 SV=1	0.0087	Up
E3 ubiquitin-protein ligase CHIP OS=Homo sapiens GN=STUB1 PE=1 SV=2	0.015	Down		Cluster of Testicular tissue protein Li 192 OS=Homo sapiens PE=2 SV=1 (A0A140VJW5_HUMAN)	0.0063	Up
Synaptogyrin-2 (Fragment) OS=Homo sapiens GN=SYNGR2 PE=1 SV=1	0.014	Down		Cluster of Hepatoma-derived growth factor OS=Homo sapiens GN=HDGF PE=1 SV=1 (HDGF_HUMAN)	0.0053	Up
DNA replication licensing factor MCM6 OS=Homo	0.013	Down		Phosphoserine phosphatase, isoform	0.0052	Up

sapiens GN=MCM6 PE=1 SV=1				CRA_b OS=Homo sapiens GN=PSPH PE=4 SV=1		
Cluster of Epididymis luminal protein 220 OS=Homo sapiens GN=HEL-S-70 PE=2 SV=1 (V9HW80_HUMAN)	0.013	Down		Peroxiredoxin-5, mitochondrial OS=Homo sapiens GN=PRDX5 PE=1 SV=4	0.0047	Up
Proteasome subunit beta type OS=Homo sapiens PE=2 SV=1	0.013	Down		Cluster of RNA-binding motif protein, X chromosome OS=Homo sapiens GN=RBMX PE=1 SV=3 (RBMX_HUMAN)	0.0044	Up
Splicing factor 3B subunit 5 OS=Homo sapiens GN=SF3B5 PE=1 SV=1	0.01	Down		cDNA FLJ90381 fis, clone NT2RP2005035, highly similar to Calumenin OS=Homo sapiens PE=2 SV=1	0.0021	Up
Cluster of Epiplakin OS=Homo sapiens GN=EPPK1 PE=1 SV=1 (A0A087X1U6_HUMAN)	0.01	Down		Asparagine--tRNA ligase, cytoplasmic OS=Homo sapiens GN=NARS PE=1 SV=1	0.0011	Up
UPF1 regulator of nonsense transcripts homolog (Yeast), isoform CRA_b OS=Homo sapiens GN=UPF1 PE=4 SV=1	0.0087	Down		Aspartate aminotransferase OS=Homo sapiens PE=2 SV=1	0.0008 8	Up
Cluster of Glutamate dehydrogenase OS=Homo sapiens PE=2 SV=1 (B4DMF5_HUMAN)	0.0083	Down		Glyoxylate reductase/hydroxypyruvate reductase OS=Homo sapiens GN=GRHPR PE=1 SV=1	0.0008	Up
40S ribosomal protein S10 OS=Homo sapiens GN=RPS10 PE=1 SV=1	0.0075	Down		Dynein heavy chain 14, axonemal OS=Homo sapiens GN=DNAH14 PE=2 SV=3	< 0.0001 0	Up
S-(hydroxymethyl)glutathione dehydrogenase OS=Homo sapiens GN=ADH5 PE=2 SV=1	0.0073	Down				
Aminoacylase-1 OS=Homo sapiens GN=ACY1 PE=4 SV=1	0.0065	Down				
Phosphomannomutase OS=Homo sapiens GN=PMM2 PE=1 SV=1	0.0059	Down				

Fatty acid synthase OS=Homo sapiens GN=FASN PE=1 SV=3	0.0012	Down				
Cluster of BUB3-interacting and GLEBS motif-containing protein ZNF207 OS=Homo sapiens GN=ZNF207 PE=1 SV=1 (J3QRS9_HUMAN)	0.00033	Down				

Table 8 Proteins responding to treatment with ribavirin.

Identified Proteins	T-Test (p-Value)	Up or Down regulated		Identified Proteins	T-Test (p-Value)	Up or Down regulated
Cluster of Histone H2B type 1-J OS=Homo sapiens GN=HIST1H2BJ PE=1 SV=3 (H2B1J_HUMAN)	0.0067	Down		Ribosomal L1 domain-containing protein 1 OS=Homo sapiens GN=RSL1D1 PE=1 SV=3	0.0087	Down
Cluster of Epididymis luminal protein 220 OS=Homo sapiens GN=HEL-S-70 PE=2 SV=1 (V9HW80_HUMAN)	0.037	Down		cDNA FLJ56566, highly similar to Small glutamine-rich tetratricopeptiderepeat-containing protein A OS=Homo sapiens PE=2 SV=1	0.046	Down
Cluster of Probable ATP-dependent RNA helicase DDX17 OS=Homo sapiens GN=DDX17 PE=1 SV=1 (A0A1W2PQ51_HUMAN)	0.014	Down		Cluster of cDNA, FLJ92825, highly similar to Homo sapiens SAR1a gene homolog 1 (S. cerevisiae) (SARA1), mRNA OS=Homo sapiens PE=2 SV=1 (B2R679_HUMAN)	0.021	Down
Cluster of RPS4X protein (Fragment) OS=Homo sapiens GN=RPS4X PE=2 SV=2 (Q96IR1_HUMAN)	0.019	Down		Cluster of NOP56 protein (Fragment) OS=Homo sapiens GN=NOP56 PE=2 SV=1 (A0PJ92_HUMAN)	0.038	Down
Cluster of Serine hydroxymethyltransferase, mitochondrial (Fragment) OS=Homo sapiens GN=SHMT2 PE=1 SV=1 (G3V4W5_HUMAN)	0.00086	Down		Protein dpy-30 homolog OS=Homo sapiens GN=DPY30 PE=1 SV=1	0.017	Down
Cluster of Ribosomal protein L7, isoform CRA_a OS=Homo sapiens GN=RPL7 PE=4 SV=1 (A0A024R814_HUMAN)	0.029	Down		Hypoxanthine-guanine phosphoribosyltransferase OS=Homo sapiens GN=HPRT1 PE=1 SV=2	0.027	Down
Ribosomal protein L23, isoform CRA_b OS=Homo sapiens GN=RPL23 PE=3 SV=1	0.0075	Down		DNA helicase OS=Homo sapiens GN=MCM3 PE=2 SV=1	0.0016	Down
40S ribosomal protein S3 OS=Homo sapiens GN=RPS3 PE=1 SV=2	0.033	Down		ATP synthase subunit delta, mitochondrial OS=Homo sapiens GN=ATP5D PE=1 SV=2	0.002	Down

Cluster of Epididymis secretory protein Li 71 OS=Homo sapiens GN=HEL-S-71 PE=2 SV=1 (V9HW41_HUMAN)	0.038	Down		BUB3-interacting and GLEBS motif-containing protein ZNF207 OS=Homo sapiens GN=ZNF207 PE=1 SV=1	1.00E-04	Down
Cluster of Staphylococcal nuclease domain-containing protein 1 OS=Homo sapiens GN=SND1 PE=1 SV=1 (SND1_HUMAN)	0.009	Down		cDNA FLJ57877, highly similar to Cleavage and polyadenylation specificity factor 7 OS=Homo sapiens PE=2 SV=1	0.046	Down
40S ribosomal protein S3a OS=Homo sapiens GN=RPS3A PE=2 SV=1	0.045	Down		Endothelial differentiation-related factor 1 OS=Homo sapiens GN=EDF1 PE=1 SV=1	0.029	Down
Cluster of cDNA FLJ59240, highly similar to Far upstream element-binding protein 1 OS=Homo sapiens PE=2 SV=1 (B4DWL1_HUMAN)	0.014	Down		RNA-binding protein 42 OS=Homo sapiens GN=RBM42 PE=1 SV=1	0.00061	Down
Cluster of Hydroxysteroid (17-beta) dehydrogenase 4, isoform CRA_b (Fragment) OS=Homo sapiens GN=HSD17B4 PE=2 SV=1 (A0A0S2Z4J1_HUMAN)	0.048	Down				
40S ribosomal protein S13 OS=Homo sapiens GN=RPS13 PE=1 SV=2	0.043	Down		Cluster of Keratin, type I cytoskeletal 18 OS=Homo sapiens GN=KRT18 PE=1 SV=2 (K1C18_HUMAN)	0.043	Up
ATP synthase subunit O, mitochondrial OS=Homo sapiens GN=ATP5O PE=1 SV=1	0.03	Down		Cluster of Actin, alpha skeletal muscle OS=Homo sapiens GN=ACTA1 PE=1 SV=3 (A6NL76_HUMAN)	0.036	Up
60S ribosomal protein L10a OS=Homo sapiens GN=RPL10A PE=1 SV=2	0.0051	Down		Cluster of Annexin OS=Homo sapiens GN=ANXA2 PE=3 SV=1 (A0A024R5Z7_HUMAN)	0.04	Up
40S ribosomal protein S30 OS=Homo sapiens GN=FAU PE=1 SV=1	0.015	Down		Heterogeneous nuclear ribonucleoprotein K OS=Homo sapiens GN=HNRNPK PE=1 SV=1	0.021	Up

Cluster of Cyclin-dependent kinase 16 OS=Homo sapiens GN=CDK16 PE=1 SV=1 (CDK16_HUMAN)	0.014	Down		Cluster of Annexin A1 OS=Homo sapiens GN=ANXA1 PE=1 SV=2 (ANXA1_HUMAN)	0.00095	Up
2'-5'-oligoadenylate synthetase 3, 100kDa, isoform CRA_a OS=Homo sapiens GN=OAS3 PE=4 SV=1	0.024	Down		Protein S100-A6 OS=Homo sapiens GN=S100A6 PE=1 SV=1	0.049	Up
Heterogeneous nuclear ribonucleoprotein R OS=Homo sapiens GN=HNRNPR PE=1 SV=1	0.043	Down		Cluster of Aspartate aminotransferase OS=Homo sapiens GN=GOT2 PE=4 SV=1 (A0A024R6W0_HUMAN)	0.0081	Up
Protein POF1B OS=Homo sapiens GN=POF1B PE=1 SV=3	0.012	Down		Cluster of MHC class I antigen (Fragment) OS=Homo sapiens GN=HLA-A PE=3 SV=1 (E5BBI6_HUMAN)	0.042	Up
Testicular tissue protein Li 75 OS=Homo sapiens PE=2 SV=1	0.033	Down		Cluster of Proteasome subunit alpha type OS=Homo sapiens GN=PSMA6 PE=1 SV=1 (G3V295_HUMAN)	0.02	Up
cDNA FLJ76387, highly similar to Homo sapiens splicing factor, arginine/serine-rich 9 (SFRS9), mRNA OS=Homo sapiens PE=2 SV=1	0.041	Down		Cluster of ARP3 actin-related protein 3 homolog (Yeast), isoform CRA_a OS=Homo sapiens GN=ACTR3 PE=3 SV=1 (A0A024RAI1_HUMAN)	0.011	Up
Cluster of DNA helicase OS=Homo sapiens PE=2 SV=1 (B3KMX0_HUMAN)	0.046	Down		Epididymis secretory sperm binding protein Li 47e OS=Homo sapiens GN=HEL-S-47e PE=2 SV=1	0.047	Up
Epidermal growth factor receptor kinase substrate 8-like protein 1 OS=Homo sapiens GN=EPS8L1 PE=1 SV=1	0.046	Down		Prefoldin subunit 2 OS=Homo sapiens GN=PFDN2 PE=1 SV=1	0.00014	Up
Small nuclear ribonucleoprotein Sm D2 OS=Homo sapiens GN=SNRPD2 PE=1 SV=1	0.003	Down		Ubiquitin carboxyl-terminal hydrolase 14 OS=Homo sapiens GN=USP14 PE=1 SV=2	0.022	Up

U1 small nuclear ribonucleoprotein 70 kDa OS=Homo sapiens GN=SNRNP70 PE=1 SV=2	0.022	Down		14-3-3 protein sigma OS=Homo sapiens GN=SFN PE=1 SV=1	0.033	Up
Cluster of Hydroxysteroid dehydrogenase-like protein 2 OS=Homo sapiens GN=HSDL2 PE=1 SV=1 (HSDL2_HUMAN)	0.0084	Down		Cluster of Kallikrein I OS=Homo sapiens GN=KLNI PE=3 SV=1 (A0A1R3UCE8_HUMAN)	0.0086	Up
ADP-sugar pyrophosphatase OS=Homo sapiens GN=NUDT5 PE=1 SV=1	0.032	Down		Ubiquitin thioesterase OS=Homo sapiens PE=2 SV=1	0.01	Up
Cluster of 40S ribosomal protein S6 OS=Homo sapiens GN=RPS6 PE=2 SV=1 (Q96DV6_HUMAN)	0.032	Down		Cluster of Tight junction protein ZO-1 (Fragment) OS=Homo sapiens GN=TJP1 PE=2 SV=1 (A9CQZ8_HUMAN)	0.02	Up
Septin-9 OS=Homo sapiens GN=SEPT9 PE=1 SV=2	0.0077	Down		SUMO-activating enzyme subunit 2 OS=Homo sapiens GN=UBA2 PE=1 SV=2	0.043	Up
Cluster of FGFR2-BICC1 fusion kinase protein OS=Homo sapiens GN=FGFR2-BICC1 PE=2 SV=1 (V5YQU3_HUMAN)	0.027	Down		ATP synthase subunit gamma OS=Homo sapiens PE=2 SV=1	0.00072	Up
Cluster of UPF1 regulator of nonsense transcripts homolog (Yeast), isoform CRA_b OS=Homo sapiens GN=UPF1 PE=4 SV=1 (A0A024R7L5_HUMAN)	0.04	Down		ATP-binding cassette sub-family E member 1 OS=Homo sapiens GN=ABCE1 PE=1 SV=1	0.045	Up
Cluster of 40S ribosomal protein S10 OS=Homo sapiens GN=RPS10 PE=1 SV=1 (RS10_HUMAN)	0.038	Down		Nuclear transport factor 2 OS=Homo sapiens GN=NUTF2 PE=1 SV=1	0.05	Up
Ras-GTPase activating protein SH3 domain-binding protein 2, isoform CRA_a OS=Homo sapiens GN=G3BP2 PE=4 SV=1	0.0082	Down		Coatomer subunit delta OS=Homo sapiens GN=ARCN1 PE=2 SV=1	0.015	Up
Phosphoserine aminotransferase OS=Homo sapiens PE=2 SV=1	0.0067	Down		Tubulin-folding cofactor B (Fragment) OS=Homo sapiens GN=TBCB PE=1 SV=8	0.015	Up
Cluster of Pyrroline-5-carboxylate reductase	0.04	Down		SEC13-like 1 isoform b variant (Fragment)	0.0058	Up

OS=Homo sapiens PE=2 SV=1 (E7D7X9_HUMAN)				OS=Homo sapiens PE=2 SV=1		
Endoribonuclease LACTB2 OS=Homo sapiens GN=LACTB2 PE=1 SV=2	0.018	Down		Apoptosis-associated speck-like protein containing a CARD OS=Homo sapiens GN=PYCARD PE=1 SV=2	0.04	Up
Cluster of Acetyl-CoA acetyltransferase, cytosolic variant (Fragment) OS=Homo sapiens PE=2 SV=1 (Q59GW6_HUMAN)	0.0057	Down		Cluster of cDNA, FLJ93976, highly similar to Homo sapiens COP9 homolog (COP9), mRNA OS=Homo sapiens PE=2 SV=1 (B2R8N1_HUMAN)	0.046	Up
Cluster of cDNA FLJ75871, highly similar to Homo sapiens staufen, RNA binding protein (STAU), transcript variant T3, mRNA OS=Homo sapiens PE=2 SV=1 (A8K622_HUMAN)	0.024	Down		Cluster of cDNA FLJ55936, highly similar to Polypyrimidine tract-binding protein 2 OS=Homo sapiens PE=2 SV=1 (B4DSS8_HUMAN)	0.049	Up
Nucleolar RNA helicase 2 OS=Homo sapiens GN=DDX21 PE=1 SV=5	0.018	Down		26S proteasome non-ATPase regulatory subunit 14 OS=Homo sapiens GN=PSMD14 PE=1 SV=1	0.0034	Up
Cluster of Rho guanine nucleotide exchange factor 1 OS=Homo sapiens GN=ARHGEF1 PE=1 SV=2 (ARHG1_HUMAN)	0.0012	Down		Putative uncharacterized protein DKFZp686B04128 OS=Homo sapiens GN=DKFZp686B04128 PE=2 SV=1	0.0069	Up

Table 9 Proteins responding to treatment with 4E1RCat

Identified Proteins	T-Test (p-Value)	Up or Down regulated		Identified Proteins	T-Test (p-Value)	Up or Down regulated
Cluster of Keratin, type I cytoskeletal 18 OS=Homo sapiens GN=KRT18 PE=1 SV=2 (K1C18_HUMAN)	0.034	Down		60S ribosomal protein L8 OS=Homo sapiens GN=RPL8 PE=1 SV=2	0.034	Up
Cluster of Epididymis luminal protein 33 OS=Homo sapiens GN=HEL-S-72p PE=2 SV=1 (V9HW22_HUMAN)	0.047	Down		Cluster of Hypoxia up-regulated protein 1 OS=Homo sapiens GN=HYOU1 PE=1 SV=1 (HYOU1_HUMAN)	0.025	Up
Cluster of Dehydrogenase/reductase SDR family member 2, mitochondrial OS=Homo sapiens GN=DHRS2 PE=1 SV=4 (DHRS2_HUMAN)	0.024	Down		Cluster of ATP-dependent RNA helicase A OS=Homo sapiens GN=DHX9 PE=1 SV=4 (DHX9_HUMAN)	0.05	Up
Cluster of Titin OS=Homo sapiens GN=TTN PE=1 SV=1 (A0A0A0MTS7_HUMAN)	0.0014	Down		Peptidyl-prolyl cis-trans isomerase FKBP4 OS=Homo sapiens GN=FKBP4 PE=1 SV=3	0.012	Up
Cluster of Adenylate kinase 2, mitochondrial OS=Homo sapiens GN=AK2 PE=1 SV=2 (KAD2_HUMAN)	0.014	Down		Cluster of Bifunctional glutamate/proline--tRNA ligase OS=Homo sapiens GN=EPRS PE=1 SV=5 (SYEP_HUMAN)	0.027	Up
Trifunctional enzyme subunit beta, mitochondrial OS=Homo sapiens GN=HADHB PE=1 SV=3	0.032	Down		Cluster of Proteasome subunit alpha type-1 OS=Homo sapiens GN=PSMA1 PE=1 SV=1 (PSA1_HUMAN)	0.002	Up
Cluster of Adenylyl cyclase-associated protein OS=Homo sapiens PE=2 SV=1 (B2RDY9_HUMAN)	0.022	Down		Cluster of Sequestosome-1 OS=Homo sapiens GN=SQSTM1 PE=1	0.015	Up

				SV=1 (SQSTM_HUMAN)		
Cluster of ATPase family AAA domain-containing protein 3A (Fragment) OS=Homo sapiens GN=ATAD3A PE=1 SV=1 (H0Y2W2_HUMAN)	0.043	Down		cDNA FLJ75881, highly similar to Homo sapiens transferrin receptor (p90, CD71) (TFRC), mRNA OS=Homo sapiens PE=2 SV=1	0.013	Up
Lysozyme C OS=Homo sapiens GN=LYZ PE=1 SV=1	0.022	Down		cDNA, FLJ93269, highly similar to Homo sapiens mitochondrial ribosomal protein L15 (MRPL15), nuclear gene encoding mitochondrial protein, mRNA OS=Homo sapiens PE=2 SV=1	0.044	Up
Cluster of EH-domain containing 4, isoform CRA_a OS=Homo sapiens GN=EHD4 PE=3 SV=1 (A0A024R9N6_HUMAN)	0.02	Down		60S ribosomal protein L34 OS=Homo sapiens GN=RPL34 PE=1 SV=3	0.0095	Up
Cytochrome c oxidase subunit 6B1 OS=Homo sapiens GN=COX6B1 PE=1 SV=2	0.048	Down		Isocitrate dehydrogenase [NADP] OS=Homo sapiens PE=2 SV=1	0.023	Up
Ubiquitin/ISG15-conjugating enzyme E2 L6 OS=Homo sapiens GN=UBE2L6 PE=1 SV=4	0.019	Down		60S ribosomal protein L35 OS=Homo sapiens GN=RPL35 PE=1 SV=2	0.015	Up
Cysteine--tRNA ligase, cytoplasmic OS=Homo sapiens GN=CARS PE=1 SV=1	0.048	Down		Epididymis secretory protein Li 102 OS=Homo sapiens GN=HEL-S-102 PE=2 SV=1	0.0016	Up
H/ACA ribonucleoprotein complex subunit 3 OS=Homo sapiens GN=NOP10 PE=1 SV=1	1.00 E-04	Down		Aspartate aminotransferase OS=Homo sapiens PE=2 SV=1	0.043	Up
Cluster of PURA protein (Fragment) OS=Homo sapiens GN=PURA PE=2 SV=1 (Q2NLC9_HUMAN)	0.011	Down		Cluster of Heat shock 70 kDa protein 4L OS=Homo sapiens	0.014	Up

				GN=HSPA4L PE=1 SV=1 (E9PDE8_HUMAN)		
Mitochondrial transcription factor A OS=Homo sapiens PE=4 SV=1	0.021	Down		cDNA FLJ60607, highly similar to Acyl-protein thioesterase 1 (EC 3.1.2.-) OS=Homo sapiens PE=2 SV=1	0.037	Up
DNA helicase OS=Homo sapiens GN=MCM3 PE=2 SV=1	0.005	Down		Glutamate--cysteine ligase regulatory subunit OS=Homo sapiens GN=GCLM PE=1 SV=1	0.042	Up
Isochorismatase domain-containing protein 2 OS=Homo sapiens GN=ISOC2 PE=1 SV=1	0.024	Down		Acyl-protein thioesterase 2 OS=Homo sapiens GN=LYPLA2 PE=1 SV=1	0.00073	Up
				Cluster of Heme oxygenase 2 (Fragment) OS=Homo sapiens GN=HMOX2 PE=1 SV=1 (I3L159_HUMAN)	0.035	Up
Cluster of 60S ribosomal protein L3 OS=Homo sapiens GN=RPL3 PE=1 SV=2 (RL3_HUMAN)	0.012	Up		Cluster of cDNA FLJ54671, highly similar to Calcium-binding mitochondrial carrier protein Aralar2 OS=Homo sapiens PE=2 SV=1 (B7Z2E2_HUMAN)	0.033	Up
Cluster of Ribosomal protein L10 isoform A (Fragment) OS=Homo sapiens GN=RPL10 PE=2 SV=1 (X5D2T3_HUMAN)	0.0034	Up		Bifunctional coenzyme A synthase OS=Homo sapiens GN=COASY PE=1 SV=4	0.0063	Up
Cluster of 60S ribosomal protein L7a OS=Homo sapiens GN=RPL7A PE=1 SV=2 (RL7A_HUMAN)	0.046	Up		Sulfiredoxin-1 OS=Homo sapiens GN=SRXN1 PE=1 SV=2	0.018	Up
Cluster of Thioredoxin reductase 1, cytoplasmic OS=Homo sapiens	0.041	Up		Nuclear protein localization 4 homolog (S.	0.044	Up

GN=TXNRD1 PE=1 SV=3 (TRXR1_HUMAN)				cerevisiae), isoform CRA_a OS=Homo sapiens GN=NPLOC4 PE=4 SV=1		
60S ribosomal protein L18a OS=Homo sapiens GN=RPL18A PE=1 SV=2	0.0082	Up		Translocon-associated protein subunit delta OS=Homo sapiens GN=SSR4 PE=1 SV=1	0.031	Up

Table 10 Proteins responding to treatment with DMSO

Identified Proteins	**T-Test (p-Value)**	**Up or Down regulated**		**Identified Proteins**	**T-Test (p-Value)**	**Up or Down regulated**
Cluster of Epididymis luminal protein 33 OS=Homo sapiens GN=HEL-S-72p PE=2 SV=1 (V9HW22_HUMAN)	0.00068	Down		Cluster of D-dopachrome tautomerase OS=Homo sapiens GN=DDT PE=2 SV=1 (Q53Y51_HUMAN)	0.042	Down
Cluster of Filamin-A OS=Homo sapiens GN=FLNA PE=1 SV=4 (FLNA_HUMAN)	0.00013	Down		Cluster of Alpha-enolase OS=Homo sapiens GN=ENO1 PE=1 SV=2 (ENOA_HUMAN)	0.043	Down
Cluster of Polyadenylate-binding protein OS=Homo sapiens PE=2 SV=1 (B4DQX0_HUMAN)	2.00E-04	Down		Cluster of Eukaryotic translation initiation factor 5A (Fragment) OS=Homo sapiens GN=EIF5A PE=1 SV=8 (I3L397_HUMAN)	0.043	Down
Cluster of Heterogeneous nuclear ribonucleoprotein K, isoform CRA_d OS=Homo sapiens GN=HNRPK PE=4 SV=1 (A0A024R228_HUMAN)	0.00034	Down		Cluster of Heterogeneous nuclear ribonucleoprotein H2 OS=Homo sapiens GN=HNRNPH2 PE=1 SV=1 (HNRH2_HUMAN)	0.043	Down
Cluster of 60S acidic ribosomal protein P2 OS=Homo sapiens GN=RPLP2 PE=1 SV=1 (RLA2_HUMAN)	0.00066	Down		Protein DJ-1 OS=Homo sapiens GN=PARK7 PE=1 SV=1	0.043	Down
Cluster of T-complex protein 1 subunit zeta-2	0.0011	Down		Splicing factor 3A subunit 1 OS=Homo	0.043	Down

OS=Homo sapiens GN=CCT6B PE=1 SV=5 (TCPW_HUMAN)				sapiens GN=SF3A1 PE=1 SV=1		
Thioredoxin OS=Homo sapiens GN=TXN PE=2 SV=1	0.00046	Down		Cluster of SWI/SNF related, matrix associated, actin dependent regulator of chromatin, subfamily e, member 1, isoform CRA_a OS=Homo sapiens GN=SMARCE1 PE=4 SV=1 (A0A024R1S7_HUMAN)	0.043	Down
Protein S100 OS=Homo sapiens GN=HEL-S-43 PE=2 SV=1	0.00058	Down		cDNA FLJ37476 fis, clone BRAWH2012827, highly similar to Homo sapiens BH3 interacting domain death agonist (BID), transcript variant 1, mRNA OS=Homo sapiens PE=2 SV=1	0.044	Down
Cluster of cDNA FLJ75422, highly similar to Homo sapiens capping protein (actin filament) muscle Z-line, alpha 1, mRNA OS=Homo sapiens PE=2 SV=1 (A8K0T9_HUMAN)	0.0011	Down		Methylosome subunit pICln OS=Homo sapiens GN=CLNS1A PE=1 SV=1	0.044	Down
Cluster of Nucleosome assembly protein 1-like 1 (Fragment) OS=Homo sapiens GN=NAP1L1 PE=1 SV=1 (H0YHC3_HUMAN)	0.00079	Down		Pyridoxine 5'-phosphate oxidase variant (Fragment) OS=Homo sapiens PE=2 SV=1	0.044	Down
Cluster of Cold shock domain containing E1, RNA-binding, isoform CRA_a OS=Homo sapiens GN=CSDE1 PE=4 SV=1 (A0A024R0E2_HUMAN)	0.00084	Down		Cluster of Ribonuclease T2 OS=Homo sapiens GN=RNASET2 PE=1 SV=1 (A0A087WZM2_HUMAN)	0.045	Down
Protein POF1B OS=Homo sapiens GN=POF1B PE=1 SV=3	0.00049	Down		Cluster of UPF1 regulator of nonsense transcripts homolog (Yeast), isoform CRA_b OS=Homo sapiens GN=UPF1 PE=4 SV=1 (A0A024R7L5_HUMAN)	0.045	Down

Cluster of Chromobox protein homolog 3 OS=Homo sapiens GN=CBX3 PE=1 SV=4 (CBX3_HUMAN)	0.00042	Down		Chloride intracellular channel protein OS=Homo sapiens PE=3 SV=1	0.046	Down
Catechol O-methyltransferase OS=Homo sapiens GN=COMT PE=1 SV=2	0.00084	Down		Coactosin-like protein OS=Homo sapiens GN=COTL1 PE=1 SV=3	0.046	Down
GRB2 protein (Fragment) OS=Homo sapiens GN=GRB2 PE=2 SV=1	0.0011	Down		Apoptosis inhibitor 5 OS=Homo sapiens GN=API5 PE=1 SV=3	0.046	Down
Cluster of PDZ and LIM domain protein 5 OS=Homo sapiens GN=PDLIM5 PE=1 SV=5 (PDLI5_HUMAN)	0.00081	Down		Eukaryotic translation elongation factor 1 beta 2, isoform CRA_a OS=Homo sapiens GN=EEF1B2 PE=3 SV=1	0.047	Down
Cluster of Testicular secretory protein Li 8 OS=Homo sapiens PE=2 SV=1 (A0A140VK08_HUMAN)	0.00041	Down		Casein kinase II alpha 1 subunit isoform a (Fragment) OS=Homo sapiens GN=CSNK2A1 PE=2 SV=1	0.047	Down
Protein S100-P OS=Homo sapiens GN=S100P PE=1 SV=2	1.00E-04	Down		Proteasome subunit alpha type-3 OS=Homo sapiens GN=PSMA3 PE=1 SV=2	0.048	Down
Cluster of cDNA FLJ56531, highly similar to UV excision repair protein RAD23 homolog B OS=Homo sapiens PE=2 SV=1 (B4DEA3_HUMAN)	0.00068	Down		Cluster of Proteasome subunit beta type (Fragment) OS=Homo sapiens PE=2 SV=1 (Q53FT8_HUMAN)	0.048	Down
Proteasome subunit beta type-6 OS=Homo sapiens GN=PSMB6 PE=1 SV=4	0.00065	Down		Cluster of ATP synthase subunit beta (Fragment) OS=Homo sapiens GN=ATP5B PE=2 SV=1 (Q0QEN7_HUMAN)	0.049	Down
Cluster of Band 4.1-like protein 1 OS=Homo sapiens GN=EPB41L1 PE=1 SV=2 (E41L1_HUMAN)	0.0011	Down		Cluster of Septin-9 OS=Homo sapiens GN=SEPT9 PE=1 SV=2 (SEPT9_HUMAN)	0.049	Down
Clathrin interactor 1 isoform 2 (Fragment) OS=Homo sapiens GN=CLINT1 PE=2 SV=1	0.00067	Down		Cluster of 26S proteasome regulatory subunit 8 OS=Homo sapiens GN=PSMC5	0.049	Down

				PE=1 SV=1 (PRS8_HUMAN)		
Aminoacylase-1 OS=Homo sapiens GN=ACY1 PE=4 SV=1	0.00031	Down		Cluster of Histone H4 OS=Homo sapiens GN=HIST1H4A PE=1 SV=2 (H4_HUMAN)	0.00099	Up
ATP synthase subunit delta, mitochondrial OS=Homo sapiens GN=ATP5D PE=1 SV=2	1.00E-04	Down		Cluster of Thioredoxin reductase 1, cytoplasmic OS=Homo sapiens GN=TXNRD1 PE=1 SV=3 (TRXR1_HUMAN)	0.00059	Up
BJ-HCC-24 tumor antigen OS=Homo sapiens PE=2 SV=1	0.00035	Down		Cluster of 4F2 cell-surface antigen heavy chain OS=Homo sapiens GN=SLC3A2 PE=1 SV=3 (4F2_HUMAN)	0.001	Up
Cluster of Myosin light chain 6B OS=Homo sapiens GN=MYL6B PE=1 SV=1 (F8W1I5_HUMAN)	0.0013	Down		Histone H1.5 OS=Homo sapiens GN=HIST1H1B PE=1 SV=3	6.00E-04	Up
Cluster of Ras-GTPase activating protein SH3 domain-binding protein 2, isoform CRA_a OS=Homo sapiens GN=G3BP2 PE=4 SV=1 (A0A024RDE5_HUMAN)	0.0013	Down		High mobility group protein B2 OS=Homo sapiens GN=HMGB2 PE=1 SV=2	0.00064	Up
Cluster of Tropomyosin alpha-3 chain OS=Homo sapiens GN=TPM3 PE=1 SV=2 (TPM3_HUMAN)	0.0014	Down		Cluster of 40S ribosomal protein S10 OS=Homo sapiens GN=RPS10 PE=1 SV=1 (RS10_HUMAN)	0.00017	Up
Inorganic pyrophosphatase OS=Homo sapiens GN=PPA1 PE=1 SV=2	0.0016	Down		Cluster of Voltage-dependent anion channel 2, isoform CRA_c OS=Homo sapiens GN=VDAC2 PE=4 SV=1 (A0A024QZT0_HUMAN)	0.00073	Up
Acyl carrier protein, mitochondrial OS=Homo sapiens GN=NDUFAB1 PE=1 SV=3	0.0016	Down		Histone H2A.V OS=Homo sapiens GN=H2AFV PE=1 SV=3	0.00099	Up
Cluster of Epidermal growth factor receptor kinase substrate 8-like protein 1 OS=Homo sapiens GN=EPS8L1 PE=1 SV=1 (B4DKV7_HUMAN)	0.0017	Down		ATP synthase subunit gamma OS=Homo sapiens PE=2 SV=1	0.00034	Up

Cluster of S100A10 protein (Fragment) OS=Homo sapiens GN=S100A10 PE=2 SV=1 (Q6FGE5_HUMAN)	0.0023	Down		Cluster of Methylcrotonoyl-CoA carboxylase beta chain, mitochondrial OS=Homo sapiens GN=MCCC2 PE=1 SV=1 (MCCB_HUMAN)	0.0009 6	Up
Lactoylglutathione lyase OS=Homo sapiens GN=HEL-S-74 PE=2 SV=1	0.0022	Down		Cluster of Transcriptional activator protein Pur-alpha OS=Homo sapiens GN=PURA PE=1 SV=2 (PURA_HUMAN)	0.0009 6	Up
Cluster of Nuclear autoantigenic sperm protein OS=Homo sapiens GN=NASP PE=1 SV=2 (NASP_HUMAN)	0.0021	Down		Dolichyl-diphosphooligosaccharide-protein glycosyltransferase subunit 2 OS=Homo sapiens GN=RPN2 PE=1 SV=3	0.001	Up
Cluster of cDNA FLJ76823, highly similar to Homo sapiens splicing factor, arginine/serine-rich 6 (SFRS6), mRNA OS=Homo sapiens PE=2 SV=1 (A8K588_HUMAN)	0.0023	Down		Isocitrate dehydrogenase [NAD] subunit, mitochondrial OS=Homo sapiens GN=IDH3B PE=1 SV=1	0.0007 5	Up
Proteasome subunit beta type OS=Homo sapiens PE=2 SV=1	0.002	Down		ATP-dependent 6-phosphofructokinase, liver type OS=Homo sapiens GN=PFKL PE=1 SV=6	0.0004 7	Up
Spermine synthase OS=Homo sapiens GN=SMS PE=1 SV=2	0.0022	Down		cDNA FLJ52100 OS=Homo sapiens PE=2 SV=1	0.0003 6	Up
Succinate--CoA ligase [GDP-forming] subunit beta, mitochondrial OS=Homo sapiens GN=SUCLG2 PE=1 SV=2	0.0018	Down		SF3A2 protein (Fragment) OS=Homo sapiens GN=SF3A2 PE=2 SV=1	0.0012	Up
cDNA FLJ59206, highly similar to Eukaryotic translation initiation factor 4B OS=Homo sapiens PE=2 SV=1	0.0019	Down		Cytochrome c1, heme protein, mitochondrial OS=Homo sapiens GN=CYC1 PE=1 SV=3	0.0013	Up
Cluster of DDAH2 OS=Homo sapiens GN=HEL-S-277 PE=1	0.002	Down		Cluster of Epididymis tissue sperm binding protein Li 3a OS=Homo	0.0015	Up

SV=1 (V9HW53_HUMAN)				sapiens PE=1 SV=1 (E9KL35_HUMAN)		
Cluster of Inorganic pyrophosphatase 2, mitochondrial OS=Homo sapiens GN=PPA2 PE=1 SV=2 (IPYR2_HUMAN)	0.0025	Down		Cluster of Transmembrane 9 superfamily member OS=Homo sapiens GN=SMBP PE=2 SV=1 (Q96JZ5_HUMAN)	0.0016	Up
Cluster of Keratin, type I cytoskeletal 18 OS=Homo sapiens GN=KRT18 PE=1 SV=2 (K1C18_HUMAN)	0.003	Down		RNA binding protein (Autoantigenic, hnRNP-associated with lethal yellow) long isoform variant (Fragment) OS=Homo sapiens GN=RALY PE=1 SV=1	0.0017	Up
Cluster of Alpha-actinin-4 OS=Homo sapiens GN=ACTN4 PE=1 SV=2 (ACTN4_HUMAN)	0.0032	Down		Succinate--CoA ligase [ADP/GDP-forming] subunit alpha, mitochondrial OS=Homo sapiens GN=SUCLG1 PE=1 SV=4	0.0017	Up
Cluster of Peptidyl-prolyl cis-trans isomerase A OS=Homo sapiens GN=PPIA PE=1 SV=2 (PPIA_HUMAN)	0.0029	Down		Cluster of Histone H2B type 1-J OS=Homo sapiens GN=HIST1H2BJ PE=1 SV=3 (H2B1J_HUMAN)	0.0021	Up
40S ribosomal protein S12 OS=Homo sapiens GN=RPS12 PE=1 SV=3	0.003	Down		Cluster of MHC class I antigen (Fragment) OS=Homo sapiens GN=HLA-A PE=3 SV=1 (E5BBI6_HUMAN)	0.0022	Up
Cluster of Eukaryotic peptide chain release factor GTP-binding subunit ERF3A OS=Homo sapiens GN=GSPT1 PE=1 SV=1 (ERF3A_HUMAN)	0.0027	Down		Cluster of Histone 1, H1e OS=Homo sapiens GN=HIST1H1E PE=2 SV=1 (A3R0T8_HUMAN)	0.002	Up
Cluster of Dynein heavy chain 12, axonemal OS=Homo sapiens GN=DNAH12 PE=1 SV=2 (E9PG32_HUMAN-DECOY)	0.0032	Down		RPL21 protein OS=Homo sapiens GN=RPL21 PE=2 SV=1	0.0022	Up
Cluster of Putative deoxyribonuclease TATDN1 OS=Homo sapiens GN=TATDN1	0.0032	Down		Cluster of Ras-related C3 botulinum toxin substrate 1 (Rho family, small GTP binding protein Rac1) OS=Homo	0.0023	Up

PE=1 SV=2 (TATD1_HUMAN)				sapiens GN=RAC1 PE=2 SV=1 (A4D2P1_HUMAN)		
Alcohol dehydrogenase [NADP(+)] OS=Homo sapiens GN=AKR1A1 PE=1 SV=3	0.0032	Down		Cluster of TOB3 OS=Homo sapiens PE=2 SV=1 (Q96T67_HUMAN)	0.0023	Up
Cluster of Triosephosphate isomerase OS=Homo sapiens GN=TPI1 PE=1 SV=3 (TPIS_HUMAN)	0.0035	Down		H/ACA ribonucleoprotein complex subunit 3 OS=Homo sapiens GN=NOP10 PE=1 SV=1	0.0019	Up
Cluster of 26S proteasome non-ATPase regulatory subunit 4 OS=Homo sapiens GN=PSMD4 PE=1 SV=1 (PSMD4_HUMAN)	0.0035	Down		Cluster of Mitochondrial transcription factor A OS=Homo sapiens PE=4 SV=1 (E5KSX8_HUMAN)	0.0018	Up
Cluster of ADP-ribosylation factor 1 OS=Homo sapiens GN=ARF1 PE=1 SV=2 (ARF1_HUMAN)	0.0036	Down		Cysteine-tRNA ligase, cytoplasmic OS=Homo sapiens GN=CARS PE=1 SV=1	0.0021	Up
cDNA FLJ54170, highly similar to Cytosolic nonspecific dipeptidase OS=Homo sapiens PE=2 SV=1	0.0037	Down		cDNA, FLJ96465, highly similar to Homo sapiens solute carrier family 25 (mitochondrial carrier;phosphate carrier), member 3 (SLC25A3), nuclear gene encodingmitochondrial protein, transcript variant 1b... OS=Homo sapiens PE=2 SV=1	0.0025	Up
Tumor protein D52 OS=Homo sapiens GN=TPD52 PE=1 SV=2	0.0037	Down		Cluster of Histone H2A type 3 OS=Homo sapiens GN=HIST3H2A PE=1 SV=3 (H2A3_HUMAN)	0.0032	Up
Serine-threonine kinase receptor-associated protein OS=Homo sapiens GN=STRAP PE=1 SV=1	0.0038	Down		Cluster of Histone H3.3 OS=Homo sapiens GN=H3F3A PE=1 SV=2 (H33_HUMAN)	0.0027	Up
Cluster of T-complex protein 1 subunit gamma OS=Homo sapiens PE=2 SV=1 (Q2TU64_HUMAN)	0.0039	Down		Cluster of NPC-A-16 OS=Homo sapiens GN=RPL9 PE=2 SV=1 (Q53Z07_HUMAN)	0.003	Up

Cluster of Nucleosome assembly protein 1-like 4, isoform CRA_b OS=Homo sapiens GN=NAP1L4 PE=3 SV=1 (A0A024RCC9_HUMAN)	0.0039	Down		Cluster of Dehydrogenase/reductase SDR family member 2, mitochondrial OS=Homo sapiens GN=DHRS2 PE=1 SV=4 (DHRS2_HUMAN)	0.0029	Up
Eukaryotic translation initiation factor 3 subunit M OS=Homo sapiens GN=EIF3M PE=1 SV=1	0.0042	Down		Polyribonucleotide nucleotidyltransferase 1, mitochondrial OS=Homo sapiens GN=PNPT1 PE=1 SV=2	0.0028	Up
Cluster of 14-3-3 protein zeta/delta OS=Homo sapiens GN=YWHAZ PE=1 SV=1 (1433Z_HUMAN)	0.0043	Down		Cluster of Dolichyl-diphosphooligosaccharide-protein glycosyltransferase subunit 1 OS=Homo sapiens GN=RPN1 PE=1 SV=1 (RPN1_HUMAN)	0.0028	Up
Costars family protein ABRACL OS=Homo sapiens GN=ABRACL PE=1 SV=1	0.0043	Down		Cluster of 60S ribosomal protein L14 OS=Homo sapiens GN=RPL14 PE=1 SV=4 (RL14_HUMAN)	0.0032	Up
Cluster of cDNA, FLJ95650, highly similar to Homo sapiens karyopherin (importin) beta 1 (KPNB1), mRNA OS=Homo sapiens PE=2 SV=1 (B2RBR9_HUMAN)	0.0045	Down		Cluster of Phosphoenolpyruvate carboxykinase [GTP], mitochondrial OS=Homo sapiens GN=PCK2 PE=1 SV=3 (PCKGM_HUMAN)	0.0028	Up
Cluster of cDNA FLJ53116, highly similar to T-complex protein 1 subunit epsilon OS=Homo sapiens PE=2 SV=1 (B4DZT5_HUMAN)	0.0048	Down		Ubiquitin/ISG15-conjugating enzyme E2 L6 OS=Homo sapiens GN=UBE2L6 PE=1 SV=4	0.0031	Up
Solute carrier family 2, facilitated glucose transporter member 1 OS=Homo sapiens GN=SLC2A1 PE=1 SV=2	0.0048	Down		cDNA FLJ75180, highly similar to Homo sapiens mitochondrial isoleucine tRNA synthetase, mRNA OS=Homo sapiens PE=2 SV=1	0.0031	Up
Myotrophin OS=Homo sapiens GN=MTPN PE=1 SV=2	0.0055	Down		AFG3-like protein 2 OS=Homo sapiens GN=AFG3L2 PE=1 SV=2	0.0026	Up
Profilin-1 OS=Homo sapiens GN=PFN1 PE=1 SV=2	0.0059	Down		39S ribosomal protein L39, mitochondrial	0.0034	Up

				OS=Homo sapiens GN=MRPL39 PE=1 SV=3		
Testicular tissue protein Li 75 OS=Homo sapiens PE=2 SV=1	0.0059	Down		Cluster of Histone deacetylase OS=Homo sapiens GN=HDAC1 PE=2 SV=1 (Q6IT96_HUMAN)	0.0035	Up
Drebrin-like protein OS=Homo sapiens GN=DBNL PE=1 SV=1	0.0059	Down		Cluster of G protein-binding protein CRFG variant (Fragment) OS=Homo sapiens PE=2 SV=1 (Q53GS0_HUMAN)	0.0035	Up
Cluster of HSPA1L OS=Homo sapiens PE=3 SV=1 (A0A1U9X7X4_HUMAN)	0.0063	Down		Leucine-rich repeat-containing protein 59 OS=Homo sapiens GN=LRRC59 PE=1 SV=1	0.0037	Up
Niban-like protein 1 OS=Homo sapiens GN=FAM129B PE=1 SV=3	0.0063	Down		Asparagine synthetase [glutamine-hydrolyzing] OS=Homo sapiens GN=ASNS PE=1 SV=4	0.0044	Up
Cluster of Nucleolar and coiled-body phosphoprotein 1 OS=Homo sapiens GN=NOLC1 PE=1 SV=2 (NOLC1_HUMAN)	0.0064	Down		Cluster of Calnexin OS=Homo sapiens GN=CANX PE=1 SV=2 (CALX_HUMAN)	0.0046	Up
Serine/arginine repetitive matrix 1 isoform 2 (Fragment) OS=Homo sapiens GN=SRRM1 PE=2 SV=1	0.0064	Down		Septin-2 OS=Homo sapiens GN=SEPT2 PE=1 SV=1	0.0049	Up
Malignant T-cell-amplified sequence 1 OS=Homo sapiens GN=MCTS1 PE=1 SV=1	0.0062	Down		Lon protease homolog, mitochondrial OS=Homo sapiens GN=LONP1 PE=2 SV=1	0.0053	Up
Cluster of cDNA FLJ32482 fis, clone SKNMC2001324, highly similar to Importin-4 OS=Homo sapiens PE=2 SV=1 (B3KPY9_HUMAN)	0.0066	Down		Cluster of RPS4X protein (Fragment) OS=Homo sapiens GN=RPS4X PE=2 SV=2 (Q96IR1_HUMAN)	0.0054	Up
Cluster of Hsp70-binding protein 1 OS=Homo sapiens GN=HSPBP1 PE=1 SV=1 (HPBP1_HUMAN)	0.0065	Down		Cluster of cDNA PSEC0016 fis, clone NT2RM1001076, highly similar to Procollagen-lysine,2-oxoglutarate 5-dioxygenase 3 (EC 1.14.11.4) OS=Homo	0.0055	Up

				sapiens PE=2 SV=1 (B3KQQ3_HUMAN)		
Spectrin alpha chain, non-erythrocytic 1 OS=Homo sapiens GN=SPTAN1 PE=1 SV=1	0.0069	Down		Topoisomerase (DNA) I OS=Homo sapiens GN=TOP1 PE=2 SV=1	0.0057	Up
Cluster of Neuroblast differentiation-associated protein AHNAK OS=Homo sapiens GN=AHNAK PE=1 SV=2 (AHNK_HUMAN)	0.0075	Down		Ribosome-binding protein 1 OS=Homo sapiens GN=RRBP1 PE=1 SV=1	0.0058	Up
Nascent polypeptide-associated complex subunit alpha, muscle-specific form OS=Homo sapiens GN=NACA PE=1 SV=1	0.0073	Down		Peptidyl-prolyl cis-trans isomerase B OS=Homo sapiens GN=PPIB PE=1 SV=2	0.0064	Up
Chromobox protein homolog 1 OS=Homo sapiens GN=CBX1 PE=1 SV=1	0.0075	Down		Cluster of Small nuclear ribonucleoprotein-associated protein N OS=Homo sapiens GN=SNRPN PE=1 SV=1 (RSMN_HUMAN)	0.0064	Up
Isocitrate dehydrogenase [NADP] OS=Homo sapiens PE=2 SV=1	0.0078	Down		Cluster of Chromodomain-helicase-DNA-binding protein 4 OS=Homo sapiens GN=CHD4 PE=1 SV=1 (A0A0C4DGG9_HUMAN)	0.0064	Up
Cluster of Calmodulin-1 OS=Homo sapiens GN=CALM1 PE=1 SV=1 (CALM1_HUMAN)	0.0079	Down		60S ribosomal protein L35 OS=Homo sapiens GN=RPL35 PE=1 SV=2	0.0066	Up
Cluster of Heterogeneous nuclear ribonucleoprotein L OS=Homo sapiens GN=HNRNPL PE=1 SV=2 (HNRPL_HUMAN)	0.0084	Down		Trifunctional enzyme subunit beta, mitochondrial OS=Homo sapiens GN=HADHB PE=1 SV=3	0.0068	Up
Endoribonuclease LACTB2 OS=Homo sapiens GN=LACTB2 PE=1 SV=2	0.0089	Down		Cluster of cDNA FLJ61290, highly similar to Neutral alpha-glucosidase AB OS=Homo sapiens PE=2 SV=1 (B4DJ30_HUMAN)	0.0071	Up

Cluster of Barrier to autointegration factor 1, isoform CRA_a OS=Homo sapiens GN=BANF1 PE=4 SV=1 (A0A024R5H0_HUMAN)	0.0091	Down		Deoxynucleoside triphosphate triphosphohydrolase SAMHD1 OS=Homo sapiens GN=SAMHD1 PE=1 SV=2	0.0074	Up
Cluster of Epididymis secretory protein Li 85 OS=Homo sapiens GN=PCBP1 PE=2 SV=1 (Q53SS8_HUMAN)	0.0092	Down		Testis derived transcript (3 LIM domains) OS=Homo sapiens GN=TES PE=4 SV=1	0.0075	Up
Cluster of Calponin (Fragment) OS=Homo sapiens PE=2 SV=1 (Q53GK7_HUMAN)	0.0094	Down		Cluster of ADP/ATP translocase 2 OS=Homo sapiens GN=SLC25A5 PE=1 SV=7 (ADT2_HUMAN)	0.0079	Up
BAG6 OS=Homo sapiens GN=BAT3 PE=1 SV=1	0.01	Down		Cluster of GTP-binding nuclear protein Ran (Fragment) OS=Homo sapiens GN=RAN PE=1 SV=1 (J3KQE5_HUMAN)	0.0082	Up
Cluster of Keratin, type II cytoskeletal 8 OS=Homo sapiens GN=KRT8 PE=1 SV=7 (K2C8_HUMAN)	0.011	Down		Voltage-dependent anion-selective channel protein 1 OS=Homo sapiens GN=VDAC1 PE=1 SV=2	0.0088	Up
Fatty acid synthase OS=Homo sapiens GN=FASN PE=1 SV=3	0.011	Down		Adenylate kinase 1 variant (Fragment) OS=Homo sapiens PE=2 SV=1	0.0088	Up
Cluster of Cofilin-1 OS=Homo sapiens GN=CFL1 PE=1 SV=3 (COF1_HUMAN)	0.011	Down		Nodal modulator 3 OS=Homo sapiens GN=NOMO3 PE=1 SV=1	0.0089	Up
Cluster of Transgelin-2 OS=Homo sapiens GN=TAGLN2 PE=1 SV=3 (TAGL2_HUMAN)	0.011	Down		60S ribosomal protein L11 OS=Homo sapiens GN=RPL11 PE=1 SV=2	0.009	Up
Splicing factor U2AF 65 kDa subunit OS=Homo sapiens GN=U2AF2 PE=1 SV=4	0.011	Down		PGRMC1 protein OS=Homo sapiens GN=PGRMC1 PE=2 SV=1	0.0095	Up
HDCMB21P OS=Homo sapiens PE=2 SV=1	0.011	Down		Eukaryotic translation initiation factor 2 beta OS=Homo sapiens GN=EIF2S2 PE=2 SV=1	0.0096	Up
cDNA FLJ75699, highly similar to Homo sapiens	0.011	Down		Cluster of Basigin OS=Homo sapiens	0.0097	Up

osteoclast stimulating factor 1 (OSTF1), mRNA OS=Homo sapiens PE=2 SV=1				GN=BSG PE=1 SV=2 (BASI_HUMAN)		
Cluster of Annexin A1 OS=Homo sapiens GN=ANXA1 PE=1 SV=2 (ANXA1_HUMAN)	0.012	Down		60S ribosomal protein L24 OS=Homo sapiens GN=RPL24 PE=1 SV=1	0.01	Up
Cluster of BolA-like protein 2 OS=Homo sapiens GN=BOLA2 PE=1 SV=2 (A0A087WZT3_HUMAN)	0.012	Down		Putative peripheral benzodiazepine receptor-related protein (Fragment) OS=Homo sapiens GN=TSPO PE=1 SV=1	0.0099	Up
Cluster of Glyceraldehyde-3-phosphate dehydrogenase OS=Homo sapiens GN=GAPDH PE=1 SV=3 (G3P_HUMAN)	0.013	Down		NADPH--cytochrome P450 reductase OS=Homo sapiens GN=POR PE=2 SV=1	0.01	Up
Cluster of Protein disulfide-isomerase OS=Homo sapiens GN=P4HB PE=2 SV=1 (A0A024R8S5_HUMAN)	0.013	Down		Cluster of Transketolase variant (Fragment) OS=Homo sapiens PE=2 SV=1 (Q53EM5_HUMAN)	0.011	Up
Cluster of Heat shock 70kDa protein 4 isoform a variant (Fragment) OS=Homo sapiens PE=2 SV=1 (Q59GF8_HUMAN)	0.013	Down		Cluster of 2'-5'-oligoadenylate synthetase 3, 100kDa, isoform CRA_a OS=Homo sapiens GN=OAS3 PE=4 SV=1 (A0A024RBQ5_HUMAN)	0.011	Up
Multifunctional methyltransferase subunit TRM112-like protein OS=Homo sapiens GN=TRMT112 PE=1 SV=1	0.013	Down		Flavin reductase (NADPH) OS=Homo sapiens GN=BLVRB PE=1 SV=3	0.011	Up
Cluster of Tumor protein D54 OS=Homo sapiens GN=TPD52L2 PE=1 SV=1 (A0A087WYR3_HUMAN)	0.013	Down		Cluster of Glutamine-fructose-phosphate aminotransferase [isomerizing] 1 OS=Homo sapiens GN=GFPT1 PE=1 SV=3 (GFPT1_HUMAN)	0.011	Up

Testicular tissue protein Li 138 OS=Homo sapiens PE=2 SV=1	0.013	Down		cDNA, FLJ93510, highly similar to Homo sapiens JTV1 gene (JTV1), mRNA OS=Homo sapiens PE=2 SV=1	0.011	Up
Synaptogyrin OS=Homo sapiens GN=SYNGR2 PE=3 SV=1	0.014	Down		Lysine-tRNA ligase OS=Homo sapiens GN=KARS PE=1 SV=3	0.012	Up
Cluster of ELAV-like protein 1 OS=Homo sapiens GN=ELAVL1 PE=1 SV=2 (ELAV1_HUMAN)	0.015	Down		E3 ubiquitin-protein ligase RNF213 OS=Homo sapiens GN=RNF213 PE=1 SV=1	0.012	Up
Cluster of Cellular retinoic acid-binding protein 2 OS=Homo sapiens GN=CRABP2 PE=1 SV=2 (RABP2_HUMAN)	0.015	Down		Cluster of Cytochrome b-c1 complex subunit 2, mitochondrial OS=Homo sapiens GN=UQCRC2 PE=1 SV=3 (QCR2_HUMAN)	0.013	Up
cDNA FLJ52068, highly similar to Microtubule-associated protein RP/EB family member 1 OS=Homo sapiens PE=2 SV=1	0.015	Down		Cluster of cDNA FLJ54020, highly similar to Heterogeneous nuclear ribonucleoprotein U OS=Homo sapiens PE=2 SV=1 (B4DLR3_HUMAN)	0.014	Up
Cluster of SET OS=Homo sapiens GN=SET PE=2 SV=1 (Q5VXV3_HUMAN)	0.015	Down		40S ribosomal protein S3a OS=Homo sapiens GN=RPS3A PE=2 SV=1	0.014	Up
Cluster of Nuclease sensitive element binding protein-1 OS=Homo sapiens PE=2 SV=1 (Q7KZ24_HUMAN)	0.015	Down		Cluster of Core histone macro-H2A.1 OS=Homo sapiens GN=H2AFY PE=1 SV=4 (H2AY_HUMAN)	0.014	Up
Cluster of La-related protein 1 OS=Homo sapiens GN=LARP1 PE=1 SV=2 (LARP1_HUMAN)	0.015	Down		X-ray repair cross-complementing protein 6 OS=Homo sapiens GN=XRCC6 PE=1 SV=1	0.015	Up
Cluster of T-complex protein 1 subunit beta OS=Homo sapiens GN=CCT2 PE=1 SV=4 (TCPB_HUMAN)	0.016	Down		Mitochondrial carrier homolog 2 OS=Homo sapiens GN=MTCH2 PE=1 SV=1	0.015	Up
Cluster of Histone-binding protein RBBP7 OS=Homo sapiens GN=RBBP7 PE=1 SV=1 (RBBP7_HUMAN)	0.016	Down		Cluster of Isocitrate dehydrogenase [NAD] subunit, mitochondrial OS=Homo sapiens GN=IDH3G PE=1 SV=1 (E7EQB8_HUMAN)	0.015	Up

Peptidyl-prolyl cis-trans isomerase NIMA-interacting 1 OS=Homo sapiens GN=PIN1 PE=1 SV=1	0.016	Down		Prohibitin-2 OS=Homo sapiens GN=PHB2 PE=1 SV=1	0.016	Up
Calreticulin variant (Fragment) OS=Homo sapiens PE=2 SV=1	0.017	Down		Cluster of Interferon-induced protein with tetratricopeptide repeats 1 OS=Homo sapiens GN=IFIT1 PE=1 SV=2 (IFIT1_HUMAN)	0.016	Up
Cluster of CSTB protein OS=Homo sapiens GN=CSTB PE=2 SV=1 (Q76LA1_HUMAN)	0.017	Down		Ubiquitin carboxyl-terminal hydrolase 14 OS=Homo sapiens GN=USP14 PE=1 SV=2	0.016	Up
Cluster of Far upstream element-binding protein 2 OS=Homo sapiens GN=KHSRP PE=1 SV=1 (A0A087WTP3_HUMAN)	0.017	Down		Cluster of Tubulin alpha chain OS=Homo sapiens GN=TUBA1C PE=1 SV=1 (F5H5D3_HUMAN)	0.017	Up
Eukaryotic translation initiation factor 3 subunit A OS=Homo sapiens GN=EIF3A PE=1 SV=1	0.017	Down		Cluster of Proteasome subunit alpha type OS=Homo sapiens GN=PSMA6 PE=1 SV=1 (G3V295_HUMAN)	0.017	Up
Proteasome subunit alpha type OS=Homo sapiens PE=2 SV=1	0.017	Down		DNA-dependent protein kinase catalytic subunit OS=Homo sapiens GN=PRKDC PE=1 SV=3	0.017	Up
EF-hand domain-containing protein D2 OS=Homo sapiens GN=EFHD2 PE=1 SV=1	0.017	Down		Apoptosis-inducing factor 1, mitochondrial OS=Homo sapiens GN=AIFM1 PE=1 SV=1	0.018	Up
cDNA FLJ56566, highly similar to Small glutamine-rich tetratricopeptiderepeat-containing protein A OS=Homo sapiens PE=2 SV=1	0.017	Down		Eukaryotic translation initiation factor 3 subunit D OS=Homo sapiens GN=EIF3D PE=2 SV=1	0.018	Up
Cluster of Prosaposin (Variant Gaucher disease and variant metachromatic leukodystrophy), isoform CRA_b OS=Homo sapiens GN=PSAP PE=4 SV=1 (A0A024QZQ2_HUMAN)	0.017	Down		Bifunctional glutamate/proline-tRNA ligase OS=Homo sapiens GN=EPRS PE=1 SV=5	0.019	Up

Cluster of cDNA FLJ55694, highly similar to Dipeptidyl-peptidase 1 (EC 3.4.14.1) OS=Homo sapiens PE=2 SV=1 (B4DJQ8_HUMAN)	0.018	Down		Histone H1x OS=Homo sapiens GN=H1FX PE=1 SV=1	0.019	Up
Cluster of Myosin regulatory light chain 12A OS=Homo sapiens GN=MYL12A PE=1 SV=2 (ML12A_HUMAN)	0.018	Down		Cluster of 40S ribosomal protein S16 OS=Homo sapiens GN=RPS16 PE=1 SV=2 (RS16_HUMAN)	0.02	Up
Drug-sensitive protein 1 OS=Homo sapiens GN=YA61 PE=2 SV=1	0.018	Down		60S ribosomal protein L34 OS=Homo sapiens GN=RPL34 PE=1 SV=3	0.02	Up
Cluster of Myeloid-derived growth factor OS=Homo sapiens GN=MYDGF PE=1 SV=1 (MYDGF_HUMAN)	0.018	Down		EPHX1 protein (Fragment) OS=Homo sapiens GN=EPHX1 PE=2 SV=1	0.02	Up
Cluster of Polypyrimidine tract binding protein 1, isoform CRA_b OS=Homo sapiens GN=PTBP1 PE=1 SV=4 (A6NLN1_HUMAN)	0.019	Down		60S ribosomal protein L30 (Fragment) OS=Homo sapiens GN=RPL30 PE=1 SV=1	0.021	Up
Nuclear migration protein nudC OS=Homo sapiens GN=NUDC PE=1 SV=1	0.019	Down		Flap endonuclease 1 OS=Homo sapiens GN=FEN1 PE=2 SV=1	0.021	Up
Integrin alpha-6 OS=Homo sapiens GN=ITGA6 PE=1 SV=5	0.019	Down		Cluster of 40S ribosomal protein S19 OS=Homo sapiens GN=RPS19 PE=2 SV=1 (B0ZBD0_HUMAN)	0.024	Up
Gamma-glutamylcyclotransferase OS=Homo sapiens GN=GGCT PE=1 SV=1	0.019	Down		Cluster of 60S ribosomal protein L17 OS=Homo sapiens GN=RPL17 PE=1 SV=3 (RL17_HUMAN)	0.024	Up
Annexin A10 OS=Homo sapiens GN=ANXA10 PE=1 SV=3	0.019	Down		Cluster of Serine hydroxymethyltransferase, mitochondrial (Fragment) OS=Homo sapiens GN=SHMT2 PE=1 SV=1 (G3V4W5_HUMAN)	0.025	Up
Cluster of Elongation factor 1-delta (Fragment) OS=Homo sapiens	0.02	Down		Regulator of chromosome condensation 2, isoform CRA_a OS=Homo	0.025	Up

GN=EEF1D PE=1 SV=1 (E9PIZ1_HUMAN)				sapiens GN=RCC2 PE=4 SV=1		
Cluster of Transcription factor BTF3 OS=Homo sapiens GN=BTF3 PE=1 SV=1 (BTF3_HUMAN)	0.02	Down		Cluster of Glutamate dehydrogenase OS=Homo sapiens PE=2 SV=1 (B4DMF5_HUMAN)	0.025	Up
Stathmin OS=Homo sapiens GN=STMN1 PE=2 SV=1	0.02	Down		Histone H1.0 OS=Homo sapiens GN=H1F0 PE=1 SV=3	0.025	Up
Cluster of Translationally-controlled tumor protein (Fragment) OS=Homo sapiens GN=TPT1 PE=1 SV=1 (E9PJF7_HUMAN)	0.02	Down		Phosphoserine aminotransferase OS=Homo sapiens PE=2 SV=1	0.025	Up
Small nuclear ribonucleoprotein F OS=Homo sapiens GN=SNRPF PE=1 SV=1	0.02	Down		Cluster of 60S ribosomal protein L13 OS=Homo sapiens GN=RPL13 PE=1 SV=1 (Q6NZ55_HUMAN)	0.026	Up
Cluster of Plectin OS=Homo sapiens GN=PLEC PE=1 SV=3 (PLEC_HUMAN)	0.021	Down		Cluster of Ribosomal protein L19 OS=Homo sapiens GN=RPL19 PE=1 SV=1 (J3KTE4_HUMAN)	0.027	Up
Obg-like ATPase 1 OS=Homo sapiens GN=OLA1 PE=1 SV=2	0.021	Down		Cluster of Peroxisome proliferator activated receptor interacting complex protein OS=Homo sapiens GN=PRIC295 PE=2 SV=1 (E1NZA1_HUMAN)	0.027	Up
Cluster of Ran GTPase-activating protein 1 OS=Homo sapiens GN=RANGAP1 PE=1 SV=1 (RAGP1_HUMAN)	0.021	Down		Cluster of cDNA FLJ45395 fis, clone BRHIP3027191, highly similar to 150 kDa oxygen-regulated protein (Orp150) OS=Homo sapiens PE=2 SV=1 (B3KXH0_HUMAN)	0.028	Up
Peflin OS=Homo sapiens GN=PEF1 PE=1 SV=1	0.021	Down		Cluster of cDNA FLJ76789, highly similar to Homo sapiens methionine-tRNA synthetase (MARS), mRNA OS=Homo sapiens PE=2 SV=1 (A8K492_HUMAN)	0.028	Up

cDNA FLJ78041, highly similar to Homo sapiens NADH dehydrogenase (ubiquinone) flavoprotein 2, 24kDa (NDUFV2), mRNA OS=Homo sapiens PE=2 SV=1	0.022	Down		2'-5'-oligoadenylate synthase 2 OS=Homo sapiens GN=OAS2 PE=1 SV=1	0.028	Up
SH3 domain binding glutamic acid-rich protein like 3, isoform CRA_a (Fragment) OS=Homo sapiens GN=SH3BGRL3 PE=4 SV=1	0.023	Down		Emerin OS=Homo sapiens GN=EMD PE=1 SV=1	0.028	Up
Cluster of Ran-binding protein 6 OS=Homo sapiens GN=RANBP6 PE=1 SV=2 (RNBP6_HUMAN)	0.023	Down		Cluster of 60S ribosomal protein L7a OS=Homo sapiens GN=RPL7A PE=1 SV=2 (RL7A_HUMAN)	0.029	Up
Cluster of UMP-CMP kinase OS=Homo sapiens GN=CMPK1 PE=1 SV=3 (KCY_HUMAN)	0.024	Down		Cluster of CTNND1 protein (Fragment) OS=Homo sapiens GN=CTNND1 PE=2 SV=2 (Q96FS1_HUMAN)	0.029	Up
Sorting nexin 1 isoform a variant (Fragment) OS=Homo sapiens PE=2 SV=1	0.024	Down		39S ribosomal protein L4, mitochondrial OS=Homo sapiens GN=MRPL4 PE=1 SV=1	0.029	Up
Cytochrome c oxidase subunit 5A, mitochondrial OS=Homo sapiens GN=COX5A PE=1 SV=2	0.025	Down		Cluster of Ribosomal protein L23, isoform CRA_b OS=Homo sapiens GN=RPL23 PE=3 SV=1 (A0A024R1Q8_HUMAN)	0.03	Up
Leucine-rich repeat-containing protein 47 OS=Homo sapiens GN=LRRC47 PE=1 SV=1	0.025	Down		Leucine-rich PPR-motif containing OS=Homo sapiens GN=LRPPRC PE=4 SV=1	0.03	Up
Acyl-CoA-binding protein OS=Homo sapiens GN=DBI PE=1 SV=2	0.025	Down		ATP synthase subunit g, mitochondrial OS=Homo sapiens GN=ATP5L PE=1 SV=3	0.03	Up
Splicing factor 3B subunit 5 OS=Homo sapiens GN=SF3B5 PE=1 SV=1	0.025	Down		Cluster of Signal recognition particle subunit SRP72 OS=Homo sapiens	0.03	Up

				GN=HEL103 PE=2 SV=1 (V9HWK0_HUMAN)		
Ribosomal protein, large, P1, isoform CRA_a OS=Homo sapiens GN=RPLP1 PE=3 SV=1	0.026	Down		Protein NipSnap homolog 2 OS=Homo sapiens GN=NIPSNAP2 PE=1 SV=1	0.03	Up
HCG26477 OS=Homo sapiens GN=RPS28 PE=2 SV=1	0.026	Down		40S ribosomal protein S11 OS=Homo sapiens GN=RPS11 PE=1 SV=3	0.031	Up
Asparagine-tRNA ligase, cytoplasmic OS=Homo sapiens GN=NARS PE=1 SV=1	0.026	Down		Cluster of Protein NipSnap homolog 1 OS=Homo sapiens GN=NIPSNAP1 PE=1 SV=1 (NIPS1_HUMAN)	0.031	Up
Cluster of Epiplakin OS=Homo sapiens GN=EPPK1 PE=1 SV=1 (A0A087X1U6_HUMAN)	0.027	Down		Cluster of Peptidyl-prolyl cis-trans isomerase OS=Homo sapiens PE=2 SV=1 (B2R6X6_HUMAN)	0.031	Up
Alanine-tRNA ligase, cytoplasmic OS=Homo sapiens GN=AARS PE=1 SV=2	0.027	Down		Cytochrome c oxidase subunit 6C OS=Homo sapiens GN=COX6C PE=1 SV=2	0.031	Up
Cluster of cDNA FLJ60127, highly similar to Ubiquilin-2 OS=Homo sapiens PE=2 SV=1 (B4DM19_HUMAN)	0.029	Down		Cluster of Citrate synthase OS=Homo sapiens GN=CS PE=1 SV=1 (B4DJV2_HUMAN)	0.032	Up
SARS protein OS=Homo sapiens GN=SARS PE=2 SV=1	0.029	Down		Heterochromatin protein 1-binding protein 3 OS=Homo sapiens GN=HP1BP3 PE=1 SV=1	0.032	Up
Cluster of Eukaryotic translation initiation factor 4H OS=Homo sapiens GN=EIF4H PE=1 SV=5 (IF4H_HUMAN)	0.03	Down		Cluster of RPL26 protein OS=Homo sapiens GN=RPL26 PE=2 SV=1 (Q6IBH6_HUMAN)	0.033	Up
cDNA FLJ76387, highly similar to Homo sapiens splicing factor, arginine/serine-rich 9 (SFRS9), mRNA OS=Homo sapiens PE=2 SV=1	0.031	Down		Regulation of nuclear pre-mRNA domain-containing protein 1B OS=Homo sapiens GN=RPRD1B PE=1 SV=1	0.033	Up
182 kDa tankyrase-1-binding protein OS=Homo sapiens	0.031	Down		Mago nashi protein OS=Homo sapiens GN=FLJ10292 PE=2 SV=1	0.033	Up

GN=TNKS1BP1 PE=1 SV=4						
Splicing factor arginine/serine-rich 3 OS=Homo sapiens GN=SFRS3 PE=2 SV=1	0.032	Down		Tryptophan--tRNA ligase, cytoplasmic OS=Homo sapiens GN=WARS PE=1 SV=2	0.034	Up
Cluster of Epididymis secretory protein Li 102 OS=Homo sapiens GN=HEL-S-102 PE=2 SV=1 (V9HW43_HUMAN)	0.032	Down		Calcium load-activated calcium channel OS=Homo sapiens GN=TMCO1 PE=2 SV=1	0.034	Up
Methionine aminopeptidase 2 OS=Homo sapiens GN=METAP2 PE=1 SV=1	0.032	Down		Cluster of Protein PML OS=Homo sapiens GN=PML PE=1 SV=1 (H3BT57_HUMAN)	0.035	Up
Cluster of Epithelial-splicing regulatory protein 1 (Fragment) OS=Homo sapiens GN=ESRP1 PE=1 SV=1 (H0YBR2_HUMAN)	0.032	Down		Cluster of 40S ribosomal protein S2 (Fragment) OS=Homo sapiens GN=RPS2 PE=1 SV=1 (E9PMM9_HUMAN)	0.036	Up
Na(+)/H(+) exchange regulatory cofactor NHERF1 OS=Homo sapiens GN=SLC9A3R1 PE=1 SV=4	0.033	Down		Cluster of DNA helicase (Fragment) OS=Homo sapiens PE=2 SV=1 (Q53FG5_HUMAN)	0.036	Up
Cluster of Calpain small subunit 1 OS=Homo sapiens GN=CAPNS1 PE=1 SV=1 (A0A0C4DGQ5_HUMAN)	0.034	Down		cDNA FLJ54723, highly similar to Poly (ADP-ribose) polymerase 9 (EC 2.4.2.30) OS=Homo sapiens PE=2 SV=1	0.036	Up
Ran-specific GTPase activating protein OS=Homo sapiens GN=RANBP1 PE=1 SV=1	0.035	Down		Cluster of 2-oxoglutarate dehydrogenase, mitochondrial OS=Homo sapiens GN=OGDH PE=1 SV=1 (A0A0D9SFS3_HUMAN)	0.037	Up
Cluster of DNA damage Einding protein 1 OS=Homo sapiens GN=DDB1 PE=1 SV=1 (DDB1_HUMAN)	0.035	Down		Delta-1-pyrroline 5-carboxylate synthase OS=Homo sapiens GN=ALDH18A1 PE=1 SV=2	0.038	Up
Cluster of Pyruvate kinase OS=Homo sapiens GN=PKM PE=1 SV=1 (B4DNK4_HUMAN)	0.036	Down		cDNA FLJ76962, highly similar to Homo sapiens nucleolar protein 5A (56kDa with KKE/D	0.038	Up

				repeat) (NOL5A), mRNA OS=Homo sapiens PE=2 SV=1		
Adenylosuccinate synthetase isozyme 2 OS=Homo sapiens GN=ADSS PE=1 SV=3	0.036	Down		cDNA FLJ13654 fis, clone PLACE1011477, highly similar to Sorting nexin-2 OS=Homo sapiens PE=2 SV=1	0.039	Up
Cluster of T-complex protein 1 subunit delta OS=Homo sapiens PE=2 SV=1 (A8K3C3_HUMAN)	0.037	Down		40S ribosomal protein S8 OS=Homo sapiens GN=RPS8 PE=2 SV=1	0.04	Up
Cluster of Serine/threonine protein phosphatase 2A 65 kDa regulatory subunit A alpha isoform OS=Homo sapiens GN=PPP2R1A PE=1 SV=4 (2AAA_HUMAN)	0.037	Down		Splicing factor 3B subunit 1 OS=Homo sapiens GN=SF3B1 PE=1 SV=3	0.04	Up
Protein kinase C substrate 80K-H, isoform CRA_a OS=Homo sapiens GN=PRKCSH PE=4 SV=1	0.037	Down		40S ribosomal protein S24 OS=Homo sapiens GN=RPS24 PE=1 SV=1	0.041	Up
Cluster of Methylenetetrahydrofolate dehydrogenase (NADP+ dependent) 1, methenyltetrahydrofolate cyclohydrolase, formyltetrahydrofolate synthetase, isoform CRA_a OS=Homo sapiens GN=MTHFD1 PE=3 SV=1 (A0A024R652_HUMAN)	0.038	Down		Cluster of Protein FAM162A OS=Homo sapiens GN=FAM162A PE=1 SV=2 (F162A_HUMAN)	0.042	Up
RcNSEP1 (Fragment) OS=Homo sapiens PE=4 SV=1	0.038	Down		Procollagen galactosyltransferase 1 OS=Homo sapiens GN=COLGALT1 PE=1 SV=1	0.042	Up
Cluster of S-methyl-5'-thioadenosine phosphorylase OS=Homo sapiens GN=MTAP PE=2 SV=1 (Q6FHT1_HUMAN)	0.038	Down		Catenin beta-1 OS=Homo sapiens GN=CTNNB1 PE=1 SV=1	0.043	Up
Cluster of Dimethylarginine dimethylaminohydrolase	0.038	Down		Cluster of eIF2AK2 protein OS=Homo sapiens GN=EIF2AK2	0.045	Up

1, isoform CRA_b OS=Homo sapiens GN=DDAH1 PE=2 SV=1 (B1AKK2_HUMAN)				PE=2 SV=1 (B7ZKK7_HUMAN)		
Cluster of Adenylyl cyclase associated protein OS=Homo sapiens PE=2 SV=1 (B2RDY9_HUMAN)	0.039	Down		Cluster of Cathepsin D OS=Homo sapiens GN=CTSD PE=1 SV=1 (A0A1B0GVD5_HUMAN)	0.046	Up
Prefoldin subunit 2 OS=Homo sapiens GN=PFDN2 PE=1 SV=1	0.039	Down		tRNA-splicing ligase RtcB homolog OS=Homo sapiens GN=RTCB PE=1 SV=1	0.046	Up
Testicular tissue protein Li 198 OS=Homo sapiens PE=2 SV=1	0.04	Down		MRE11 meiotic recombination 11 homolog A (S. cerevisiae), isoform CRA_a OS=Homo sapiens GN=MRE11A PE=3 SV=1	0.046	Up
Thioredoxin domain-containing protein 17 OS=Homo sapiens GN=TXNDC17 PE=1 SV=1	0.04	Down		Tripeptidyl peptidase I, isoform CRA_a OS=Homo sapiens GN=TPP1 PE=4 SV=1	0.047	Up
Ubiquitin-conjugating enzyme E2 variant 2 (Fragment) OS=Homo sapiens GN=UBE2V2 PE=1 SV=1	0.04	Down		Cluster of cDNA FLJ51914, highly similar to Protein DEK OS=Homo sapiens PE=2 SV=1 (B4DNW3_HUMAN)	0.047	Up
Cluster of Tubulin beta-4A chain OS=Homo sapiens GN=TUBB4A PE=1 SV=2 (TBB4A_HUMAN)	0.041	Down		Cytochrome c oxidase subunit 4 isoform 1, mitochondrial OS=Homo sapiens GN=COX4I1 PE=1 SV=1	0.048	Up
Pyridoxal kinase OS=Homo sapiens GN=PDXK PE=1 SV=1	0.041	Down		Nuclear transport factor 2 OS=Homo sapiens GN=NUTF2 PE=1 SV=1	0.048	Up
Cluster of cDNA, FLJ96580, highly similar to Homo sapiens hepatoma-derived growth factor (high-mobility group protein 1-like) (HDGF), mRNA OS=Homo sapiens PE=2 SV=1 (B2RDE8_HUMAN)	0.042	Down		E3 ubiquitin-protein ligase DTX3L OS=Homo sapiens GN=DTX3L PE=1 SV=1	0.049	Up

Heterogeneous nuclear ribonucleoprotein D0 (Fragment) OS=Homo sapiens GN=HNRNPD PE=1 SV=8	0.042	Down		Cluster of Reticulon-4 OS=Homo sapiens GN=RTN4 PE=1 SV=2 (RTN4_HUMAN)	0.05	Up

Table 11 Proteome response of HT29 cells to treatment with cycloheximide from the perspective of a gene ontological (GO) analysis

Cycloheximide UPs			
source	term name	adjusted p value	term size
GO:BP	RNA splicing, via transesterification reactions with bulged adenosine as nucleophile	0.045679	334
GO:BP	mRNA splicing, via spliceosome	0.045679	334
GO:BP	RNA splicing, via transesterification reactions	0.048032	337
GO:CC	ribonucleoprotein complex	1.53 X 10-05	862
GO:CC	catalytic step 2 spliceosome	6.10 X 10-05	85
GO:CC	spliceosomal complex	8.82 X 10-05	176

Cycloheximide DOWNs			
source	term name	adjusted p value	term size
GO:MF	ubiquitin protein ligase binding	0.011285	286
GO:MF	ubiquitin-like protein ligase binding	0.015028	301
GO:MF	peptidase activator activity	0.031093	39
GO:MF	ubiquitin-like protein conjugating enzyme activity	0.036163	41
GO:BP	protein catabolic process	3.72 X 10-05	911
GO:BP	regulation of protein catabolic process	0.000107	372
GO:BP	positive regulation of protein modification by small protein conjugation or removal	0.000463	127
GO:BP	regulation of protein modification by small protein conjugation or removal	0.000619	220
GO:BP	proteolysis involved in cellular protein catabolic process	0.002204	696
GO:BP	cellular protein catabolic process	0.004378	751
GO:BP	proteasomal protein catabolic process	0.00669	451
GO:BP	regulation of proteolysis involved in cellular protein catabolic process	0.007841	206
GO:BP	regulation of catabolic process	0.016192	870
GO:BP	regulation of cellular protein catabolic process	0.017517	237
GO:BP	proteasom x 10-mediated ubiquitin-dependent protein catabolic process	0.027965	391
GO:CC	proteasome complex	0.002105	67
GO:CC	endopeptidase complex	0.002233	68
GO:CC	peptidase complex	0.006792	90

GO:CC	ubiquitin conjugating enzyme complex	0.03161	9
GO:CC	MCM complex	0.048174	11
CORUM	PA28-20S proteasome	0.046775	16
CORUM	MCM4-MCM6-MCM7 complex	0.049917	3
CORUM	OTUB1-UBC13-MMS2 complex	0.049917	3

Table 12 Proteome response of HT29 cells to treatment with ribavirin from the perspective of a GO analysis

Ribavirin UPs			
source	term name	adjusted p value	term size
GO:MF	cadherin binding involved in cell-cell adhesion	0.001339	19
GO:MF	cadherin binding	0.004298	323
GO:MF	cell-cell adhesion mediator activity	0.026171	50
GO:MF	cell adhesion mediator activity	0.042976	59
GO:MF	cell adhesion molecule binding	0.043532	489
GO:CC	cell-cell adherens junction	0.005655	112
GO:CC	adherens junction	0.032212	537
GO:CC	proteasome complex	0.033012	67
GO:CC	endopeptidase complex	0.034499	68
GO:CC	anchoring junction	0.037428	552

Ribavirin DOWNs			
source	term name	adjusted p value	term size
GO:MF	structural constituent of ribosome	0.004931	168
GO:MF	helicase activity	0.039684	150
GO:BP	protein targeting to ER	6.04E-05	108
GO:BP	establishment of protein localization to endoplasmic reticulum	7.78E-05	112
GO:BP	mRNA metabolic process	9.37E-05	784
GO:BP	ribonucleoprotein complex biogenesis	0.000134	447
GO:BP	nuclear-transcribed mRNA catabolic process, nonsense mediated decay	0.000141	122
GO:BP	protein localization to endoplasmic reticulum	0.000296	136
GO:BP	SRP-dependent cotranslational protein targeting to membrane	0.000772	96
GO:BP	cotranslational protein targeting to membrane	0.001043	101
GO:BP	Nucleobase containing compound catabolic process	0.001124	553
GO:BP	RNA catabolic process	0.001463	345

GO:BP	heterocycle catabolic process	0.002584	602
GO:BP	cellular nitrogen compound catabolic process	0.002626	603
GO:BP	protein targeting to membrane	0.002847	190
GO:BP	aromatic compound catabolic process	0.003232	616
GO:BP	RNA processing	0.00351	902
GO:BP	rRNA processing	0.004007	200
GO:BP	organic cyclic compound catabolic process	0.005355	649
GO:BP	nuclear-transcribed mRNA catabolic process	0.005538	210
GO:BP	mRNA catabolic process	0.007079	311
GO:BP	rRNA metabolic process	0.012281	237
GO:BP	regulation of mRNA metabolic process	0.025407	265
GO:BP	maturation of LSU-rRNA	0.0314	17
GO:BP	ribosome biogenesis	0.037944	282
GO:CC	ribonucleoprotein complex	2.81E-08	862
GO:CC	cytosolic ribosome	0.000273	119
GO:CC	nucleolus	0.000371	934
GO:CC	polysome	0.000582	75
GO:CC	cytosolic part	0.001415	244
GO:CC	ribosomal subunit	0.004585	194
GO:CC	ribosome	0.017723	247
KEGG	Ribosome	0.002587	149
CORUM	Nop56p-associated pre-rRNA complex	0.001674	104
CORUM	Ribosome, cytoplasmic	0.040959	80

Table 13 Proteome response of HT29 cells to treatment with 4E1RCat from the perspective of a GO analysis

4E1RCat UPs			
source	term name	adjusted p value	term size
GO:MF	structural constituent of ribosome	5.88 X 10-08	168
GO:MF	structural molecule activity	0.010018	809
GO:BP	SRP-dependent cotranslational protein targeting to membrane	2.46 X 10-07	96
GO:BP	cotranslational protein targeting to membrane	3.53 X 10-07	101
GO:BP	peptide metabolic process	4.34 X 10-07	884
GO:BP	protein targeting to ER	5.68 X 10-07	108
GO:BP	establishment of protein localization to endoplasmic reticulum	7.35 X 10-07	112
GO:BP	peptide biosynthetic process	7.36 X 10-07	727
GO:BP	translational initiation	1.13 X 10-06	198
GO:BP	nuclear-transcribed mRNA catabolic process, nonsens x 10-mediated decay	1.34 X 10-06	122
GO:BP	mRNA catabolic process	1.52 X 10-06	311
GO:BP	protein localization to endoplasmic reticulum	2.89 X 10-06	136
GO:BP	RNA catabolic process	3.79 X 10-06	345
GO:BP	amide biosynthetic process	4.80 X 10-06	857
GO:BP	translation	8.83 X 10-06	704
GO:BP	protein targeting to membrane	2.97 X 10-05	190
GO:BP	heterocycle catabolic process	3.03 X 10-05	602
GO:BP	cellular nitrogen compound catabolic process	3.07 X 10-05	603
GO:BP	establishment of protein localization to membrane	3.47 X 10-05	306
GO:BP	aromatic compound catabolic process	3.76 X 10-05	616
GO:BP	nuclear-transcribed mRNA catabolic process	5.91 X 10-05	210

GO:BP	organic cyclic compound catabolic process	6.17 X 10-05	649
GO:BP	nucleobas x 10-containing compound catabolic process	0.000224	553
GO:BP	protein localization to membrane	0.000367	586
GO:BP	protein targeting	0.000384	418
GO:BP	establishment of protein localization to organelle	0.002354	531
GO:BP	mRNA metabolic process	0.0042	784
GO:BP	ribosomal large subunit biogenesis	0.009208	71
GO:BP	protein localization to organelle	0.010942	881
GO:CC	cytosolic large ribosomal subunit	1.26 X 10-09	64
GO:CC	large ribosomal subunit	2.16 X 10-09	122
GO:CC	ribosome	1.82 X 10-08	247
GO:CC	ribosomal subunit	8.98 X 10-08	194
GO:CC	cytosolic ribosome	1.07 X 10-07	119
GO:CC	ribonucleoprotein complex	4.62 X 10-07	862
GO:CC	cytosolic part	1.57 X 10-05	244
GO:CC	polysome	2.18 X 10-05	75
GO:CC	polysomal ribosome	2.72 X 10-05	30
KEGG	Ribosome	1.68 X 10-06	149
CORUM	60S ribosomal subunit, cytoplasmic	5.48 X 10-07	47
CORUM	Ribosome, cytoplasmic	2.55 X 10-05	80
CORUM	Nop56p-associated pr x 10-rRNA complex	0.000161	104

4E1RCat DOWNs			
source	term name	adjusted p value	term size
GO:CC	nucleoid	0.001483	43
GO:CC	mitochondrial nucleoid	0.001483	43
GO:CC	nuclear replisome	0.042695	25

Table 14 Proteome response of HT29 cells to treatment with DMSO from the perspective of a GO analysis

DMSO UPs			
source	term name	adjusted p value	term size
GO:BP	SRP-dependent cotranslational protein targeting to membrane	3.20 X 10-25	96
GO:BP	cotranslational protein targeting to membrane	1.24 X 10-24	101
GO:BP	protein targeting to ER	7.24 X 10-24	108
GO:BP	establishment of protein localization to endoplasmic reticulum	1.87 X 10-23	112
GO:BP	protein localization to endoplasmic reticulum	9.38 X 10-23	136
GO:BP	nuclear-transcribed mRNA catabolic process, nonsens x 10-mediated decay	1.71 X 10-22	122
GO:BP	translational initiation	7.82 X 10-20	198
GO:BP	translation	4.04 X 10-19	704
GO:BP	peptide biosynthetic process	1.34 X 10-18	727
GO:BP	protein targeting to membrane	1.07 X 10-17	190
GO:BP	cellular nitrogen compound catabolic process	1.14 X 10-17	603
GO:BP	aromatic compound catabolic process	2.35 X 10-17	616
GO:BP	nucleobas x 10-containing compound catabolic process	5.73 X 10-17	553
GO:BP	RNA catabolic process	6.68 X 10-17	345
GO:BP	amide biosynthetic process	7.67 X 10-17	857
GO:BP	heterocycle catabolic process	9.86 X 10-17	602
GO:BP	nuclear-transcribed mRNA catabolic process	1.19 X 10-16	210
GO:BP	peptide metabolic process	2.43 X 10-16	884
GO:BP	organic cyclic compound catabolic process	1.15 X 10-15	649
GO:BP	mRNA catabolic process	8.20 X 10-15	311
GO:BP	establishment of protein localization to membrane	6.63 X 10-14	306

GO:BP	establishment of protein localization to organelle	1.10 X 10-13	531
GO:BP	protein localization to organelle	2.96 X 10-12	881
GO:BP	protein targeting	1.08 X 10-11	418
GO:BP	protein localization to membrane	4.14 X 10-09	586
GO:BP	ncRNA metabolic process	4.89 X 10-09	544
GO:BP	mRNA metabolic process	2.31 X 10-08	784
GO:BP	rRNA metabolic process	6.98 X 10-06	237
GO:BP	DNA conformation change	8.04 X 10-06	278
GO:BP	ribosome biogenesis	9.86 X 10-06	282
GO:BP	ribonucleoprotein complex biogenesis	3.80 X 10-05	447
GO:BP	rRNA processing	5.93 X 10-05	200
GO:BP	generation of precursor metabolites and energy	6.66 X 10-05	463
GO:BP	positive regulation of gene expression, epigenetic	0.000119	60
GO:BP	DNA metabolic process	0.000122	999
GO:BP	nucleoside triphosphate metabolic process	0.000125	294
GO:BP	purine nucleoside triphosphate metabolic process	0.000363	275
GO:BP	tRNA aminoacylation for protein translation	0.000379	47
GO:BP	ncRNA processing	0.000401	368
GO:BP	tRNA aminoacylation	0.000588	50
GO:BP	cellular amino acid metabolic process	0.000629	333
GO:BP	amino acid activation	0.000676	51
GO:BP	drug metabolic process	0.000719	770
GO:BP	aerobic respiration	0.000781	76
GO:BP	nucleobas x 10-containing small molecule metabolic process	0.001094	728
GO:BP	nucleosome assembly	0.001275	143
GO:BP	carboxylic acid metabolic process	0.001329	989
GO:BP	purine ribonucleoside triphosphate metabolic process	0.001757	268
GO:BP	ribonucleoside triphosphate metabolic process	0.002253	274
GO:BP	nucleotide metabolic process	0.002259	640
GO:BP	nucleoside phosphate metabolic process	0.002547	645
GO:BP	ATP metabolic process	0.003151	238

GO:BP	cytoplasmic translation	0.003416	92
GO:BP	tricarboxylic acid metabolic process	0.00381	42
GO:BP	chromatin assembly	0.004222	163
GO:BP	chromosome condensation	0.005052	44
GO:BP	DNA packaging	0.005259	207
GO:BP	cellular respiration	0.005546	168
GO:BP	interspecies interaction between organisms	0.00649	811
GO:BP	telomere organization	0.006503	171
GO:BP	ribosomal large subunit biogenesis	0.006694	71
GO:BP	RNA processing	0.010605	902
GO:BP	nucleosome organization	0.010802	181
GO:BP	chromatin assembly or disassembly	0.015838	189
GO:BP	nucleosome positioning	0.015975	15
GO:BP	oxidative phosphorylation	0.01604	113
GO:BP	chromatin organization involved in regulation of transcription	0.01604	113
GO:BP	doubl x 10-strand break repair via nonhomologous end joining	0.022388	85
GO:BP	tricarboxylic acid cycle	0.024778	34
GO:BP	purine nucleotide metabolic process	0.025024	506
GO:BP	telomere maintenance	0.025356	158
GO:BP	ribose phosphate metabolic process	0.025643	507
GO:BP	negative regulation of gene expression, epigenetic	0.028211	122
GO:BP	non-recombinational repair	0.037721	92
GO:BP	regulation of DNA metabolic process	0.037729	409
GO:BP	citrate metabolic process	0.043431	38
GO:BP	negative regulation of chromatin silencing	0.044117	19
GO:BP	energy derivation by oxidation of organic compounds	0.045598	260
GO:BP	purine ribonucleotide metabolic process	0.04707	474
GO:CC	cytosolic ribosome	1.21 X 10-25	119
GO:CC	ribosome	5.07 X 10-25	247
GO:CC	ribonucleoprotein complex	5.01 X 10-22	862
GO:CC	ribosomal subunit	2.06 X 10-21	194
GO:CC	cytosolic part	8.23 X 10-19	244
GO:CC	cytosolic large ribosomal subunit	5.75 X 10-14	64
GO:CC	large ribosomal subunit	1.97 X 10-12	122

GO:CC	mitochondrial matrix	4.27 X 10-10	466
GO:CC	cytosolic small ribosomal subunit	2.23 X 10-09	48
GO:CC	nucleoid	2.48 X 10-08	43
GO:CC	mitochondrial nucleoid	2.48 X 10-08	43
GO:CC	protein-DNA complex	6.31 X 10-08	203
GO:CC	organelle inner membrane	1.03 X 10-07	506
GO:CC	small ribosomal subunit	2.33 X 10-07	75
GO:CC	focal adhesion	5.03 X 10-07	404
GO:CC	cell-substrate adherens junction	5.69 X 10-07	407
GO:CC	cell-substrate junction	6.68 X 10-07	411
GO:CC	mitochondrial envelope	6.75 X 10-07	723
GO:CC	mitochondrial membrane	9.85 X 10-07	680
GO:CC	chromosomal part	1.22 X 10-06	924
GO:CC	mitochondrial inner membrane	2.83 X 10-06	449
GO:CC	polysome	4.38 X 10-06	75
GO:CC	nucleolus	6.48 X 10-06	934
GO:CC	pigment granule	6.51 X 10-06	105
GO:CC	melanosome	6.51 X 10-06	105
GO:CC	nucleosome	9.35 X 10-06	109
GO:CC	adherens junction	9.47 X 10-06	537
GO:CC	anchoring junction	1.49 X 10-05	552
GO:CC	nuclear chromosome	1.51 X 10-05	608
GO:CC	DNA packaging complex	1.85 X 10-05	117

GO:CC	nuclear chromosome, telomeric region	3.21 X 10-05	124
GO:CC	polysomal ribosome	5.28 X 10-05	30
GO:CC	mitochondrial protein complex	0.000108	260
GO:CC	nuclear chromosome part	0.000119	570
GO:CC	chromosome, telomeric region	0.00029	157
GO:CC	aminoacyl-tRNA synthetase multienzyme complex	0.000727	12
GO:CC	chromatin	0.001508	553
GO:CC	chromosomal region	0.002642	347
GO:CC	organelle outer membrane	0.02339	209
GO:CC	outer membrane	0.025162	211
GO:CC	catalytic step 2 spliceosome	0.026484	85
GO:CC	inner mitochondrial membrane protein complex	0.037937	130
KEGG	Ribosome	3.51 X 10-16	149
KEGG	Biosynthesis of amino acids	0.000168	73
KEGG	Citrate cycle (TCA cycle)	0.000521	30
KEGG	Carbon metabolism	0.001097	115
KEGG	Parkinson disease	0.003001	129
KEGG	Non-homologous end-joining	0.003257	13
KEGG	Aminoacyl-tRNA biosynthesis	0.005164	44
KEGG	Huntington disease	0.013718	185
CORUM	Ribosome, cytoplasmic	1.70 X 10-16	80
CORUM	Nop56p-associated pr x 10-rRNA complex	7.48 X 10-15	104
CORUM	60S ribosomal subunit, cytoplasmic	1.38 X 10-09	47
CORUM	40S ribosomal subunit, cytoplasmic	1.49 X 10-05	31
CORUM	40S ribosomal subunit, cytoplasmic	2.74 X 10-05	33
CORUM	TRBP containing complex (DICER, RPL7A, EIF6, MOV10 and subunits of the 60S ribosomal particle)	3.71 X 10-05	25
CORUM	Multisynthetase complex	0.037748	11
CORUM	prohibitin 2 complex, mitochondrial	0.049881	5

DMSO UPs			
source	term name	adjusted p value	term size
GO:BP	mRNA metabolic process	6.35 X 10-10	784

GO:BP	peptide metabolic process	2.09 X 10-08	884
GO:BP	peptide biosynthetic process	4.72 X 10-08	727
GO:BP	RNA splicing	1.11 X 10-07	422
GO:BP	amide biosynthetic process	1.72 X 10-07	857
GO:BP	RNA splicing, via transesterification reactions	3.61 X 10-07	337
GO:BP	protein folding	4.19 X 10-07	211
GO:BP	translation	4.68 X 10-07	704
GO:BP	negative regulation of mRNA metabolic process	5.71 X 10-07	70
GO:BP	nucleobas x 10-containing compound catabolic process	1.06 X 10-06	553
GO:BP	regulation of mRNA metabolic process	1.95 X 10-06	265
GO:BP	mRNA splicing, via spliceosome	2.01 X 10-06	334
GO:BP	RNA splicing, via transesterification reactions with bulged adenosine as nucleophile	2.01 X 10-06	334
GO:BP	regulated exocytosis	2.10 X 10-06	750
GO:BP	aromatic compound catabolic process	2.22 X 10-06	616
GO:BP	RNA catabolic process	3.52 X 10-06	345
GO:BP	mRNA catabolic process	3.86 X 10-06	311
GO:BP	heterocycle catabolic process	6.31 X 10-06	602
GO:BP	cellular nitrogen compound catabolic process	6.54 X 10-06	603
GO:BP	organic cyclic compound catabolic process	6.82 X 10-06	649
GO:BP	neutrophil degranulation	8.91 X 10-06	483
GO:BP	neutrophil activation involved in immune response	1.00 X 10-05	486
GO:BP	symbiont process	1.26 X 10-05	762
GO:BP	exocytosis	1.43 X 10-05	864

GO:BP	neutrophil activation	1.47 X 10-05	496
GO:BP	neutrophil mediated immunity	1.53 X 10-05	497
GO:BP	granulocyte activation	1.91 X 10-05	503
GO:BP	viral process	2.99 X 10-05	696
GO:BP	leukocyte degranulation	4.86 X 10-05	529
GO:BP	interspecies interaction between organisms	4.99 X 10-05	811
GO:BP	myeloid cell activation involved in immune response	6.63 X 10-05	538
GO:BP	protein localization to organelle	8.29 X 10-05	881
GO:BP	nuclear transport	8.35 X 10-05	337
GO:BP	mRNA processing	8.40 X 10-05	501
GO:BP	interleukin-12-mediated signaling pathway	8.47 X 10-05	47
GO:BP	myeloid leukocyte mediated immunity	8.68 X 10-05	546
GO:BP	negative regulation of mRNA splicing, via spliceosome	0.000115	20
GO:BP	cellular response to interleukin-12	0.000119	49
GO:BP	response to interleukin-12	0.000141	50
GO:BP	regulation of mRNA stability	0.000173	119
GO:BP	regulation of catabolic process	0.000226	870
GO:BP	establishment of protein localization to organelle	0.000232	531
GO:BP	regulation of RNA stability	0.000339	127
GO:BP	nucleocytoplasmic transport	0.000401	334
GO:BP	RNA processing	0.000482	902
GO:BP	negative regulation of RNA splicing	0.000501	25
GO:BP	drug metabolic process	0.000856	770
GO:BP	regulation of mRNA catabolic process	0.000978	141
GO:BP	myeloid leukocyte activation	0.001267	635
GO:BP	negative regulation of mRNA processing	0.001295	29
GO:BP	protein localization to nucleus	0.001379	247
GO:BP	leukocyte activation involved in immune response	0.001623	694
GO:BP	cytoplasmic translation	0.001634	92
GO:BP	negative regulation of programmed cell death	0.001733	960
GO:BP	cell activation involved in immune response	0.001797	698

GO:BP	cellular amino acid metabolic process	0.001986	333
GO:BP	regulation of cellular catabolic process	0.002288	759
GO:BP	positive regulation of protein localization to Cajal body	0.003443	9
GO:BP	regulation of protein localization to Cajal body	0.003443	9
GO:BP	RNA localization	0.003762	231
GO:BP	negative regulation of apoptotic process	0.004064	946
GO:BP	translational initiation	0.004373	198
GO:BP	ribonucleoprotein complex assembly	0.00455	235
GO:BP	regulation of RNA splicing	0.004889	134
GO:BP	protein stabilization	0.004922	166
GO:BP	ATP metabolic process	0.005235	238
GO:BP	chaperon x 10-mediated protein folding	0.005321	56
GO:BP	protein localization to Cajal body	0.005688	10
GO:BP	positive regulation of establishment of protein localization to telomere	0.005688	10
GO:BP	protein localization to nuclear body	0.005688	10
GO:BP	positive regulation of organelle organization	0.007231	602
GO:BP	cofactor metabolic process	0.007491	554
GO:BP	ribonucleoprotein complex subunit organization	0.008596	249
GO:BP	regulation of establishment of protein localization to telomere	0.008861	11
GO:BP	carboxylic acid metabolic process	0.0095	989
GO:BP	nucleoside triphosphate metabolic process	0.010643	294
GO:BP	protein export from nucleus	0.01261	183
GO:BP	regulation of establishment of protein localization to chromosome	0.013176	12
GO:BP	positive regulation of protein localization to chromosome, telomeric region	0.013176	12
GO:BP	protein localization to nucleoplasm	0.013176	12
GO:BP	proteasomal ubiquitin-independent protein catabolic process	0.013791	25
GO:BP	ribonucleotide metabolic process	0.01796	489
GO:BP	purine ribonucleoside triphosphate metabolic process	0.019033	268
GO:BP	regulation of translation	0.019468	398
GO:BP	purin x 10-containing compound metabolic process	0.019549	541
GO:BP	ribonucleoside triphosphate metabolic process	0.024107	274
GO:BP	purine nucleoside triphosphate metabolic process	0.02506	275
GO:BP	sulfur compound metabolic process	0.02604	362
GO:BP	regulation of protein localization to chromosome, telomeric region	0.026184	14

GO:BP	nuclear export	0.026583	198
GO:BP	positive regulation of catabolic process	0.027289	409
GO:BP	regulation of mRNA splicing, via spliceosome	0.028151	99
GO:BP	purine nucleotide metabolic process	0.028473	506
GO:BP	negative regulation of protein polymerization	0.029089	72
GO:BP	ribose phosphate metabolic process	0.029236	507
GO:BP	supramolecular fiber organization	0.029339	660
GO:BP	generation of precursor metabolites and energy	0.033165	463
GO:BP	cellular aldehyde metabolic process	0.034877	74
GO:BP	positive regulation of telomerase RNA localization to Cajal body	0.035395	15
GO:BP	cytoplasmic translational initiation	0.041777	31
GO:BP	purine ribonucleotide metabolic process	0.044737	474
GO:CC	cytoplasmic vesicle lumen	5.76 X 10-12	336
GO:CC	vesicle lumen	6.17 X 10-12	337
GO:CC	secretory granule lumen	1.58 X 10-11	319
GO:CC	adherens junction	1.49 X 10-10	537
GO:CC	anchoring junction	2.96 X 10-10	552
GO:CC	ribonucleoprotein complex	7.94 X 10-09	862
GO:CC	cell-substrate junction	2.42 X 10-08	411
GO:CC	focal adhesion	1.09 X 10-07	404
GO:CC	cell-substrate adherens junction	1.26 X 10-07	407
GO:CC	ficolin-1-rich granule lumen	2.10 X 10-07	123
GO:CC	ficolin-1-rich granule	2.10 X 10-07	123
GO:CC	cytosolic part	2.45 X 10-06	244
GO:CC	chaperone complex	7.91 X 10-06	18
GO:CC	chaperonin-containing T-complex	1.12 X 10-05	10
GO:CC	proteasome complex	1.23 X 10-05	67
GO:CC	endopeptidase complex	1.41 X 10-05	68

GO:CC	contractile fiber part	2.59 X 10-05	216
GO:CC	contractile fiber	6.28 X 10-05	232
GO:CC	supramolecular fiber	6.60 X 10-05	941
GO:CC	actin cytoskeleton	6.82 X 10-05	482
GO:CC	supramolecular polymer	7.71 X 10-05	948
GO:CC	supramolecular complex	7.88 X 10-05	949
GO:CC	secretory vesicle	0.000144	977
GO:CC	zona pellucida receptor complex	0.000155	7
GO:CC	peptidase complex	0.000165	90
GO:CC	myofibril	0.000224	220
GO:CC	secretory granule	0.000232	831
GO:CC	cell-cell junction	0.000491	450
GO:CC	spliceosomal complex	0.000983	176
GO:CC	cytoplasmic stress granule	0.001033	59
GO:CC	proteasome core complex	0.001678	24
GO:CC	sarcomere	0.003199	199
GO:CC	cell cortex part	0.003342	163
GO:CC	cytoplasmic region	0.004385	476
GO:CC	cell cortex	0.004522	289
GO:CC	cortical cytoskeleton	0.004924	103
GO:CC	perinuclear region of cytoplasm	0.004951	693
GO:CC	hemidesmosome	0.014924	7
GO:CC	myelin sheath	0.025036	166
GO:CC	polymeric cytoskeletal fiber	0.026699	719
GO:CC	ribonucleoprotein granule	0.040086	218
KEGG	Spliceosome	0.00028	132
KEGG	Proteasome	0.000299	45
CORUM	26S proteasome	0.000344	22
CORUM	20S proteasome	0.006425	14
CORUM	CCT complex (chaperonin containing TCP1 complex)	0.009222	8
CORUM	PA28gamma-20S proteasome	0.009421	15
CORUM	PA700-20S-PA28 complex	0.012117	36
CORUM	PA28-20S proteasome	0.013395	16
CORUM	PABPC1-HSPA8-HNRPD-EIF4G1 complex	0.020393	4
CORUM	BBS-chaperonin complex	0.026472	10
CORUM	Multiprotein complex (mRNA turnover)	0.049927	5

7 References

Argilés, J. M., Busquets, S., Stemmler, B., & López-Soriano, F. J. (2014). Cancer cachexia: Understanding the molecular basis. *Nature Reviews Cancer*, *14*(11), 754–762. https://doi.org/10.1038/nrc3829

Asara, J. M., Christofk, H. R., Freimark, L. M., & Cantley, L. C. (2008). A label-free quantification method by MS/MS TIC compared to SILAC and spectral counting in a proteomics screen. *Proteomics*, *8*(5), 994–999. https://doi.org/10.1002/pmic.200700426

Barabási, A.-L., Gulbahce, N., & Loscalzo, J. (2011). An Integrative Systems Medicine Approach to Mapping Human Metabolic Diseases. *Nat Rev Genet*, *12*(1), 56–68. https://doi.org/10.1038/nrg2918.Network

Birnie, G. D. (1988). The HL60 cell line: A model system for studying human myeloid cell differentiation. *British Journal of Cancer*.

Bordeleau, M.-E., Matthews, J., Wojnar, J. M., Lindqvist, L., Novac, O., Jankowsky, E., … Pelletier, J. (2005). Stimulation of mammalian translation initiation factor eIF4A activity by a small molecule inhibitor of eukaryotic translation. *Proceedings of the National Academy of Sciences*, *102*(30), 10460–10465. https://doi.org/10.1073/pnas.0504249102

Cencic, R., Hall, D. R., Robert, F., Du, Y., Min, J., Li, L., … Lewis, I. (2010). Reversing chemoresistance by small molecule inhibition of the translation initiation complex eIF4F. *Proceedings of the National Academy of Sciences*, *108*(3), 1046–1051. https://doi.org/10.1073/pnas.1011477108

Cencic, R., & Pelletier, J. (2016). Hippuristanol - A potent steroid inhibitor of eukaryotic initiation factor 4A. *Translation*, *4*(1), e1137381. https://doi.org/10.1080/21690731.2015.1137381

Chambers, J. M., Lindqvist, L. M., Webb, A., Huang, D. C. S., Savage, G. P., & Rizzacasa, M. A. (2013). Synthesis of Biotinylated Episilvestrol : Highly Selective Targeting of the Translation Factors eIF4AI / II, (7), 13–16. https://doi.org/10.1021/ol400401d

Cho, P. F., Osler, W., & Hg, Q. (2008). Cap-Dependent Translational Inhibition Establishes Two Opposing Morphogen Gradients in Drosophila Embryos, *16*(20), 2035–2041.

Clark, A. L., Coats, A. J. S., Krum, H., Katus, H. A., Mohacsi, P., Salekin, D., … Anker, S. D. (2017). Effect of beta-adrenergic blockade with carvedilol on cachexia in severe chronic heart failure : results from the COPERNICUS trial, (February), 549–556. https://doi.org/10.1002/jcsm.12191

Cramer, Z., Sadek, J., Vazquez, G. G., Di Marco, S., Pause, A., Pelletier, J., & Gallouzi, I. E. (2018). EIF4A inhibition prevents the onset of cytokin x 10-induced muscle wasting by blocking the STAT3 and iNOS pathways. *Scientific Reports*, *8*(1), 2–11. https://doi.org/10.1038/s41598-018-26625-9

Crotty, S., Cameron, C. E., & Andino, R. (2001). RNA virus error catastrophe : Direct molecular test by using ribavirin, *98*(12).

Di Marco, S., Cammas, A., Lian, X. J., Kovacs, E. N., Ma, J. F., Hall, D. T., … Gallouzi, I. E. (2012). The translation inhibitor pateamine A prevents cachexia-induced muscle wasting in mice. *Nature Communications*, *3*(May), 812–896. https://doi.org/10.1038/ncomms1899

Dobs, A. S. (2013). Effects of enobosarm on muscle wasting and physical function in patients with cancer: a doubl x 10-blind, randomised controlled phase 2 trial. *Lancet Oncology*, *4*(14), 335–345. https://doi.org/10.1183/09031936.00063810.The

Duffy, A. G., Makarova-Rusher, O. V., & Ulahannan, S. V. (2016). Modulation of tumor eIF4E by antisense inhibition: A phase I/II translational clinical trial of ISIS 183750—an antisense oligonucleotide against eIF4E—in combination with irinotecan in solid tumors and irinotecan-refractory colorectal cancer, *1657*, 1648–1657. https://doi.org/10.1002/ijc.30199

Evans, W. J., Morley, J. E., Argilés, J., Bales, C., Baracos, V., Guttridge, D., … Anker, S. D. (2008). Cachexia: A new definition. *Clinical Nutrition*, *27*(6), 793–799. https://doi.org/10.1016/j.clnu.2008.06.013

Frey, N. P., & Davis, E. P. (2016). Launch and commissioning the deep space climate observatory. *Advances in the Astronautical Sciences*, *157*(October 2013), 999–1010. https://doi.org/10.1002/pbc

Frydryskova, K., Masek, T., Borcin, K., Mrvova, S., Venturi, V., & Pospisek, M. (2016). Distinct recruitment of human eIF4E isoforms to processing bodies and stress granules. *BMC Molecular Biology*, *17*(1), 1–19. https://doi.org/10.1186/s12867-016-0072-x

Gordon, J. N., Trebble, T. M., Ellis, R. D., Duncan, H. D., Johns, T., & Goggin, P. M. (2005). Thalidomide in the treatment of cancer cachexia: a randomised placebo controlled trial, 540–545. https://doi.org/10.1136/gut.2004.047563

Harms, U., Andreou, A. Z., Gubaev, A., & Klostermeier, D. (2014). EIF4B, eIF4G and RNA regulate eIF4A activity in translation initiation by modulating the eIF4A conformational cycle. *Nucleic Acids Research*, *42*(12), 7911–7922. https://doi.org/10.1093/nar/gku440

Hayano, T., Yanagida, M., Yamauchi, Y., Shinkawa, T., Isobe, T., & Takahashi, N. (2003). Proteomic Analysis of Human Nop56p-associated Pr x 10-ribosomal Ribonucleoprotein Complexes. *Journal of Biological Chemistry*, *278*(36), 34309–34319. https://doi.org/10.1074/jbc.m304304200

Hemi Cumming, A., Brown, S. L., Tao, X., Cuyamendous, C., Field, J. J., Miller, J. H., … Teesdal x 10-Spittle, P. H. (2016). Synthesis of a simplified triazole analogue of pateamine A. *Organic and Biomolecular Chemistry*, *14*(22), 5117–5127. https://doi.org/10.1039/c6ob00086j

Ho, J., Hyun, Y., Young, S., Min, J., Kim, A., & Chang, Y. (2009). Crystal structure of the eIF4A – PDCD4 complex, 1–6.

Iwasaki, S., Floor, S. N., & Ingolia, N. T. (2016). Rocaglates convert DEAD-box protein eIF4A into a sequenc x 10-selective translational repressor. *Nature*, *534*(7608), 558–561. https://doi.org/10.1038/nature17978

Iwasaki, S., Iwasaki, W., Takahashi, M., Sakamoto, A., Watanabe, C., Shichino, Y., … Ingolia, N. T. (2019). The Translation Inhibitor Rocaglamide Targets a Bimolecular Cavity between eIF4A and Polypurine RNA. *Molecular Cell*, *73*(4), 738–748.e9. https://doi.org/10.1016/j.molcel.2018.11.026

Joshi, B., Lee, K., Maeder, D. L., & Jagus, R. (2005). Phylogenetic analysis of eIF4 X 10-family members, *20*, 1–20. https://doi.org/10.1186/1471-2148-5-48

Katakami, N., Uchino, J., Yokoyama, T., Naito, T., Kondo, M., Yamada, K., … Eguchi, K. (2018). Anamorelin (ONO-7643) for the treatment of patients with non–small cell lung cancer and cachexia: Results from a randomized, doubl x 10-blind, placebo-controlled, multicenter study of Japanese patients (ONO-7643-04). *Cancer*, *124*(3), 606–616. https://doi.org/10.1002/cncr.31128

Kentsis, A., Topisirovic, I., Culjkovic, B., Shao, L., & Borden, K. L. B. (2004). Ribavirin suppresses eIF4 X 10-mediated oncogenic transformation by physical mimicry of the 7-methyl guanosine mRNA cap, *101*(52), 18105–18110.

Kentsis, A., Volpon, L., Topisirovic, I., Soll, C. E., Culjkovic, B., Shao, L., & Borden, K. L. B. (2005). Further evidence that ribavirin interacts with eIF4E. *Rna*, *11*(12), 1762–1766. https://doi.org/10.1261/rna.2238705

Kislinger, T., Gramolini, A. O., MacLennan, D. H., & Emili, A. (2005). Multidimensional protein identification technology (MudPIT): Technical overview of a profiling method optimized for the comprehensive proteomic investigation of normal and diseased heart tissue. *Journal of the American Society for Mass Spectrometry*, *16*(8), 1207–1220. https://doi.org/10.1016/j.jasms.2005.02.015

Korneeva, N. L., Lamphear, B. J., Hennigan, F. L. C., Merrick, W. C., & Rhoads, R. E. (2001). Characterization of the Two eIF4A-binding Sites on Human eIF4G-1. *Journal of Biological Chemistry*, *276*(4), 2872–2879. https://doi.org/10.1074/jbc.M006345200

Kuznetsov, G., Xu, Q., Rudolph-Owen, L., TenDyke, K., Liu, J., Towle, M., … Littlefield, B. A. (2009). Potent in vitro and in vivo anticancer activities of des-methyl, des-amino pateamine A, a synthetic analogue of marine natural product pateamine A. *Molecular Cancer Therapeutics*, *8*(5), 1250–1260. https://doi.org/10.1158/1535-7163.MCT-08-1026

Lanford, R. E., Hong, Z., Chavez, D., Guerra, B., Lau, J. Y. N., Beames, B., & Brasky, K. M. (2002). Ribavirin Induces Error-Prone Replication of GB Virus B in Primary Tamarin Hepatocytes. *Journal of Virology*, *75*(17), 8074–8081. https://doi.org/10.1128/jvi.75.17.8074-8081.2001

Le Hir, H., Gatfield, D., Izaurralde, E., & Moore, M. J. (2001). The exon-exon junction complex provides a binding platform for factors involved in mRNA export and nonsens x 10-mediated mRNA decay. *EMBO Journal*, *20*(17), 4987–4997. https://doi.org/10.1093/emboj/20.17.4987

Leyssen, P., Clercq, E. De, & Neyts, J. (2006). The Anti-Yellow Fever Virus Activity of Ribavirin Is Independent of Error-Prone Replication, *69*(4), 1461–1467. https://doi.org/10.1124/mol.105.020057.for

Li, S., & Rousseau, D. (2012). ATAD3, a vital membrane bound mitochondrial ATPase involved in tumor progression. *Journal of Bioenergetics and Biomembranes*, *44*(1), 189–197. https://doi.org/10.1007/s10863-012-9424-5

Lindqvist, L., Oberer, M., Reibarkh, M., Cencic, R., Bordeleau, M. E., Vogt, E., … Pelletier, J. (2008). Selective pharmacological targeting of a DEAD box RNA helicase. *PLoS ONE*, *3*(2). https://doi.org/10.1371/journal.pone.0001583

Litonin, D., Sologub, M., Shi, Y., Savkina, M., Anikin, M., Falkenberg, M., … Temiakov, D. (2010). Human Mitochondrial Transcription Revisited. *Journal of Biological Chemistry*, *285*(24), 18129–18133. https://doi.org/10.1074/jbc.C110.128918

Low, W. K., Dang, Y., Bhat, S., Romo, D., & Liu, J. O. (2007). Substrat x 10-Dependent Targeting of Eukaryotic Translation Initiation Factor 4A by Pateamine A: Negation of Domain-Linker Regulation of Activity. *Chemistry and Biology*, *14*(6), 715–727. https://doi.org/10.1016/j.chembiol.2007.05.012

Low, W. K., Dang, Y., Schneider-Poetsch, T., Shi, Z., Choi, N. S., Merrick, W. C., … Liu, J. O. (2005). Inhibition of eukaryotic translation initiation by the marine natural product pateamine A. *Molecular Cell*, *20*(5), 709–722. https://doi.org/10.1016/j.molcel.2005.10.008

Marcotrigiano, J., Gingras, A. C., Sonenberg, N., & Burley, S. K. (1999). Cap-dependent translation initiation in eukaryotes is regulated by a molecular mimic of eIF4G. *Molecular Cell*, *3*(6), 707–716. https://doi.org/10.1016/S1097-2765(01)80003-4

Matthews, J. H. (2010). THESIS: The Molecular Pharmacology of Pateamine A.

Matthews, J. H., Maass, D. R., Northcote, P. T., Atkinson, P. H., & Teesdal x 10-Spittle, P. H. (2013). The cellular target specificity of pateamine A. *Zeitschrift Fur Naturforschung - Section C Journal of Biosciences*, *68 C*(9–10), 406–415. https://doi.org/10.1515/znc-2013-9-1008

Merrick, W. C. (1992). Mechanism and regulation of eukaryotic protein synthesis. *Microbiological Reviews*, *56*(2), 291–315. https://doi.org/10.1101/gad.11.21.2755

Migliaccio, A., Rotondi, A., & Auricchio, F. (2006). Calmodulin-stimulated phosphorylation of 17 beta-estradiol receptor on tyrosine. *Proceedings of the National Academy of Sciences*, *81*(19), 5921–5925. https://doi.org/10.1073/pnas.81.19.5921

Milne, A. C., Potter, J., & Avenell, A. (2005). Protein and energy supplementation in elderly people at risk from malnutrition. *Cochrane Database of Systematic Reviews*, (2). https://doi.org/10.1002/14651858.CD003288.pub2

Minich, W. B., Balastat, M. L., Gosst, D. J., & Rhoads, R. E. (1994). Chromatographic resolution of in vivo phosphorylated and nonphosphorylated eukaryotic translation initiation factor eIF-4E : Increased cap affinity of the phosphorylated form, *91*(August), 7668–7672.

Moerke, N. J., Aktas, H., Chen, H., Cantel, S., Reibarkh, M. Y., Fahmy, A., … Wagner, G. (2007). Small-Molecule Inhibition of the Interaction between the Translation Initiation Factors eIF4E and eIF4G. *Cell*, *128*(2), 257–267. https://doi.org/10.1016/j.cell.2006.11.046

Morin, P. J., Vogelstein, B., & Kinzlertt, K. W. (1996). Apoptosis and APC in colorectal tumorigenesis. *Medical Sciences*, *93*(July), 7950–7954. https://doi.org/10.1073/pnas.93.15.7950

Morino, S., Imataka, H., Svitkin, Y. V, Pestova, T. V, & Sonenberg, N. (2000). Eukaryotic translation initiation factor 4E (eIF4E) binding site and the middle on x 10-third of eIF4GI constitute the core domain for cap-dependent translation, and the C-terminal on x 10-third functions as a modulatory region. *Molecular & Cellular Biology*, *20*(2), 468–477. https://doi.org/10.1128/MCB.20.2.468-477.2000

Morley, J., Thomas, D., & Wilson, M.-M. (2006). Cachexia: Pathophysiology and clinical relevance. *American Journal of Clinical Nutrition*, *83*(4), 735–743. https://doi.org/10.1093/ajcn/83.4.735

Naiki, M., Ochi, N., Kato, Y. S., Purevsuren, J., Yamada, K., Kimura, R., … Wakamatsu, N. (2014). Mutations in HADHB, which encodes the β-subunit of mitochondrial trifunctional protein, cause infantile onset hypoparathyroidism and peripheral polyneuropathy. *American Journal of Medical Genetics, Part A*, *164*(5), 1180–1187. https://doi.org/10.1002/ajmg.a.36434

Ngagore, L., Nadeau, R. J., Guo, Q., Jadhav, Y., Jarrett, H., & Haskins, W. (2013). Purification & Characterization of Transcription Factors, *5*(32), 386–398. https://doi.org/10.1002/bmb.20244.DNA

Nielsen, P. J., & Trachsel, H. (1988). The mouse protein synthesis initiation factor 4A gene family includes two related functional genes which are differentially expressed. *The EMBO Journal*, *7*(7), 2097–2105. https://doi.org/10.1093/jxb/erx229

Northcote, P. T., Blunt, J. W., & Munro, M. H. G. (1991). Pateamine: a potent cytotoxin from the New Zealand Marine sponge, mycale sp. *Tetrahedron Letters*, *32*(44), 6411–6414. https://doi.org/10.1016/0040-4039(91)80182-6

Oberer, M., Marintchev, A., & Wagner, G. (2005). Structural basis for the enhancement of eIF4A helicase activity by eIF4G. *Genes and Development*, *19*(18), 2212–2223. https://doi.org/10.1101/gad.1335305

Oguro, A., Ohtsu, T., Svitkin, Y. V, Sonenberg, N., & Nakamura, Y. (2003). RNA aptamers to initiation

factor 4A helicase hinder cap-dependent translation by blocking ATP hydrolysis, 394–407. https://doi.org/10.1261/rna.2161303.)

Owen, J. G., Charlop-Powers, Z., Smith, A. G., Ternei, M. A., Calle, P. Y., Reddy, B. V. B., … Brady, S. F. (2015). Multiplexed metagenome mining using short DNA sequence tags facilitates targeted discovery of epoxyketone proteasome inhibitors. *Proceedings of the National Academy of Sciences*, *112*(14), 4221–4226. https://doi.org/10.1073/pnas.1501124112

Page, M. J., Handley, S. J., Northcote, P. T., Cairney, D., & Willan, R. C. (2011). Successes and pitfalls of the aquaculture of the sponge Mycale hentscheli. *Aquaculture*, *312*(1–4), 52–61. https://doi.org/10.1016/j.aquaculture.2010.12.006

Page, T., & Connor, J. D. (1990). The metabolism of ribavirin in erythrocytes and nucleated cells. *International Journal of Biochemistry*, *22*(4), 379–383. https://doi.org/10.1016/0020-711X(90)90140-X

Pelletier, J., Graff, J., Ruggero, D., & Sonenberg, N. (2015). TARGETING THE eIF4F TRANSLATION INITIATION COMPLEX: A CRITICAL NEXUS FOR CANCER DEVELOPMENT. *Cancer Research*, *75*(2), 250–263. https://doi.org/10.1158/0008-5472.CAN-14-2789

Pestova, T. V, & Kolupaeva, V. G. (2002). The roles of individual eukaryotic translation initiation factors in ribosomal scanning and initiation codon selection, *3*, 2906–2922. https://doi.org/10.1101/gad.1020902.5

Peters, T. L., Tillotson, J., Yeomans, A. M., Wilmore, S., Lemm, E., Jimenez-Romero, C., … Schatz, J. H. (2018). Target-based screening against eIF4A1 reveals the marine natural product elatol as a novel inhibitor of translation initiation with in vivo antitumor activity. *Clinical Cancer Research*, *24*(17), 4256–4270. https://doi.org/10.1158/1078-0432.CCR-17-3645

Pichon, X., A. Wilson, L., Stoneley, M., Bastide, A., A King, H., Somers, J., & E Willis, A. (2012). RNA Binding Protein/RNA Element Interactions and the Control of Translation. *Current Protein & Peptide Science*, *13*(4), 294–304. https://doi.org/10.2174/138920312801619475

Rakesh, R., Joseph, A. P., Bhaskara, R. M., & Srinivasan, N. (2016). Structural and mechanistic insights into human splicing factor SF3b complex derived using an integrated approach guided by the cryo-EM density maps. *RNA Biology*, *13*(10), 1025–1040. https://doi.org/10.1080/15476286.2016.1218590

Reid, M. B., & Li, Y. P. (2001). Tumor necrosis factor-α and muscle wasting: A cellular perspective. *Respiratory Research*, *2*(5), 269–272. https://doi.org/10.1186/rr67

Reimand, J., Arak, T., Adler, P., Kolberg, L., Reisberg, S., Peterson, H., & Vilo, J. (2016). g:Profiler-a web server for functional interpretation of gene lists (2016 update). *Nucleic Acids Research*, *44*(W1), W83–W89. https://doi.org/10.1093/nar/gkw199

Rendón-Huerta, E. P., Torres-Martínez, A., Charles-Niño, C., Rivas-Estilla, A. M., Paez, A., Fortoul, T. I., & Montaño, L. F. (2013). Pegylated interferon-α2b and ribavirin decrease claudin-1 and X 10-cadherin expression in HepG2 and Huh-7.5 cells. *Annals of Hepatology*, *12*(4), 448–457.

Romo, D., Choi, N. S., Li, S., Buchler, I., Shi, Z., & Liu, J. O. (2004). Evidence for separate binding and scaffolding domains in the immunosuppressive and antitumor marine natural product, pateamine A: Design, synthesis, and activity studies leading to a potent simplified derivative. *Journal of the American Chemical Society*, *126*(34), 10582–10588. https://doi.org/10.1021/ja040065s

Romo, D., Rzasa, R. M., Shea, H. A., Park, K., Langenhan, J. M., Sun, L., … Liu, J. O. (1998). Total synthesis and immunosuppressive activity of (-)-pateamine A and related compounds:

Implementation of a β-lactam-based macrocyclization. *Journal of the American Chemical Society*, *120*(47), 12237–12254. https://doi.org/10.1021/ja981846u

Rozen, F., Edery, I., Meerovitch, K., Dever, T. E., Merrick, W. C., & Sonenberg, N. (1990). Bidirectional RNA helicase activity of eucaryotic translation initiation factors 4A and 4F. *Molecular and Cellular Biology*, *10*(3), 1134–1144. https://doi.org/10.1128/MCB.10.3.1134

Ryu, A. H., Eckalbar, W. L., Kreimer, A., Yosef, N., & Ahituv, N. (2017). Use antibiotics in cell culture with caution: Genom x 10-wide identification of antibiotic-induced changes in gene expression and regulation. *Scientific Reports*, *7*(1), 1–9. https://doi.org/10.1038/s41598-017-07757-w

Sadlish, H., Galicia-vazquez, G., Paris, C. G., Aust, T., Bhullar, B., Chang, L., … Movva, N. R. (2014). Evidence for a functionally relevant rocaglamide binding site on the eIF4A:RNA complex, *8*(7), 1519–1527. https://doi.org/10.1021/cb400158t.Evidence

Schneider-Poetsch, T., Ju, J., Eyler, D. E., Dang, Y., Bhat, S., Merrick, W. C., … Liu, J. O. (2010). Inhibition of eukaryotic translation elongation by cycloheximide and lactimidomycin. *Nature Chemical Biology*, *6*(3), 209–217. https://doi.org/10.1038/nchembio.304

Schwanhäusser, B., Wolf, J., Chen, W., Selbach, M., Busse, D., Dittmar, G., … Schuchhardt, J. (2011). Global quantification of mammalian gene expression control. *Nature*, *473*(7347), 337–342. https://doi.org/10.1038/nature10098

Serkan Kir, S., White, J. P., Kleiner, S., Kazak, L., Cohen, P., Baracos, aVikie E., & Spiegelman, B. M. (2014). Tumor-derived PTHrP Triggers Adipose Tissue Browning and Cancer Cachexia. *Nature*, *513*(7516), 100–104. https://doi.org/10.1038/nature13528.Tumor-derived

Speicher, D. W. (2010). Target-Decoy Search Strategy for Mass Spectrometry-Based Proteomics. *Current Protocols in Protein Science*, (5), 25.0.1-25.0.2. https://doi.org/10.1002/0471140864.ps2500s60

Sun, Y., Atas, E., Lindqvist, L. M., Sonenberg, N., Pelletier, J., & Meller, A. (2014). Singl x 10-Molecule Kinetics of the Eukaryotic Initiation Factor 4AI upon RNA Unwinding. *Structure/Folding and Design*, *22*(7), 941–948. https://doi.org/10.1016/j.str.2014.04.014

Svitkin, Y., Pause, A., Haghighat, A., & Pyronnet, S. (2001). The requirement for eukaryotic initiation factor 4A (eIF4A) in translation is in direct proportion to …. *Rna*, (2001), 382–394. Retrieved from http://www.ncbi.nlm.nih.gov/entrez/query.fcgi?db=pubmed&cmd=Retrieve&dopt=AbstractPlus&list_uids=10684923970642830528related:wOQ4er15SJQJ%5Cnhttp://journals.cambridge.org/abstract_S135583820100108X

Szklarczyk, D., Gable, A. L., Lyon, D., Junge, A., Wyder, S., Huerta-Cepas, J., … Von Mering, C. (2019). STRING v11: Protein-protein association networks with increased coverage, supporting functional discovery in genom x 10-wide experimental datasets. *Nucleic Acids Research*, *47*(D1), D607–D613. https://doi.org/10.1093/nar/gky1131

Szklarczyk, D., Morris, J. H., Cook, H., Kuhn, M., Wyder, S., Simonovic, M., … Von Mering, C. (2017). The STRING database in 2017: Quality-controlled protein-protein association networks, made broadly accessible. *Nucleic Acids Research*, *45*(D1), D362–D368. https://doi.org/10.1093/nar/gkw937

Tanabe, M., & Kanehisa, M. (2012). *Using the KEGG database resource*. *Current Protocols in Bioinformatics*. https://doi.org/10.1002/0471250953.bi0112s38

Tao, X. (2015). Tristetraprolin Recruits Eukaryotic Initiation Factor 4E2 To Repress Translation of AU-Rich Element-Containing mRNAs, *35*(22), 3921–3932. https://doi.org/10.1128/MCB.00845-

15.Address

Timm, M., Saaby, L., Moesby, L., & Hansen, E. W. (2013). Considerations regarding use of solvents in in vitro cell based assays. *Cytotechnology*, *65*(5), 887–894. https://doi.org/10.1007/s10616-012-9530-6

Trudgian, D. C., Fischer, R., Guo, X., Kessler, B. M., & Mirzaei, H. (2014). GOAT - A simple LC-MS/MS gradient optimization tool. *Proteomics*, *14*(12), 1467–1471. https://doi.org/10.1002/pmic.201300524

Vanhoutte, G., Van De Wiel, M., Wouters, K., Sels, M., Bartolomeeussen, L., De Keersmaecker, S., … Peeters, M. (2016). Cachexia in cancer: what is in the definition? *BMJ Open Gastroenterology*, *3*(1), 1–11. https://doi.org/10.1136/bmjgast-2016-000097

Venturi, V., Little, R., Bircham, P. W., Rodigheri Brito, J., Atkinson, P. H., Maass, D. R., & Teesdal x 10-Spittle, P. H. (2018). Characterisation of the biological response of Saccharomyces cerevisiae to the loss of an allele of the eukaryotic initiation factor 4A. *Biochemical and Biophysical Research Communications*, *496*(4), 1082–1087. https://doi.org/10.1016/j.bbrc.2018.01.137

Verheijen, M. C. T., Lienhard, M., Schrooders, Y. J. M., Clayton, O., Nudischer, R., Timmermann, B., … Caiment, F. (2018). DMSO-induced drastic changes in cellular processes and epigenetic landscape in vitro. *Toxicology Letters*, *295*(August 2018), S215. https://doi.org/10.1016/j.toxlet.2018.06.927

Volpin, F., Casaos, J., Sesen, J., Mangraviti, A., Choi, J., Gorelick, N., … Skuli, N. (2017). Use of an anti-viral drug, Ribavirin, as an anti-glioblastoma therapeutic. *Oncogene*, *36*(21), 3037–3047. https://doi.org/10.1038/onc.2016.457

Von Haehling, S., & Anker, S. D. (2015). Treatment of cachexia: An overview of recent developments. *International Journal of Cardiology*, *184*(1), 726–742. https://doi.org/10.1016/j.ijcard.2014.10.026

Waldron, J. A., Raza, F., & Le Quesne, J. (2018). eIF4A alleviates the translational repression mediated by classical secondary structures more than by G-quadruplexes. *Nucleic Acids Research*, *46*(6), 3075–3087. https://doi.org/10.1093/nar/gky108

Warren S. (1932). 1932 Warren - The Immediate Causes of Death in Cancer.pdf. *Am J Med Sci*.

Westman, B., Beeren, L., Grudzien, E., Stepinski, J., Worch, R., Zuberek, J., … Preiss, T. (2005). The antiviral drug ribavirin does not mimic the 7-methylguanosine moiety of the mRNA cap structure in vitro. *Rna*, *11*(10), 1505–1513. https://doi.org/10.1261/rna.2132505

Williams-Hill, D. M., Duncan, R. F., Nielsen, P. J., & Tahara, S. M. (1997). Differential expression of the murine eukaryotic translation initiation factor isogenes eIF4A(I) and eIF4A(II) is dependent upon cellular growth status. *Archives of Biochemistry and Biophysics*, *338*(1), 111–120. https://doi.org/10.1006/abbi.1996.9804

Wolfe, A. L., Singh, K., Zhong, Y., Drewe, P., Rajasekhar, V. K., Sanghvi, V. R., … Rätsch, G. (2015). RNA G-quadruplexes cause eIF4A-dependent oncogene translation in cancer, *513*(7516), 65–70. https://doi.org/10.1038/nature13485.RNA

Yan, Y., Svitkin, Y., Lee, J. M., Bisaillon, M., & Pelletier, J. (2005). Ribavirin is not a functional mimic of the 7-methyl guanosine mRNA cap. *Rna*, *11*(8), 1238–1244. https://doi.org/10.1261/rna.2930805

Yeeles, J. T. P., Janska, A., Early, A., & Diffley, J. F. X. (2017). How the Eukaryotic Replisome Achieves Rapid and Efficient DNA Replication. *Molecular Cell*, *65*(1), 105–116.

https://doi.org/10.1016/j.molcel.2016.11.017

Yoder-Hill, J., Pause, A., Sonenberg, N., & Merrick, W. C. (1993). The p46 subunit of eukaryotic initiation factor (eIF)-4F exchanges with eIF-4A. *Journal of Biological Chemistry*, *268*(8), 5566–5573. https://doi.org/10.1006/BBRC.1995.1958

Yu, J. G., Bonnerud, P., Eriksson, A., Stal, P. S., Tegner, Y., & Malm, C. (2014). Effects of long term supplementation of anabolic androgen steroids on human skeletal muscle. *PLoS ONE*, *9*(9). https://doi.org/10.1371/journal.pone.0105330

Zhao, P., Liu, Q., Miller, W. A., & Goss, D. J. (2017). Eukaryotic translation initiation factor 4G (eIF4G) coordinates interactions with eIF4A, eIF4B, and eIF4E in binding and translation of the barley yellow dwarf virus 3′ cap-independent translation element (BTE). *Journal of Biological Chemistry*, *292*(14), 5921–5931. https://doi.org/10.1074/jbc.M116.764902